AD-A171 029

SECURITY CLASSIFICATION OF THIS PAGE (When Data Entered)

REPORT DOCUMENTATION PAGE		READ INSTRUCTIONS BEFORE COMPLETING FORM
1. REPORT NUMBER AFOSR-TR- 86-0506	2. GOVT ACCESSION NO.	3. RECIPIENT'S CATALOG NUMBER (2)
4. TITLE (and Subtitle) Deterministic Methods of Seismic Source Identification		5. TYPE OF REPORT & PERIOD COVERED 9/30/83 - 10/1/84
		6. PERFORMING ORG. REPORT NUMBER
7. AUTHOR(s) Charles B. Archambeau		8. CONTRACT OR GRANT NUMBER(s) F49620-83-C-0009
9. PERFORMING ORGANIZATION NAME AND ADDRESS CIRES University of Colorado Boulder, CO 80309		10. PROGRAM ELEMENT, PROJECT, TASK AREA & WORK UNIT NUMBERS 61102F, 2309, A2 NA
11. CONTROLLING OFFICE NAME AND ADDRESS Defense Advanced Research Projects Agency 1400 Wilson Blvd. Arlington, VA 22209		12. REPORT DATE November 1984
		13. NUMBER OF PAGES 84
14. MONITORING AGENCY NAME & ADDRESS (if different from Controlling Office) Air Force Office of Scientific Research Bolling Air Force Base Washington, DC 20332		15. SECURITY CLASS. (of this report) unclassified
		15a. DECLASSIFICATION/DOWNGRADING SCHEDULE

16. DISTRIBUTION STATEMENT (of this Report)

DISTRIBUTION STATEMENT A
Approved for public release;
Distribution Unlimited

17. DISTRIBUTION STATEMENT (of the abstract entered in Block 20, if different from Report)

DTIC ELECTE AUG 13 1986 S D

18. SUPPLEMENTARY NOTES

19. KEY WORDS (Continue on reverse side if necessary and identify by block number)

Discrimination, signal analysis, elastodynamics, wave propagation

20. ABSTRACT (Continue on reverse side if necessary and identify by block number)

(over)

DTIC FILE COPY

DD FORM 1 JAN 73 1473 EDITION OF 1 NOV 65 IS OBSOLETE

UNCLASSIFIED
SECURITY CLASSIFICATION OF THIS PAGE (When Data Entered)

Research on Deterministic Methods of Seismic Source Identification

Summary of Semi-Annual Technical Report for October 1, 1982 - Sept. 30, 1984

The objectives of the research conducted during the 2 year contract were to: (1) Develop and test methods of discrimination in the regional and teleseismic distance range using physical source parameter discriminants, (2) Pursue theoretical and observational studies of seismic sources; (3) To develop methods of theoretical seismogram synthesis in the near, regional and teleseismic distance ranges for structure and source definition; (4) To develop and apply advanced signal processing/analysis methods for discrimination and explosion yields estimation studies and; (5) to pursue near field studies of explosions and earthquakes for detailed source definition.

In this report we describe specific research results pertaining to: (1) The theoretical basis for automatic seismic signal detection and analysis, and (2) Analytical methods for the representation of seismic radiation fields in uniformly layered elastic/anelastic media. This modal method provides predictions of both body and surface waves in the frequency range from 0 to about 15 HZ at near and regional distances from seismic sources. This latter exposition is intended to be comprehensive and integrates new and old results and methods. The modal representation method for seismic radiation fields is being employed to describe radiation fields for the prediction of earthquake and explosion radiation fields and has been used to evaluate a variety of detection and discrimination methods.

Previous annual and semi-annual reports have described applications of the QHD signal analysis methods and the seismic synthesis methods to source discrimination problems. In particular, these earlier reports have described research results from the observational studies related to discrimination, wherein computer programs employing the theoretical results described here are used to analyze the data and provide the basis of interpretation of the data for regional discrimination and yield estimation.

ARPA Order 4669
Program Code 3D60
Name of Contractor: University of Colorado
Effective Date of Contract: 1 October 1982
Grant Expiration Date: 30 September 1984
Amount: $285,000
Contact No.: F49620-83-C-0009
Principal Investigator: C.B. Archambeau (303) 492-5643
Program Manager: William J. Best (202) 767-5011
Title of Work: Deterministic Methods of Seismic Source Identification

Annual Technical Report

October 1, 1983 - September 30, 1984

Sponsored by
Advanced Research Projects Agency (DOD)
ARPA Order No. 4669
Monitored by AFOSR Under Contract No. F49620-83-C-0009

Table of Contents

Research on Deterministic Methods of Seismic Source Identification

Summary of Semi-Annual Technical Report for October 1, 1982 - Sept. 30, 1984

The objectives of the research conducted during the 2 year contract were to: (1) Develop and test methods of discrimination in the regional and teleseismic distance range using physical source parameter discriminants, (2) Pursue theoretical and observational studies of seismic sources; (3) To develop methods of theoretical seismogram synthesis in the near, regional and teleseismic distance ranges for structure and source definition; (4) To develop and apply advanced signal processing/analysis methods for discrimination and explosion yield estimation studies and; (5) to pursue near field studies of explosions and earthquakes for detailed source definition.

In this report we describe specific research results pertaining to: (1) The theoretical basis for automatic seismic signal detection and analysis, and (2) Analytical methods for the representation of seismic radiation fields in uniformly layered elastic/anelastic media. This modal method provides predictions of both body and surface waves in the frequency range from 0 to about 15 HZ at near and regional distances from seismic sources. This latter exposition is intended to be comprehensive and integrates new and old results and methods. The modal representation method for seismic radiation fields is being employed to describe radiation fields for the prediction of earthquake and explosion radiation fields and has been used to evaluate a variety of detection and discrimination methods.

Previous annual and semi-annual reports have described applications of the QHD signal analysis methods and the seismic synthesis methods to source discrimination problems. In particular, these earlier reports have described research results from the observational studies related to discrimination, wherein computer programs employing the theoretical results described here are used to analyze the data and provide the basis of interpretation of the data for regional discrimination and yield estimation.

Part I - Methods of Seismic Signal Detection and Analysis Based on Quasi-Harmonic Decomposition (QHD)

I. INTRODUCTION

Any time series can, of course, be decomposed into Fourier or harmonic components, and in this case the outcome is that we determine the amplitude and relative phase of each harmonic component occuring within the time window chosen for such a decomposition. We do not, however, know anything about *when* the energy, associated with a particular frequency, may be arriving within this time window. That is, we have no time resolution within the window. If we attempt to sub-divide the time window and perform a Fourier analysis of these subsets of the time series in order to obtain a higher degree of time resolution then, of course, truncation effects begin to severely contaminate the amplitude spectral estimates.

It is, however, well known that information about the time of energy arrival (i.e., the group time) can be retained if one is prepared to accept a certain amount of uncertainty in the frequency value to be associated with the spectral amplitude (or energy magnitude) and phase estimate (e.g., Helstrom, 1960). In particular, simple narrow band filtering of the time series, x(t), at a set of filter center frequencies f_k, can be used to generate an associated set of quasi-harmonic time series, $y(t;f_k)$, having properties such that the spectral amplitudes and phases of pulses making up the original time series can be estimated, along with the *time* at which each pulse spectral component has arrived within the time window. That is, the spectral character and arrival time of each frequency component of the individual "signal" or "noise" pulses, making up the original time series, may be estimated.

The price to be paid for this simultaneous estimate of both frequency content and (energy) arrival time is an uncertainty in the precise time and frequency to be assigned to the spectral components of each pulse or transient making up the original time series. Thus if Δf is the bandwidth of one

particular narrow band filter at its half power point, then the uncertainty in the estimate of the energy arrival time is related to Δf by an "uncertainty principle" in the *form*[+]:

$$\overline{\Delta\omega}\ \overline{\Delta t} \geq \frac{1}{2}$$

where $\overline{\Delta t}$ is the uncertainty (variance) in the estimate of the energy or group arrival time and $\overline{\Delta\omega} \simeq 2\pi\Delta f$. (e.g. If a Gaussian narrow band filter is employed, then the uncertainty product is a minimum, so that $\overline{\Delta\omega}\ \overline{\Delta t} = 1/2$. For all other filters $\overline{\Delta\omega}\ \overline{\Delta t} > 1/2$.)

In the context of this "quasi-harmonic decomposition" of the time series by narrow band filtering, we may think of Fourier decomposition as the limiting case, in which the narrow band filters that are convolved with the time series have zero bandwidth. Thus Fourier decomposition corresponds to the case $\overline{\Delta\omega} = 0$ in (1), and in this limiting case, $\overline{\Delta t}$ becomes unbounded. This simply means that we obtain precise frequency information and no information about energy arrival time, within the time window chosen for analysis.

The possibility of time resolution as well as frequency resolution in analyzing a time series, however, allows "instantaneous" measures of the spectral character of the series, that is measurements of time varying phase and spectral amplitude as well as measurements of derived quantities such as the "instantaneous frequency", corresponding to the time derivative of the time varying phase. These quantities have been discussed extensively in the literature (e.g. Helstrom, 1960) and are meaningful when defined for quasi-harmonic time series. Thus, our objective here is to show how decomposition of a broadband time series into a set of quasi-harmonic time series, by Gaussian narrow

[+] See Denny and Chin (1976), for example, for a more precise definition of the quantities $\overline{\Delta\omega}$ and $\overline{\Delta t}$ appearing in (1).

band filtering, can be optimally accomplished so as to allow appropriately accurate measurements of time varying phase, amplitude and frequency for *each* quasi-harmonic component to be made. We will then show how this derived set of time dependent variables may be used to detect "desired signals", with prescribed physical properties, in the presence of "undesired signals" or "noise". Specifically we will show how a variety of "signal sensitive" filters can be defined to isolate, for example, signals with particualr dispersive properties (dispersion filters), wave number and frequency characteristics (ω–k filters) and polarization or particle motion characteristics (polarization filters). Further, we can use these instantaneous variables to define another class of "filters" designed to separate interfering (time overlapping) signals, with these latter interference detection filters being based on the variance of the instantaneous frequency variable and the splitting (jump discontinuities) in the dispersion characteristics of a multiple pulse signal.

The joint use of all such filters proves to be a very powerful "matched filter" for the isolation or decomposition of complex, multiple pulse, time series. In addition to signal detection however, the decomposition of the time series into quasi-harmonic components and the generation of time varying spectral variables allows the whole time series to be analyzed in considerable detail. In particular signal spectra, with noise corrections, can be obtained along with frequency dependent signal dispersion, polarization and wave number vector direction and magnitude. These are essentially all the signal properties that we need to (or can) know in order to interpret the time series in some physical context. In this regard, we will show how deterministic, as well as probablistic noise corrections, may be applied to isolated signal data, and how this corrected signal data may be used to make physical inferences regarding the origins of the signals. To do this we need to consider a specific kind or type of

time series, in order to not only relate it to its physical origins, but also in order to define the kinds of "signals" to be detected.

Thus, while the general signal analysis methods discussed may be applied to any type of time series regardless of its origins, we will focus on seismic wave generated time series since, aside from being familiar to us, they are particularly interesting in view of their uses (e.g. seismic methods for resource exploration, event identification for underground nuclear event detection, planetary structure investigations, earthquake prediction studies) and since they are particularly rich in structure (a vector wave field, at least two intrinsic wave propagation velocities, and a variety of guided wave possibilities in planetary structures leading to complexities in signal dispersion, polarization and wave number vector direction and magnitude). In the application of QHD methods to the seismic data discussed in this study, we will consider examples of automated signal detection and analysis that relate directly to event identification and earth structure determinations.

Numerous previous studies have addressed the analysis of seismic data using related multiple narrow band filtering techniques. In particular, in an early study, Alexander (1963) used multiple band pass filtering to determine the group velocity dispersion of seismic surface waves, from which elastic velocity structure in the earth was inferred. Archambeau *et al* (1965), Archambeau and Flinn (1965) and Archambeau, Flinn and Lambert (1966) used multiple narrow band filtering to determine the dispersion and spectral properties of both body and surface waves for earth structure and source studies. Dziewonski, Block and Landisman (1969) applied multiple filtering extensively to give seismic surface wave dispersion measurements, and studied the resolution of the method using synthetic seismograms. Dziewonski, Mills and Block (1972) investigated the effect of preprocessing strongly dispersed surface wave signals

with a matched filter in the time domain, followed by narrow-band filtering, and showed that this procedure, which they termed a residual dispersion measurement, was superior to the direct measurement of the total dispersion. Several later studies, for example by Inston, Marshall and Blamay (1971), Cara (1973) and Denny and Chin (1976), have also considered schemes for optimization of the multiple filtering method in order to achieve greater accuracy and resolution in seismic surface wave dispersion measurements.

Most of this work has focused on signal dispersion measurements, most commonly for low mode order seismic surface waves. In the present study we will generate signal dispersion results in a manner similar to that used in these earlier studies, but with an optimization approach that invokes matched filtering, when required, along with filter bandwidth variations with frequency. We will then go a step further and specify dispersion filters whose function is to isolate signals with particular dispersion (or residual dispersion) characteristics. In doing this we will also adjoin to the dispersion filter, other filters, whose function is to simultaneously search for other required signal properties, in particular polarization and wave vector directional properties.

In regard to seismic polarization filters, or particle motion detectors, early work focused on time domain analysis without the explicit use of special multiple narrow band filtering. Examples of such filters are those discussed by Shimshoni and Smith (1964) and Mims and Sax (1965). Flinn (1965) used time domain particle motion measurements to perform both polarization and directional, or wave number vector, filtering. Archambeau and Flinn (1965) defined polarization filters in the spectral domain for seismic body and surface wave detection and analysis. In later work, Archambeau, Flinn and Lambert (1969) applied these polarization filters as a means of isolating multiple body wave arrivals for study of the earth's upper mantle structure. Body wave isolation

and enhancement, with suppression of surface wave noise by polarization techniques, has been subsequently used by a number of investigators, for example by Montalbetti and Kanasewich (1970), who used an extension of the time domain approach described by Flinn (1965); and by Lewis and Meyer (1968), who employed the frequency domain approach. On the other hand, Simons (1968) applied frequency domain polarization filtering, using a moving window FFT, to detect and enhance seismic surface waves. (These earlier polarization filtering methods, and their applications, are summarized in more detail by Kanasewich (1975).) Further, both Flinn (1965) and Simons (1968) considered directionality filters using the amplitude of the ground motion recorded on the three spatial components defining the vector wave field at a single three component seismic station. This filtering amounts to "vector wave number filtering" at a single point, since the wave number vector describes the normal direction to the wave front and, for a prescribed wave type, the recorded components of ground motion can be used to determine the orientation of this vector. Thus, only certain desired wave number vector orientations are accepted by such a directionality filter.

In the present study we will combine polarization filtering with wave number vector filtering. Polarization filters can be defined in terms of the instantaneous phase variable generated by quasi-harmonic decomposition (QHD) of the individual vector components of a seismic wave. In this case the phase difference between two spatial components of the wave field serves to define the polarization. Thus we can obtain a frequency dependent, time-varying measure of the polarization of the seismic wave signals and noise making up the time series. Similarily, we can define vector wave number directions in terms of the time varying amplitude components, taken at the group arrival times; where we obtain the spectral information at the group arrival times and

define directionality that is both frequency and time dependent. Compared to previous time domain methods, this approach has the advantage of defining a polarization filter, and wave number vector filter, for each filter center frequency, so that frequency dependent polarization and directionality filtering can be performed. In addition, greater time resolution can be achieved by the QHD method than is possible by the previously used spectral methods, and truncation effects arising from moving spectral windows, are entirely avoided. Further, we can combine dispersion measurements with polarization and directionality measurements in one single operation, with the QHD procedure generating all the required information. Then optimization of the filter design for any one of the measurements, for example for accuracy in signal dispersion measurements, ensures that the filter design is also optimal for all the other measurements, such as for time varying amplitude, phase, polarization, etc. Most important, however, is the fact that we may associate a set of signals (or noise) related variables, such as spectral amplitude, phase, polarization and instantaneous frequency, with each measured group arrival time, which itself corresponds to the time at which seismic wave energy, at (or near) the filter center frequency, arrives at the sensor. This generation of time connected functions of frequency, which may be associated one to one with signal (or noise) pulses in the time series, provides us with the opportunity of performing a series of *joint* filtering operations. These filtering operations are both time varying and frequency dependent in general, and may be linear or non-linear, but are, in any case, used to extract desired signals along with estimates of their spectral properties. In the next section we will consider the appropriate seismic signal definitions so as to establish a physical context in which these filtering operations can be defined, implemented, and applied.

II. SEISMIC SIGNAL DEFINITIONS

In the previous discussion we indicated that "joint filtering" operations are to be considered. What is meant is that a number of criteria, based on known physical characteristics of the various types of seismic signals, will be used together, to detect, or search for, signals of a desired type. This is a matched filter concept with signals detected on the basis of correlations with specified signal properties. However, our application of the matched filtering approach will be quite different than the usual linear filtering method, which involves generation of what amounts to a cross-correlation of the specified signal wave form with a time series, and selection of correlation peaks above a threshold as signal detections. Instead, we will define only general "robust" characteristics of the signal types of interest, rather than attempt to specify details of wave forms or spectra, and then use quasi-harmonic decomposition methods to (continuously) monitor the time series for the signal characteristics of interest. Detections of "desired signals" would then be obtained at those time intervals during which the time series exhibited all (or most of) the characteristics of the specified signal type. Obviously how closely and in what sense the time series is to match the discrete set of specific signal properties must also be precisely defined -- and this will be considered in detail in a later section. At this point our task is to specify signal definitions, and then to devise the filter analysis proceedures which will provide data for detections. Once a desired signal form is detected, the filter output data can also provide details of the signal spectra, timing and so on.

The signal characteristis that will be used as criteria for detection and isolation of seismic signals are those invariant properties that are usually used to define the various seismic body and surface wave types. Specifically we have;

(A) Seismic body wave pulses characterized by:

(1) *Minimal dispersion;* such that each frequency component of the signal pulse has nearly the same group and phase velocity.

(2) *Linear polarization;* with compressional body waves (P waves) having particle motion in the direction of the wave number vector and normal to the wave front; and with shear waves (SV and SH) having particle motion in directions perpendicular to the wave number vector, in the plane tangent to the wave front.

(3) *Pulse-like amplitude spectrum;* where the amplitude spectrum has broad band width and is a slowly varying function of frequency.

(4) *Minimal variation in wave number orientation;* with nearly constant direction (azimuth and emergence angles) of the wave number vector as a function of frequency.

(5) *Near vertical wave vector directions;* so that the apparent emergence angle is relatively low and the apparent phase velocity is large.

(B) Seismic surface waves, characterized by:

(1) *Strong dispersion;* such that the group velocity generally increases with decreasing frequency, due to the generally increasing elastic velocities with depth in the earth.

(2) *Elliptical polarization (Rayleigh type surface waves) or transverse linear polarization (Love type surface waves);* with fundamental mode Rayleigh waves usually being retrograde elliptically polarized,[+] so that the particle motion is in elliptical orbits, with the onset of motion along the wave number axis in the opposite direction from the wave number vector. Higher mode Rayleigh waves may be either retrograde or prograde elliptically polarized, the latter with elliptical particle motion initiating in the same direction as the wave number vector.

For all Rayleigh modes, the eccentricity of the particle orbits -- or the ellipticity of the polarization -- are functions of frequency, having a variation which is similar in form to that for the wave group velocity.

(3) *Peaked amplitude spectrum:* so that the time domain signal associated with a particular surface wave mode is usually well dispersed and extended in time, with at least several cycles of

[+]Fundamental mode Rayleigh waves can, in certain structures, within particular frequency bands, also be prograde elliptically polarized.

motion present. Thus surface waves typically tend to be narrower in band width than body waves and appear to "ring" in the time domain.

(4) *Moderate variation in wave number azimuth orientation with frequency;* with higher modes showing more variability than fundamental mode surface waves, these variations being principally associated with lateral variations in the near surface velocity structure within the earth.

(5) *Horizontal wave number vector directions;* so that phase velocities are low compared to those for body waves.

These characteristics are the major fixed properties of seismic "phases" and so are the most important criteria for phase detection and identification. The signal properties are, out of necessity, rather broadly defined but, as we will show, they are sufficient to provide the basis for automated detection/identification of signals in a high noise background. Specifically, the approach is to specify, as precisely as possible, what type of signal is to be detected in terms of wave type (body wave; Rayleigh wave, etc.) and the distance and azimuth range for the originating event, so that signals with the appropriate dispersion, polarization, wave number vector orientation and spectral properties can be isolated. The first filtering process to be applied is simply one designed to continuously generate, as functions of time, the required frequency dependent dispersion, polarization, apparent wave vector and spectral information; with the detection operation then being a selection process, wherein one picks out the signals having desired properties. It is our purpose to make this selection process an objective, computer controlled, operation. Naturally the details of this process can be quite involved and will depend, at least in part, on the nature of the noise background. It is therefore necessary to also consider the character of the expected noise, or undesired signal, in order to effectively design signal isolation procedures.

III. NOISE DEFINITIONS: SEISMIC

In most applications it is desirable to be able to detect and isolate particular types of signals from seismic sources within certain prescribed distance ranges and azimuth sectors. For example, it is often most important to be able to detect compessional (P) waves from sources at teleseismic distances, occuring within some azimuth sector, and to reject signals from nearby microearthquakes as well as teleseismic signals from events outside the azimuth sector of interest. Further, it is important to be able to reject all background seismic noise due to more or less randomly distributed sources, such as are associated with atmospheric pressure fluctuations, ocean surf, and cultural effects. Clearly undesired signals from isolated seismic sources outside the distance and/or azimuth range of interest may only differ from the signals of interest in wave number vector orientation, or, if near the receiver, in high frequency content. On the other hand, characeristics of the background seismic noise, while obviously having wave characteristics that are similar to those previously enumerated for "signals", do have details of spectral and modal structure that are quite distinctive. These properties provide the basis for filtering operations which can distinguish between most signals of interest and background noise.

The noise characteristics can be described as follows:

(1) *General spectral properties and modal composition:* The average background noise spectrum, obtained from long time noise samples, is strongly peaked in the period range from 6 to 8 seconds, with a secondary peak of much lower level near 0.3 seconds. Other secondary low level maxima may occur at very long periods, but roughly speaking, the noise at lower frequencies decreases from the peak at 6 - 8 seconds, rapidly at first, then much more slowly. At high frequencies, $f > 10$ Hz, the noise is mostly wind generated and originates locally, with very high levels possible. Essentially all the low frequency noise, including that associated with the sharp spectral peaks at 6 - 8 seconds corresponds to fundamental mode Rayleigh type surface waves, with minor contributions from higher modes and from Love type surface waves. The noise peak near 0.3 seconds corresponds mainly to higher mode Rayleigh waves, with most of the noise peaks being composed of a superposition of many higher modes and

therefore having body wave-like characteristics. Thus at these higher frequencies, and particularly near the 0.3 sec. spectral peak, the noise is predominantly higher mode Rayleigh type surface waves, with some body waves contributing as well.

(2) *Spatial and temporal variability in noise spectral levels, invarience of mode composition:* The overall level of the noise spectrum is dependent on proximity to noise sources, such as ocean boundaries, and is also quite variable with time. However, the modal compostion of the noise is effectively constant, even though the overall mode excitation level may be quite variable. (This implies that all the surface wave modes, fundamental and higher, are excited by a typical noise source and that most of the fundamental mode excitation is at 6 to 8 sec. and most higher mode excitiation is near 0.3 sec.)

(3) *Pulse-like time domain composition of high frequency background noise:* Analysis of the detailed time domain structure of the background noise, for example by narrow band filtering, indicates that, especially in the intermediate to high frequency range, the noise can be described as a superposition of discrete noise "pulses" consisting of a few cycles of motion. In view of the normally random space-time distribution of sources, a noise time series is therefore composed of a random time sequence of "bursts" or pulses, with each pulse having a mode characteristic of the type previously described. Each pulse is therefore actually a coherent signal propagating as a surface wave or occasionally as a body wave.

The essential differences, between the noise and the signals we wish to detect, are that the body wave signals will be undispersed, linearly polarized pulses with wave number vectors that are oriented within a narrow spatial "cone" and with associated high values of apparent phase velocity. On the other hand, surface wave noise has, for the most part, moderate to strong dispersion, is elliptically polarized, has narrow band width compared to the signals, and has relatively low apparent phase velocity. Thus filtering, designed to exploit the differences in dispersion, polarization, frequency content and wave number characteristics, will be effective in isolating body wave signals. Further, that part of the noise field having body wave characteristics will have random wave number vector orientations and can be eliminated, in part, by wave number filtering.

On the other hand, surface wave signals of interest are typically of broader

band width than the surface wave noise, which is strongly peaked in the 6 - 8 sec. period range, and so ordinary frequency filtering can be used to reduce the surface wave noise without appreciable loss of signal power. The noise also has random wave number vector orientation characteristics, and both vector wave number filters and matched filters can, therefore, be used to select surface wave signals from particular spatial directions.

IV. ANALYTICAL REPRESENTATIONS FOR SEISMIC SIGNALS AND NOISE

The signals and the time series we are dealing with are associated with vector wave fields and so are themselves vector quantities. We will, in general, deal with one spatial component of the field at a time and will suppress component indices when the treatment applies equally to all signal components. We will only be explicit as to vector components when it is necesary to combine them, as is the case, for example, when defining single receiver polarization or wave number filters.

Modal Representation of Pulse-Like Signals and Noise

Any component of an observed seismic displacement time series, x(t), can be expressed as sum of "signals", in the form

$$x(t) = \sum_n S_n(t) = \sum_n \mathrm{Re} \int_{-\infty}^{+\infty} \mathfrak{S}_n(\omega) e^{i\omega t} df \qquad (1)$$

where Re denotes the real part of the Fourier integral. Here, since x(t) and $S_n(t)$ are real, then with the Fourier transform of $S_n(t)$ denoted by $\mathfrak{S}_n(\omega)$, we have $\mathfrak{S}_n(-\omega) = \mathfrak{S}_n^*(\omega)$, where $\mathfrak{S}_n^*$ is the complex conjugate of $\mathfrak{S}_n$. Similarily, $\tilde{x}(-\omega), = \tilde{x}^*(\omega)$, where $\tilde{x}(\omega)$ is the Fourier transform of x(t).

The sum in (1) is over "signals" $S_n(t)$ which may, in fact, be noise pulses

depending on how we choose to define what we call a signal. At this point we can simply call an energy pulse in the time series a signal of some sort. This is consistent with our previous descriptions of seismic signals and noise, where both were described as having specific wave type properties. We can, as we will demonstrate below, represent each "pulse" $S_n(t)$ as a superposition of modes, whether it is noise or signal and whether it corresponds to a body or surface wave. If S_n happens to correspond to a body wave, then its representation is a superposition of many higher modes. If it is a surface wave, then, of course, it is represented by just one mode. In any case the "signals" all have the general form of propagating vector fields and, in the mode representation form, are given in the frequency domain by:

$$\tilde{S}_n(\omega) = \sum_m A_n^m(r,\omega) \exp\left\{ -i \left[K_n^m r + \varphi_n^m(\omega) \right] \right\} \qquad (2)$$

where the sum over m is a sum over modes and r is the earth's radial coordinate. Here K_n^m is the complex wave number for the m^{th} mode of the n^{th} signal. The phase φ_n^m can be called the initial phase for the m^{th} mode term of the n^{th} signal, and is associated with the phase delay at the source. The function A_n^m is source and medium dependent, but because of its strong dependence on the source of the signal, will be called a mode excitation function. The mode excitation function for the n^{th} signal, A_n^m, may of course be zero (or negligible) for all except one mode index value, so that the (infinite) sum over m can be degenerate. For body waves this is not the case however and, for a given body wave signal, many of the A_n^m functions will be of comparable magnitude.

The detailed nature of body wave modal structure is illustrated by the mode curves of Figure (1) and (2), from Harvey (1980). Seismograms generated from the excitation of these modes by a theoretical earthquake source are shown in Figure (3).

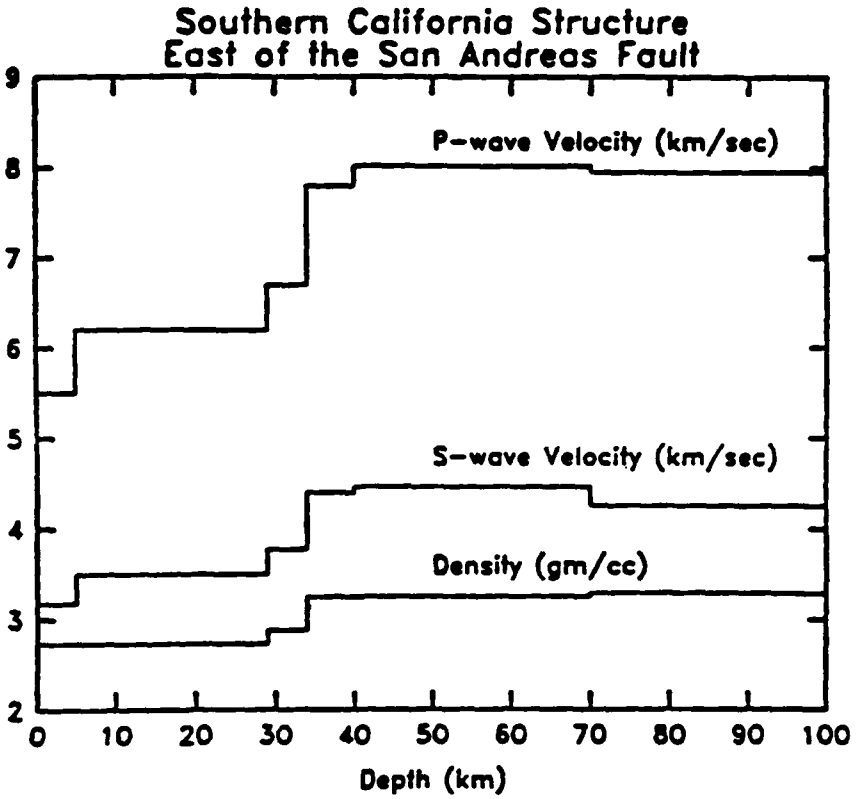

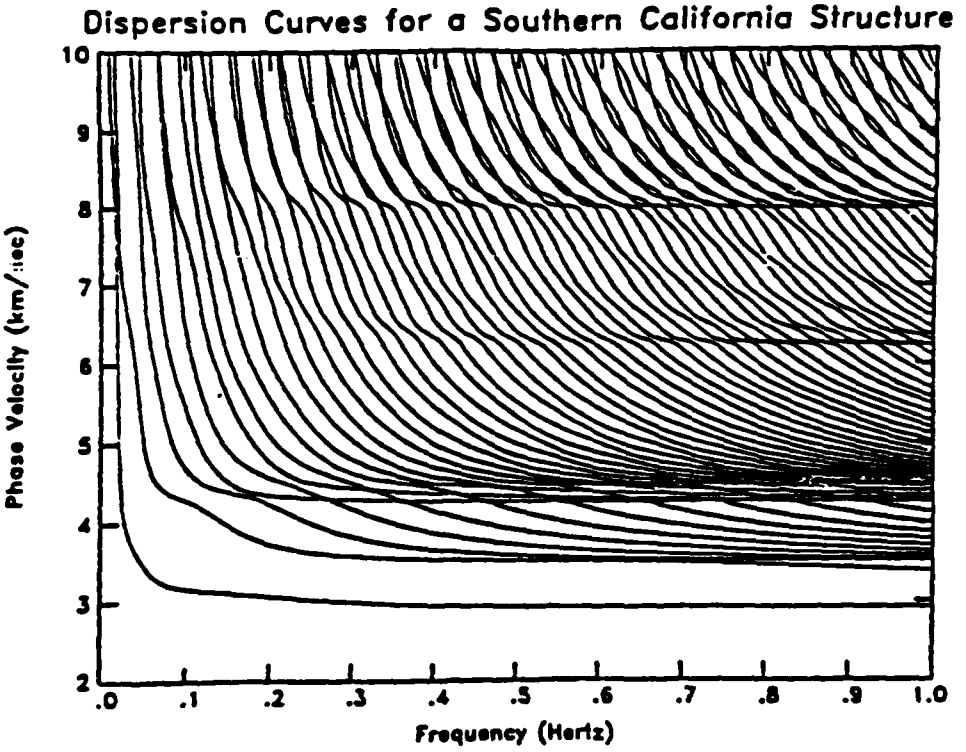

Figure 1. A section of the modal phase velocity versus frequency curves for the velocity-density structure in the Southern California region, just east of the San Andreas fault zone and south of Los Angeles (structure after Kanamori and Hadley, 1978). The prominent flattening of the higher mode curves near 4.6 km/sec, again in the range around 6.2 to 6.5 km/sec and near 8.0 km/sec produce, respectively, S, P_g and P_n body wave arrivals when the modes are summed, as shown in Figure 3.

Numerous body wave pulses are generated by the superposition of these modes, but each seismic body phase is associated with a large number of higher modes all having a flat segment in their phase velocity dispersion curves at nearly the same phase velocity value. This is illustrated in Figure 1 by the flat dispersion in the modes near the phase velocity of 8 km/sec. (This corresponds to P_n, the crust-mantle boundary refracted wave which is the first arrival on the theoretical seismogram shown in Figure 3.) When the phase velocity is constant, as it is on the flat parts of the dispersion curves in Figure 1, then the phase and group (energy) velocities are equal, and both constant. Figure 2 shows the more complex group velocity curves, where their constant group velocity near 8 km/sec. is, nevertheless, also evident. Thus, for the superposed modes, the flat sections of the phase velocity curves will contribute, in sum, to a pulse like seismic phase, with all frequency components arriving at nearly the same time (ie., with nearly constant group velocity). Because mode excitation at a given frequency is inversely proportional to the derivative of the group velocity with respect to frequency, then when the group velocity is nearly constant, as it is along the flat parts of the dispersion curves, its derivative is small and the excitation of the mode will be high. Since there are many modes with the same locally constant group and phase velocities, then not only will they all sum to give an undispersed pulse, but each mode will have relatively larger excitation in this (narrow) group velocity range than it does at either higher or lower values of group velocity, where the dispersion curves are steep. Thus, one can expect a well defined pulse, with larger amplitude than that of the more dispersed energy arriving just before and after it in time.

This description constitutes a modal representation of a classical body wave. In the other extreme, the theoretical seismograms in Figure (3) show late arriving energy corresponding to the single fundamental mode Rayleigh wave,

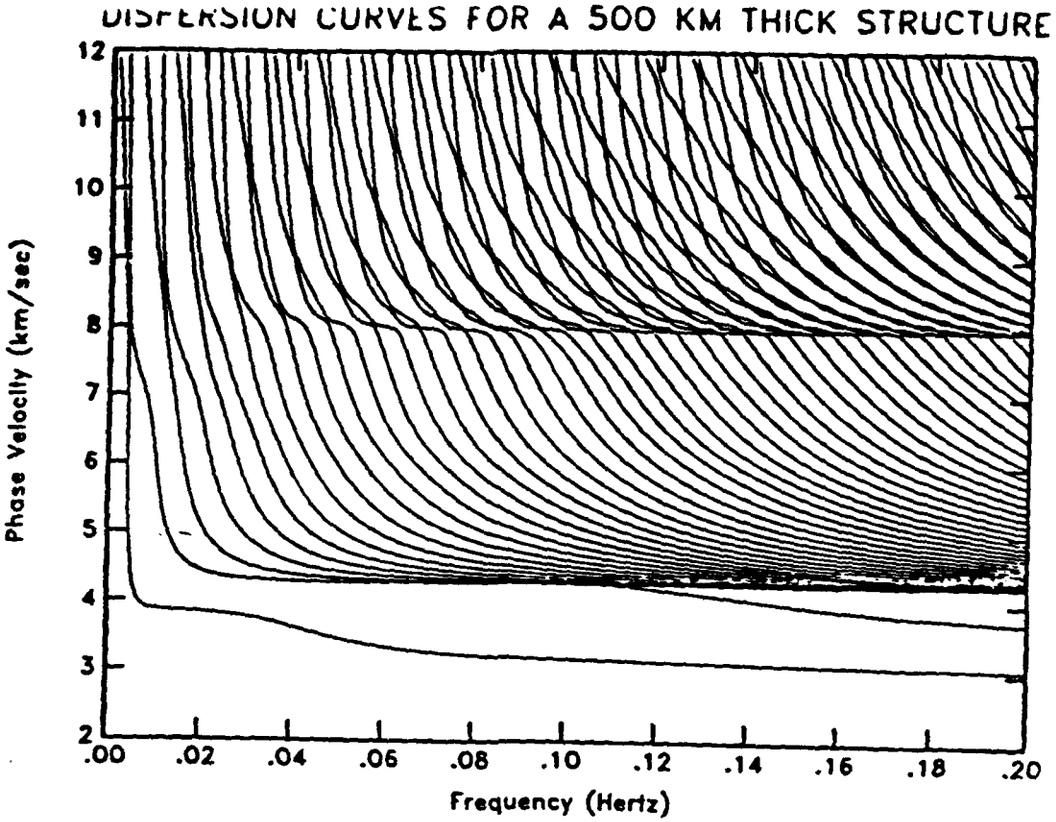

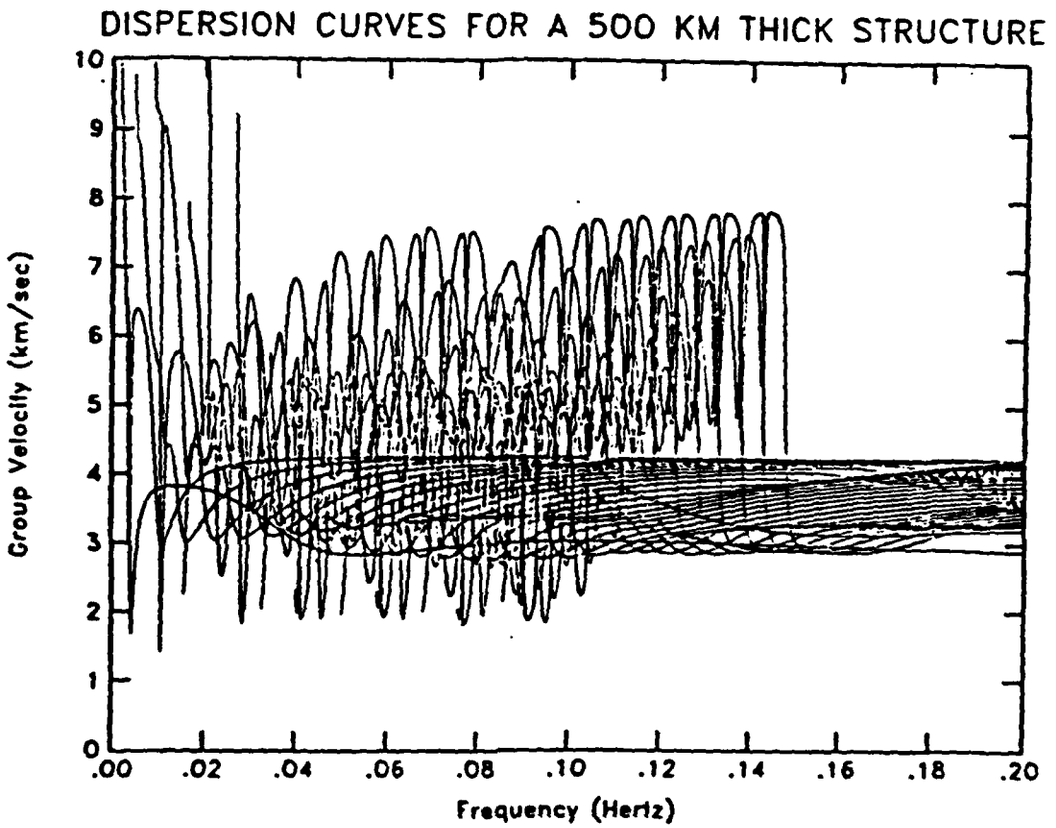

Figure 2. Low frequency sections of the phase and group velocity curves as functions of frequency. Only group velocity dispersion curves for the fundamental and first few higher modes are shown, due to the complexity of these functions in the velocity-frequency plane. Maxima and minima along the modal group velocity curves give rise to "Airy phases", where the mode excitation is relatively much larger than at other points on the curves, where the slope is larger.

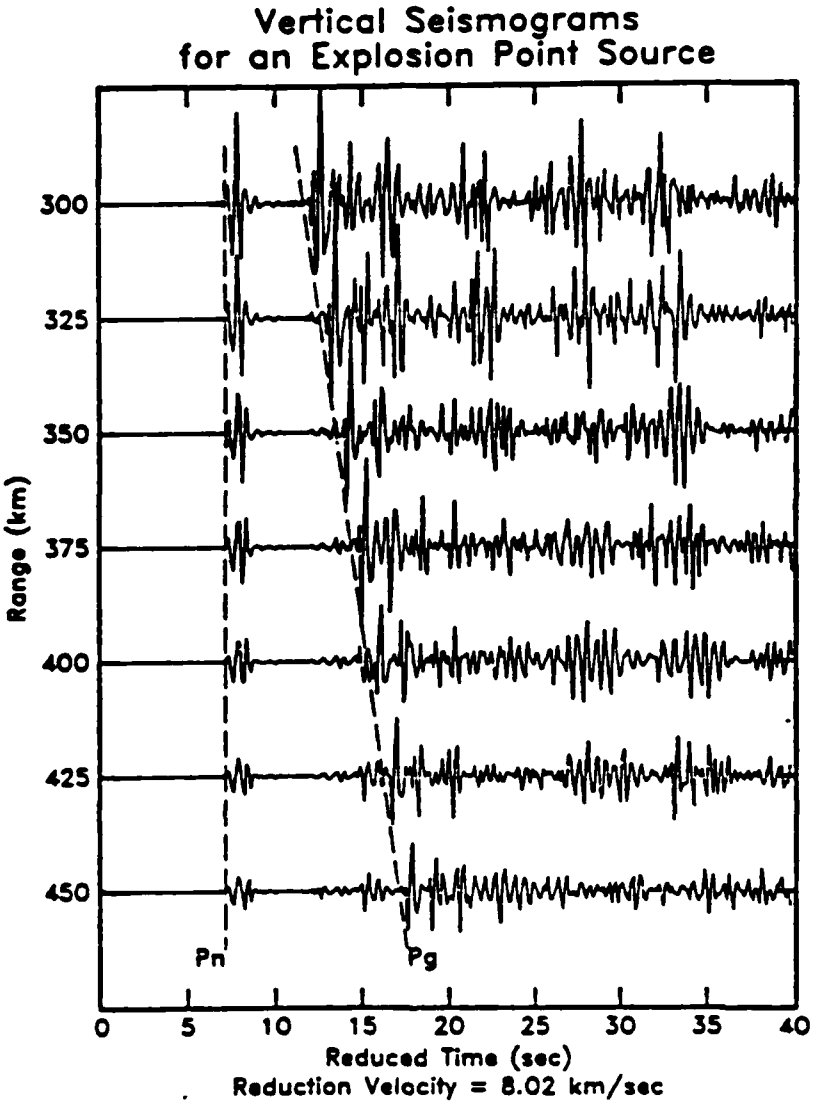

Figure 3. Early time section of the synthetic seismograms generated by mode superposition for the Southern California structure shown in Figure 1. The lines are theoretical travel times for the "body wave" phases P_n and P_g, based on simple ray theory. The complex P_g wave train results from many higher mode contributions in the phase velocity range around 6.2 to 6.5 km/sec, where the mode curves show low slopes and flattening as functions of frequency as illustrated in Figure 1. The sharp, time compressed, pulse results from the superposition of the large number of modes with very pronounced flattening in a narrow range near 8.0 km/sec.

so that for the representation of this signal, only a single mode is involved.

Much of the seismic energy propagation must, however, be described as intermediate between a classical body wave, composed of a very large number of higher modes with near constant phase and group velocities, and ordinary fundamental mode surface waves. An example of this is the P_g wave energy, arriving in the group velocity range from around 6.2 to 5.0 km/sec in the synthetic seismograms shown in Figure 3. The origins of this large amplitude, time distributed arrival are higher mode contributions, associated with the relatively slight mode curve flattening in the phase velocity range from about 7 to 9 km/sec. In this case there is no extremely well defined coincidence of flat sections in the mode curves at a constant phase and group velocity (giving a well defined body wave that can be approximated by a ray) but instead one finds a less pronounced flattening which occurs over a range of phase and group velocities. In this case the engergy transmission cannot be viewed very simply in terms of rays, as are classical body phases, but must be viewed as either a large number of higher modes, contributing over a group and phase velocity *range* or as a large number of rays with steep angles of incidence (high phase velocities) representing multiple reflections and refractions distributed in arrival time over a relatively long time interval.

Mode Groups as Isolated Signals

A modal description is a formal analytical representation that will be used here to provide a mathematically complete representation of the entire seismic wave field. We will, when appropriate however, make use of the special features of the modal superposition when dealing with body wave signals. Now, for such a representation, we can combine (1) and (2) to obtain:

$$x(t) = \sum_{n,m} \mathrm{Re} \int_{-\infty}^{+\infty} A_n^m(\mathbf{r},\omega)\exp\left\{-i\left[K_n^m r - \omega t + \varphi_n^m(\omega)\right]\right\} d\omega \qquad (3)$$

or

$$x(t) = \sum_{n,m} \mathrm{Re} \int_{-\infty}^{+\infty} D_n^m(\mathbf{r},\omega)\, e^{i\omega t} d\omega \qquad (4)$$

with

$$D_n^m(\mathbf{r},\omega) \equiv A_n^m(\mathbf{r},\omega)\exp\left\{-i\left[K_n^m r + \varphi_n^m(\omega)\right]\right\} = A_n^m(\mathbf{r},\omega)\, e^{-i\Psi_n^m(\mathbf{r},\omega)} \qquad (5\text{-a})$$

where Ψ_n^m is the phase factor for D_n^m. Thus, from previous definitions, every "signal" $S_n(t)$ is represented by a sum of modal contributions D_n^m such that

$$\tilde{S}_n(\mathbf{r},\omega) = \sum_m D_n^m(\mathbf{r},\omega) \qquad (5\text{-b})$$

Here, as elsewhere, m is restricted to a set of integers (l_n) appropriate to the n^{th} signal. Precisely how we chose to define the signals $S_n(t)$ will determine which modes, and which phase or group velocity segments of the modes, contribute to a given signal.

The wave number K_n^m is conveniently represented in terms of a phase velocity C_n^m for the $m^{\underline{th}}$ mode of the $n^{\underline{th}}$ signal, so that

$$K_n^m(\omega) = \omega / C_n^m(\omega) \qquad (6)$$

In this representation of an observed seismic time series we will use a relation like (3) to describe the entire time series and to represent a superposition of "signals" from many sources, including sources which produce "signals" that are not of interest, as well as signals from some particular source which are of interest. Thus (3), and equivalent mode sums, represent a multiple source superposition, with the sum over n representing a sum over different source signals as well as a sum over different signals from the same source. In this case only a few signals from the series are important, while all other terms in the

sum over n are viewed as noise relative to the signals to be isolated. Our objective is to devise systematic methods that may be used to pick out of this series those terms that satisfy prescribed conditions, such as those for body waves of a particular type from a source in a particular distance-azimuth range.

V. GAUSSIAN NARROW BAND FILTERING OF SEISMIC TIME SERIES

The essential tool to be used to isolate desired signals from the seismic time series will be the quasi-harmonic decomposition of the time series. This decomposition provides time varying spectral information such that particular characteristics of the sought for signals can be measured and used to automatically select, or filter out, the appropriate signals.

Narrow Band Filter Combs

In order to decompose the time series we will use a "comb", or set, of ultra narrow band Gaussian filters, with center frequencies f_k, k=1,2,....,N. The transfer function of a Gaussian filter is defined to be:

$$G_k(\omega;\alpha) = \sqrt{\frac{\alpha}{\pi}}\, e^{-\alpha(\omega-\omega_k)^2} \tag{7}$$

where $\omega_k = 2\pi f_k$ is the angular center frequency of the filter, and α is a parameter determining the bandwidth of the filter. The impulse response of the filter is given by

$$g_k(t) = F^{-1}[G_k;t] = \frac{1}{2\pi}\int_{-\infty}^{+\infty}\left[\sqrt{\frac{\alpha}{\pi}}\, e^{-\alpha(\omega-\omega_k)^2}\right] e^{i\omega t}\, d\omega$$

where F^{-1} denotes the inverse Fourier Transform operator. We therefore have, after evaluating the integral:

$$g_k(t) = \left(\frac{1}{2\pi}\right) e^{-t^2/4\alpha + i\omega_k t} \tag{8}$$

as the impulse response. Hence this is a simple sinusoid modulated by an

exponential function of time, in both time directions from t = 0. Thus this filter is phaseless and when applied to filter a signal, it will introduce no phase shift and will "ring" in both the positive and negative time directions. Clearly this modulation can be controlled by the choice of α. (Although not explicitly indicated, α can be chosed to be a function of ω_k for the set of filters (G_k).)

A useful means of specifying the filter bandwidth is by use of the filter quality factor, or Q, which is defined to be the ratio $f_k / \Delta f_k$, with Δf_k equal to half the bandwidth at the half power point of the filter. To express the parameters α in terms of the filter Q, we observe first that the power at $\omega = \omega_k$ is given by:

$$\left|G_k\right|^2 = \left[\frac{\alpha}{\pi}\right], \text{ at } \omega = \omega_k,$$

so that the half power points, at $\omega = \omega_k \pm \Delta\omega_k$, are such that

$$\left|G_k(\omega_k \pm \Delta\omega_k;\alpha)\right|^2 = \left[\frac{\alpha}{2\pi}\right]$$

Evaluating explicitly the expression for G_k, at $\omega = \omega_k \pm \Delta\omega_k$, gives the condition that:

$$e^{-2\alpha(\Delta\omega_k)^2} = 1/2$$

In terms of the half bandwidth $\Delta\omega_k$, we have for α:

$$\alpha = \left[\frac{\ln 2}{2}\right]\left[\frac{1}{\Delta\omega_k}\right]^2 \tag{9-a}$$

Using the definition for the filter Q, then:

$$\alpha = \left[\frac{\ln 2}{2}\right]\left[\frac{Q_k}{\omega_k}\right]^2 \tag{9-b}$$

Thus the set of Gaussian filters have the form

$$G_k(\omega) = \frac{1}{\Delta\omega_k}\sqrt{\frac{\beta}{\pi}}\exp\left[-\beta\left[\frac{\omega-\omega_k}{\Delta\omega_k}\right]^2\right] \tag{10-a}$$

or

$$G_k(\omega) = \sqrt{\frac{\beta}{\pi}}\left[\frac{Q_k}{\omega_k}\right]\exp\left[-\beta Q_k^2\left[\frac{\omega-\omega_k}{\omega_k}\right]^2\right] \tag{10-b}$$

where

$$\beta \equiv \frac{\ln 2}{2} \text{ and } Q_k^{-1} \equiv \frac{\Delta\omega_k}{\omega_k} = \frac{\Delta f_k}{f_k}$$

Analytical Forms of Gaussian Filter Responses

for Isolated Signals

If we apply any one of the Gaussian filters to a signal $S_n(t)$, then the output of the filter can be denoted as $\bar{S}_n(t;\omega_k)$, and is given by the inverse Fourier transform of the product of the signal transform with the filter transfer function, that is:

$$\bar{S}_n(t;\omega_k) = \frac{1}{2\pi} \mathrm{Re} \int_{-\infty}^{+\infty} \tilde{S}_n(\omega)\, G_k(\omega-\omega_k;Q_k) e^{i\omega t} d\omega$$

Here we have written out the functional dependence of the filter on the difference $\omega - \omega_k$, and on the parameter Q_k, explicitly. In order to evaluate this integral we introduce a change of variable such that

$$\omega' = \omega - \omega_k$$

so we get

$$\bar{S}_n(t;\omega_k) = \mathrm{Re}\left[\frac{e^{i\omega_k t}}{2\pi} \int_{-\infty}^{+\infty} \tilde{S}_n(\omega'+\omega_k)\, G_k(\omega';Q_k)\, e^{i\omega' t} d\omega'\right] \qquad (11)$$

and then consider the expansion of the signal spectrum $\tilde{S}_n(\omega)$ about the frequency $\omega = \omega_k$, that is about the point $\omega' = 0$.

We observe that we have from (5):

$$\tilde{S}_n(\omega) = \sum_m A_n^m(\mathbf{r},\omega) e^{-i\Psi_n^m(\mathbf{r},\omega)}$$

with the sum running over the modes. Thus, for any signal S_n we can expand A_n^m and Ψ_n^m individually about $\omega = \omega_k$, and obtain:

$$A_n^m(\mathbf{r},\omega'+\omega_k) = \sum_{l=0}^{\infty} \frac{1}{l!} \left[\frac{d^l}{d\omega^l} A_n^m(\mathbf{r},\omega)\right]_{\omega_k} (\omega')^l$$

(12)

$$\Psi_n^m(\tau,\omega'+\omega_k) = \sum_{l=0}^{\infty} \frac{1}{l!} \left[\frac{d^l}{d\omega^l} \Psi_n^m(\tau,\omega) \right]_{\omega_k} (\omega')^l$$

We will see that if the bandwidth of the filters is narrow enough, then only small values of ω' contribute to $\bar{S}_n(t,\omega_k)$, and the expansion for $\bar{S}_n$, resulting from the expansions in (12), will converge rapidly.

In order to simplify the notation somewhat, we note that the mode sum over m commutes with the integral over ω' in (11.). Thus the filter, in effect, acts on each mode independently and the total output is just the sum of the individually filtered modes. For this reason we will temporarily suppress the mode index m and the mode sum, since the manipulations and integral evaluation are independent of which mode is being considered. In this case we can, for example, write

$$\Psi_n^{(l)}(\tau,\omega_k) \equiv \left[\frac{d^l}{d\omega^l} \Psi_n^m(\tau,\omega) \right]_{\omega_k}$$

as a notational convenience in the second expansion in (12.)

We observe from (5.) that (with the index m suppressed):

$$\Psi_n(\tau,\omega_k) \equiv K_n \tau + \varphi_n(\omega)$$

Therefore,

$$\Psi_n^{(l)}(\tau,\omega_k) = \left[\frac{d^l K_n}{d\omega^l} \right]_{\omega_k} \tau + \left[\frac{d^l \varphi_n}{d\omega^l} \right]_{\omega_k}$$

Since the group velocity $U_n(\omega)$ is given by

$$U_n = \frac{d\omega}{dK_n} \tag{13}$$

then

$$\Psi_n^{(l)}(\tau,\omega_k) = \frac{d^{l-1}}{d\omega^{l-1}} \left[\frac{1}{U_n} \right]_{\omega_k} + \varphi_n^{(l)}(\omega_k) \quad ; l \geq 1 \tag{14}$$

$$\psi_n^{(0)}(r,\omega_k) = K_n(\omega_k) + \varphi_n(\omega_k) = \frac{\omega_k}{C_n(\omega_k)} + \varphi_n(\omega_k)$$

where $C_n(\omega_k)$ is the phase velocity evaluated at $\omega=\omega_k$.

Introducing group and phase delay times, t_g and t_p, defined by

$$t_g^{(n)}(\omega_k) = \frac{r}{U_n(\omega_k)} + \varphi_n^{(1)}(\omega_k)$$

$$t_p^{(n)}(\omega_k) = \frac{r}{C_n(\omega_k)} + \frac{\varphi_n(\omega_k)}{\omega_k} \qquad (15)$$

for the $n^{\underline{th}}$ signal (with the mode index again suppressed) and then using the expansions of (12) in the integral relation (11) for the filter output $\bar{S}_n(t;\omega_k)$, gives:

$$\bar{S}_n(t;\omega_k) = \mathrm{Re}\left\{ \frac{1}{\Delta\omega_k}\sqrt{\frac{\rho}{\pi}}\,\frac{e^{i\omega_k(t-t_p^{(n)})}}{2\pi} \right.$$

$$\left. \cdot \sum_{l=0}^{\infty} \frac{1}{l!} A_n^{(l)}(r,\omega_k) \int_{-\infty}^{+\infty} (\omega')^l\, e^{i\omega'(t-t_g^{(n)}) - iP(\omega')} \right.$$

$$\left. \exp\left[-\beta\left(\frac{\omega'}{\Delta\omega_k}\right)^2\right] d\omega' \right\} \qquad (16)$$

where

$$P(\omega') = \sum_{P=2}^{\infty} \frac{1}{P!}\left[\frac{d^{P-1}}{d\omega^{P-1}}\, t_g^{(n)}(\omega)\right]_{\omega_k} \omega'^P$$

To evaluate the integrals in this expansion for $\bar{S}_n$ we can express the factor $\exp\{-iP(\omega)\}$ in a power series in ω and use the integral relation:

$$\int_{-\infty}^{+\infty} (i\omega)^m\, e^{-\sigma\omega^2}\, e^{i\omega t}\, d\omega = \sqrt{\frac{\pi}{\sigma}}\,\frac{\partial^m}{\partial t^m}\left[e^{-t^2/4\sigma}\right];\ \mathrm{Re}(\sigma) > 0$$

to give (16) in series form.

The exponential expansion required has the form:

$$E(\omega) \equiv \exp[-iP(\omega)] = 1 + \sum_{m=2}^{\infty} e_m \omega^m$$

where the first few coefficients e_m are:

$$e_2 = -\frac{i}{2}\left[\frac{dt_g^{(n)}}{d\omega}\right]_{\omega_k} \; ; \; e_3 = -\frac{i}{6}\left[\frac{d^2t_g^{(n)}}{d\omega^2}\right]_{\omega_k}$$

$$e_4 = -\frac{1}{24}\left[3\left[\frac{dt_g^{(n)}}{d\omega}\right]^2_{\omega_k} + i\left[\frac{d^3t_g^{(n)}}{d\omega^3}\right]_{\omega_k}\right]$$

$$e_5 = -\frac{i}{12}\left\{\left[\frac{dt_g^{(n)}}{d\omega}\right]_{\omega_k}\left[\frac{d^2t_g^{(n)}}{d\omega^2}\right]_{\omega_k} + \frac{i}{10}\left[\frac{d^4t_g^{(n)}}{d\omega^4}\right]_{\omega_k}\right\}$$

$$e_6 = -\frac{1}{48}\left\{\left[\frac{dt_g^{(n)}}{d\omega}\right]_{\omega_k}\left[\frac{d^3t_g^{(n)}}{d\omega^3}\right]_{\omega_k} + \frac{2}{3}\left[\frac{d^2t_g^{(n)}}{d\omega^2}\right]^2 + i\left[\frac{dt_g^{(n)}}{d\omega}\right]^3_{\omega_k} - \frac{i}{15}\left[\frac{d^5t_g^{(n)}}{d\omega^5}\right]_{\omega_k}\right\}$$

Thus, the filtered output in (16) can be expressed as:

$$\mathcal{S}_n(t;\omega_k) = \mathrm{Re}\left\{\frac{1}{\Delta\omega_k}\sqrt{\frac{\beta}{\pi}}\,\frac{e^{i\omega_k(t-t_g^{(n)})}}{2\pi}\sum_{l=0}^{\infty}\frac{1}{l!}A_n^{(l)}\right.$$

$$\left.\times\int_{-\infty}^{+\infty}(\omega')^l\left[1+\sum_{m=2}^{\infty}e_m\omega'^m\right]\exp\left[-\beta\left[\frac{\omega'}{\Delta\omega_k}\right]^2\right]e^{i\omega'(t-t_g^{(n)})}\,d\omega'\right\}$$

or, combining the two summations, as:

$$\mathcal{S}_n(t;\omega_k) = \mathrm{Re}\left\{\frac{1}{\Delta\omega_k}\sqrt{\frac{\beta}{\pi}}\,\frac{e^{i\omega_k(t-t_g^{(n)})}}{2\pi}\right.$$

$$\left.\times\sum_{p=0}^{\infty}B_n^{(p)}(r,\omega_k)\int_{-\infty}^{+\infty}\omega'^p\exp\left[-\beta\left[\frac{\omega'}{\Delta\omega_k}\right]^2\right]\exp\left[i\omega'(t-t_g^{(n)})\right]d\omega'\right\} \qquad (17)$$

with

$$B_n^{(0)}(r,\omega_k) = A_n^{(0)}(r,\omega_k) \;\; ; \;\; B_n^{(1)}(r,\omega_k) = A_n^{(1)}(r,\omega_k)$$

$$B_n^{(P)}(r,\omega_k) = \frac{1}{p!} A_n^{(P)}(r,\omega_k) + \sum_{l=0}^{P-2} \frac{1}{l!} A_n^{(l)}(r,\omega_k)\, e_{P-l} \;\; ; \; P \geq 2$$

Now using the integral relation previously quoted, we get, after grouping terms in order by powers of $\Delta\omega_k$:

$$\bar{S}_n(t:\omega_k) = \left[\frac{1}{2\pi}\right] \mathrm{Re}\left\{ e^{i\omega_k(t - t_g^{(n)})} \left[B_n^{(0)}(r,\omega_k) \right.\right.$$

$$+ 2\left[B_n^{(2)}(r,\omega_k) + i(t - t_g^{(n)})\, B_n^{(1)}(r,\omega_k)\right] \Delta\omega_k^2$$

$$+ 4\left[3B_n^{(4)}(r,\omega_k) + 3i(t - t_g^{(n)})\, B_n^{(3)}(r,\omega_r) - (t - t_g^{(n)})^2\, B_n^{(2)}(r,\omega_k)\, \Delta\omega_k^4 \right.$$

$$\left.\left. + O(\Delta\omega_k^8) \right] \exp\left[- \frac{\Delta\omega_k^2}{4\beta} (t - t_g^{(n)})^2 \right] \right\} \qquad (18)$$

Here, in terms of the fundamental signal parameters, the coefficients $B_n^{(P)}$ are:

$$B_n^{(0)}(r,\omega_k) = A_n^{(0)}(r,\omega_k)$$

$$B_n^{(1)}(r,\omega_k) = A_n^{(1)}(r,\omega_k)$$

$$B_n^{(2)}(r,\omega_k) = \frac{1}{2} A_n^{(2)}(r,\omega_k) - \frac{i}{2} A_n^{(0)}(r,\omega_k) \left[\frac{dt_g^{(n)}}{d\omega}\right]_{\omega_k}$$

$$B_n^{(3)}(r,\omega_k) = \frac{1}{6} A_n^{(3)}(r,\omega_k) - \frac{i}{6} \left[A_n^{(0)}(r,\omega_k) \left[\frac{dt_g^{(n)}}{d\omega^2}\right]_{\omega_k} \right.$$

$$\left. + 3A_n^{(1)}(r,\omega_k) \left[\frac{dt_g^{(n)}}{d\omega}\right]_{\omega_k} \right]$$

$$B_n^{(4)}(r,\omega_k) = \frac{1}{24} \left[A_n^{(4)}(r,\omega_k) - 3A_n^{(0)}(r,\omega_k) \left[\frac{dt_g^{(n)}}{d\omega}\right]_{\omega_k}^2 \right]$$

$$- \frac{i}{24} \left[A_n^{(0)}(\tau,\omega_k) \left[\frac{d^3 t_g^{(n)}}{d\omega^3} \right]_{\omega_k} + 4A_n^{(1)}(\tau,\omega_k) \left[\frac{d^3 t_g^{(n)}}{d\omega^2} \right]_{\omega_k} \right.$$

$$\left. + 6A_n^{(2)}(\tau,\omega_k) \left[\frac{dt_g^{(n)}}{d\omega} \right]_{\omega_k} \right]$$

where the superscript index on the signal amplitude A_n denotes the order of derivative with respect to angular frequency, that is:

$$A_n^{(l)}(\tau,\omega_k) \equiv \left[\frac{d^l A_n(\tau,\omega)}{d\omega^l} \right]_{\omega_k}$$

This expression for the filtered signal is formally exact, under the tacit assumption that the expansions of the signal amplitude and phase functions are convergent. Such convergence is, however, assured for a physically realizable signal.

There are a number of important features in equation (18.) that deserve comment. First of all, the result is similar to the impulse response of the filter itself, in that it consists of a sinusoid, namely $e^{i\omega_k(t-t_g^{(n)})}$, modulated by a decaying exponential in time - that is modulated by

$$\exp\left\{ -\frac{\Delta\omega_k^2}{4\beta}(t - t_g^{(n)})^2 \right\}$$

In addition, however, the result contains a second complex valued modulation function, involving the signal spectrum and frequency derivatives of the spectrum, plus frequency derivatives of the group delay, $t_g^{(n)}$, all evaluated at the filter center frequency ω_k. This function therefore carries information concerning the signal spectrum and its dispersive characteristics, whereas the pure sinusoid carrier involves only the phase delay of the signal and the Gaussian exponential modulation depends only on the group delay of the signal. Further, this function has the form of a power series in $\Delta\omega_k$, so that for $\Delta\omega_k$ small it can be approximated by the first few terms. It is therefore useful to

write the filtered signal result in the form:

$$\bar{S}_n(t;\omega_k) = \left(\frac{1}{2\pi}\right)\mathrm{Re}\left[e^{i\omega_k(t-t_g^{(n)})}\, M_n(t-t_g^{(n)};\Delta\omega_k)\, e^{-\frac{\Delta\omega_k^2}{4\beta}(t-t_g^{(n)})^2}\right] \tag{19}$$

where

$$M_n(t-t_g^{(n)};\Delta\omega_k) = A_n^{(0)} + \left[A_n^{(2)} - iA_n^{(0)}\left[\frac{dt_g^{(n)}}{d\omega}\right]_{\omega_k} + 2iA_n^{(1)}(t-t_g^{(n)})\right]\overline{\Delta\omega_k^2}$$

$$+ 1/2\left[\left\{A_n^{(4)} - 3A_n^{(0)}\left[\frac{dt_g^{(n)}}{d\omega}\right]^2_{\omega_k} - iA_n^{(0)}\left[\frac{d^3t_g^{(n)}}{d\omega^3}\right]_{\omega_k} - 4iA_n^{(1)}\left[\frac{d^2t_g^{(n)}}{d\omega^2}\right]_{\omega_k}\right.\right.$$

$$\left.\left. - 6iA_n^{(2)}\left[\frac{dt_g^{(n)}}{d\omega}\right]_{\omega_k}\right\} + 4\left\{3A_n^{(1)}\left[\frac{dt_g^{(n)}}{d\omega}\right]_{\omega_k} + iA_n^{(2)} + A_n^{(0)}\left[\frac{d^2t_g^{(n)}}{d\omega^2}\right]_{\omega_k}\right\}(t-t_g^{(n)})\right.$$

$$\left. - 4\left\{A_n^{(2)} - A_n^{(0)}\left[\frac{dt_g^{(n)}}{d\omega}\right]_{\omega_k}\right\}(t-t_g^{(n)})^2\right]\overline{\Delta\omega_k^4}$$

$$+ O(\overline{\Delta\omega_k^6}) \tag{20}$$

with

$$\overline{\Delta\omega_k} \equiv \frac{\Delta\omega_k}{(4\beta)^{1/2}}\ ,\ \beta = \frac{\ln 2}{2}$$

Thus, the modulation function M_n is a relatively simple power series in $\Delta\omega_k$ with coefficients which are polynomials in the time difference $(t - t_g^{(n)})$. It is also useful to express M_n in polar form, in which case we can write the filter output as:

$$\bar{S}_n(t;\omega_k) = \frac{|M_n|}{2\pi}\, e^{-\overline{\Delta\omega_k^2}(t-t_g^{(n)})^2}\cos[\omega_k(t-t_g^{(n)}) - \Phi_g] \tag{19a}$$

with

$$|M_n| = A_n^{(0)}\left|1 + \frac{A_n^{(2)}}{A_n^{(0)}}\overline{\Delta\omega_k^2} + \left\{\left[\frac{A_n^{(4)}}{2A_n^{(0)}} - 2\left[\frac{dt_g^{(n)}}{d\omega}\right]^2_{\omega_k}\right]\right.\right.$$

$$+ 2\left[\frac{2A_n^{(1)}}{A_n^{(0)}}\left[\frac{dt_g^{(n)}}{d\omega}\right]_{\omega_k} + \left[\frac{d^2t_g^{(n)}}{d\omega^2}\right]_{\omega_k}\right](t - t_g^{(n)})$$

$$+ 2\left[\left[\left(\frac{A_n^{(1)}}{A_n^{(0)}}\right)^2 - \frac{A_n^{(2)}}{A_n^{(0)}}\right](t - t_g^{(n)})^2\right]\overline{\Delta\omega_k^4} + O(\Delta\omega_k^6)\Bigg] \qquad (20a)$$

$$\Phi_g = \tan^{-1}\left\{\left[\left[\frac{dt_g^{(n)}}{d\omega}\right]_{\omega_k} - 2\,\frac{A_n^{(1)}}{A_n^{(0)}}(t - t_g^{(n)})\right]\overline{\Delta\omega_k^2} + O(\Delta\omega_k^4)\right\} \qquad (20b)$$

Here, in expressing these last results, we have assumed $A_n^{(0)} \neq 0$.

Limiting Forms of the Quasi-Harmonic Filtered Signal, $\overline{S}_n$.

An important property of the modulation function is that

$$\lim_{\Delta\omega_k \to 0} M_n(t - t_g^{(n)};\Delta\omega_k) = A_n^{(0)}(r;\omega_k) \qquad (21)$$

$$\lim_{\Delta\omega_k \to 0} \overline{S}_n(t;\omega_k) = \left(\frac{1}{2\pi}\right) \mathrm{Re}\left[A_n^{(0)}(r;\omega_k)e^{i\omega_k(t - t_g^{(n)})}\right] \qquad (22)$$

so that, as the filter bandwith approaches zero, we obtain a pure sinusoid with amplitude and phase equal to the Fourier amplitude and phase. This of course is not unexpected, since this limit must correspond to the operation of ordinary Fourier analysis. Nevertheless this shows that we may approach the limit of Fourier spectral analysis if $\Delta\omega_k$ is made small, and we will of course wish to obtain good spectral estimates of the signal by narrow band filtering, as well as accurate group arrival time estimates, by choosing $\Delta\omega_k$ small. In this regard however, the limiting case given in (22.) shows that we can obtain exact spectral estimates by narrow band filtering when $\Delta\omega_k \to 0$, corresponding to Fourier decomposition, *but no estimate of the group arrival time*.

We observe however, from (20.), that when $t = t_g^{(n)}$ for the n^{th} signal, then most of the terms in the expression vanish, and:

$$M_n(0;\Delta\omega_k) = A_n^{(0)}\left[1 + \left\{\frac{A_n^{(2)}}{A_n^{(0)}} - i\left[\frac{dt_g^{(n)}}{d\omega}\right]_{\omega_k}\right\}\overline{\Delta\omega_k^2} + O(\Delta\omega_k^4)\right] \tag{23}$$

with the final terms being, at most, of order $\Delta\omega_k^4$ and involving products of high order derivatives of A_n and $t_g^{(n)}$ with respect to frequency. Therefore when $\Delta\omega_k$ is such that

$$\frac{\Delta\omega_k^2}{4\beta}\left[\frac{dt_g^{(n)}}{d\omega}\right]_{\omega_k} \ll 1 \tag{24}$$

then we can expand γ in powers of this small factor, which gives

$$\begin{aligned}\gamma^{-1} &\approx 1 - \frac{i}{4}\left[\frac{\Delta\omega_k^2}{\beta}\right]\left[\frac{dt_g^{(n)}}{d\omega}\right]_{\omega_k} \\ \gamma^{-2} &\approx 1 - \frac{i}{2}\left[\frac{\Delta\omega_k^2}{\beta}\right]\left[\frac{dt_g^{(n)}}{d\omega}\right]_{\omega_k}\end{aligned} \tag{25}$$

for the γ factors appearing in the function M_n. These factors can be written in polar form as

$$\gamma^{-1} \approx e^{\frac{-i}{2}\phi_g} \tag{26-a}$$

$$\gamma^{-2} \approx e^{-i\phi_g} \tag{26-b}$$

where

$$\phi_g = \tan^{-1}\left[\frac{\Delta\omega_k^2}{2\beta}\left[\frac{dt_g^{(n)}}{d\omega}\right]_{\omega_k}\right]$$

We see that as long as the condition (24) holds, then the factors γ^{-1} and γ^{-2} appearing in M_n can be approximated as simple phase shifts. In this situation, the value of M_n at $t = t_g^{(n)}$ is, from (23):

$$M_n(0;\Delta\omega_k) = A_n^{(0)} e^{\frac{-i}{2}\phi_g} + \frac{1}{2}\left[\frac{\Delta\omega_k^2}{2\beta}\right] e^{\frac{-3i}{2}\phi_g} A_n^{(2)} + O\left[\frac{\Delta\omega_k^4}{4\beta^2}\right]$$

Consequently the narrow band Gaussian filtered signal $\overline{S}_n$, at $t = t_g^{(n)}$, has the form:

$$\bar{S}_n(t_g^{(n)};\omega_k) \approx \left(\frac{1}{2\pi}\right) \mathrm{Re}\left[A_n^{(0)} e^{i\omega_k(t_g^{(n)}-t_p^{(n)}-\Phi_g/2\omega_k)}\left\{1+\frac{1}{2}\left[\frac{\Delta\omega_k^2}{2\beta}\right]\frac{A_n^{(2)}}{A_n^{(0)}}e^{-i\Phi_g}+O\left[\Delta\omega_k^4\right]\right\}\right] \tag{27}$$

for $A_n^{(0)} \neq 0$ at $\omega=\omega_k$. Comparing this to (22), the limiting case of the Fourier decomposition for which $\Delta\omega_k$ is zero, we now observe that we get a very similar result at $t=t_g^{(n)}$ when $\Delta\omega_k$ is finite, so long as:

$$(1)\quad \frac{\Delta\omega_k^2}{2\beta}\left|\left[\frac{dt_g}{d\omega}\right]_{\omega_k}\right| \ll 1$$

$$(2)\quad \frac{\Delta\omega_k^2}{4\beta}\left|\frac{A_n^{(2)}}{A_n^{(0)}}\right| \ll 1\ ;\ \left|A_n^{(0)}\right| \neq 0 \tag{28}$$

In this case we note that the phase factor Φ_g in (27) can be neglected since,

$$0 \leq \left|\Phi_g\right| = \left|\tan^{-1}\left[\frac{\Delta\omega_k^2}{2\beta}\left[\frac{dt_g^{(n)}}{d\omega}\right]_{\omega_k}\right]\right| \approx \frac{\Delta\omega_k^2}{2\beta}\left|\left[\frac{dt_g^{(n)}}{d\omega}\right]_{\omega_k}\right| \ll 1$$

by the first inequality in (28). Further when the second inequality in (28) also holds, the complex amplitude factors in (27) can be neglected relative to unity. Thus we can clearly approximate the limiting case in which the amplitude of the filtered output is equal to the Fourier amplitude at the center frequency of the filter when $\Delta\omega_k$ is finite, if we measure the amplitue of the filtered time series at $t=t_g^{(n)}$, the group arrival time. Similarily the phase of the filtered time series at $t=t_g^{(n)}$ is, to a good approximation, equal to $\omega_k(t_g^{(n)}-t_p^{(n)})$ which is the Fourier phase of the $n^{\underline{th}}$ signal at the frequency ω_k.

Filter Design and Signal Conditioning Requirements

In view of the previous limiting case results, we observe that the objective of narrow-band filtering, which is to decompose a complex time series into a series of nearly harmonic components that simultaneously retain accurate signal energy arrival time and Fourier amplitude and phase information for each signal, can be achieved provided the filter design and signal characteristics are such that the Q of each filter simultaneously satisfies the conditions

$$Q_k \gg \left| \left(\frac{dt_g^{(n)}}{d\omega} \right)_{\omega_k} \right|^{1/2} \omega_k$$

$$Q_k \gg \left| A_n^{(2)}(\omega_k) / 2A_n^{(0)}(\omega_k) \right|^{1/2} \omega_k \qquad (29)$$

where Q_k and ω_k are the quality factor and center frequency for the $k^{\underline{th}}$ filter. For the filter design criteria to be met, the expected signals within the time series should be minimally dispersed and have smooth amplitude spectra. Body wave signal pulses intrinsically have such characteristics, while other seismic "phases" require preprocessing of the time series to render them of the required form. Specifically, preprocessing with a matched filter, which is the approximate inverse of the expected signal, within the bandwidth to be covered by the set of narrow band filters, is required.

An acceptable design of the narrow band filter set is achieved using:

$$Q_k = \tau_b \omega_k$$

where τ_b is a constant such that:

$$\tau_b \gg \max_{1 \le k \le N} \left\{ \left| \left(\frac{dt_g^{(n)}}{d\omega} \right)_{\omega_k} \right| ; \left| A_n^{(2)}(\omega_k) / 2A_n^{(0)}(\omega_k) \right| \right\}$$

In this case the bandwidth, $\Delta\omega_k$, is constant for all the filters of the set, since

from the definition of the filter Q we have

$$\Delta\omega_k = 1/\tau_b$$

Hence, τ_b is a time like parameter which is a measure of the ring time of the narrow band filters. (ie. The amplitude of the impulse response of each filter is decreased by 1/e, from its peak at $t=t_p^{(n)}$, when $t=t_p^n \pm \tau_b$.) In addition, the resolution time, Δt_k, for any time measurement from a filter output is constrained by the "uncertainty principal", having the form: $\Delta\omega_k \Delta t_k \geq \varepsilon$, for all k. Here $\Delta\omega_k$ is again, the filter bandwidth and ε is some constant independent of the filter index k. Consequently the uncertainty in measuring the time at which a filter output has a maximum is proportional to τ_b, in particular:

$$\Delta t_k \geq \varepsilon\tau_b$$

Since we cannot precisely define ε , other than to say that it is greater than zero and at most of order 1, then we cannot say much more than that Δt_k increases or decreases directly with τ_b. With the choice of the filter set Q factors as indicated above however, then every filter of the set has the same theoretical resolution, as well as bandwidth. That is, Δt_k and $\Delta\omega_k$ are both constant for all k and directly or inversely proportional, respectively, to τ_b.

Filter Output For a Time Series of Superposed Pulse-Like Signals and Noise

When the narrow band filter design meets the conditions specified by (29), then the filter output, for a input series of signals $S_n(t)$, has the form:

$$Y(t;\omega_k) = \sum_n \bar{S}_n(t;\omega_k) \approx \frac{1}{2\pi}\mathrm{Re}\left\{\sum_{n,m}\left[M_{nm}(t-t_p^{(n)};\Delta\omega_k)e^{\frac{-\Delta\omega_k^2}{4\beta}(t-t_p^{(n)})^2}\right]e^{i\omega_k(t-t_p^{(n)})}\right\} \tag{30}$$

where, from (20),

$$M_{nm}(t-t_g^{(n)};\Delta\omega_k) \approx A_{nm}^{(0)}(\omega_k) + \frac{\Delta\omega_k^2}{2\beta}\left[iA_{nm}^{(1)}(\omega_k)(t-t_g^{(n)}) + \tfrac{1}{2}A_{nm}^{(2)}(\omega_k)\right] + O\left[\Delta\omega_k^4\right] \qquad (31)$$

Here the mode sum over m has been restored to the expressions for completeness. The mode index m takes on values from sets (l_n), which are determined by the signal index n. (ie. Different sets of modes are summed for different signals.) The function $Y(t;\omega_k)$ is introduced to denote the $k^{\underline{th}}$ narrow band filter output of a time series consisting of a sum of signals of pulse-like form.

The results expressed in (30) and (31) therefore apply to signals of pulse form, that is minimally dispersed and spectrally smooth. In general the time series is composed of signals of this type, plus noise, the latter being all "signals" not of this form. Thus, in general, we have a time series x(t) which is a sum of signals $S_n(t)$ and noise $N_l(t)$, where the noise is indexed to indicate that it too is composed of a series of discrete wave packets (typically overlapping in time) which are usually dispersed and/or have "non-smooth" spectral amplitude character. Nevertheless the noise can be represented by modes, however these modes are not excited by the single source responsible for the signals, but rather by a more or less random distribution of sources scattered in space and time. Thus we write the basic time series as:

$$x(t) = \sum_n S_n(t) + \sum_l N_l(t)$$

and the output of the $k^{\underline{th}}$ narrow band Gaussian filter as

$$X(t;\omega_k) = \sum_n \bar{S}_n(t;\omega_k) + \sum_l \bar{N}_l(t;\omega_k) \qquad (32)$$

where the first sum on the right side is $Y(t;\omega_k)$, as given in (30) - (31), and the second sum, representing the filtered noise, can be denoted $Z(t;\omega_k)$. From the previous general analysis it is quite evident that $Z(t;\omega_k)$ can be expressed in the same general form as is $Y(t;\omega_k)$, that is as

$$Z(t;\omega_k) = \sum_l \bar{N}_l(t;\omega_k) = \frac{1}{2\pi} Re\left\{ \sum_{l,m}\left[M_{lm}(t-t_g^{(l,m)};(\Delta\omega_k) e^{\frac{-\Delta\omega_k^2}{4\beta}(t-t_g^{(l,m)})^2}\right] e^{i\omega_k(t-t_g^{(l,m)})}\right\}$$

Here, however, the modulation function M_{lm} now has a complex form, given formally by equation (20), which cannot in general be reduced to the simple form of (31), since the various frequency derivatives of the group time and spectral amplitudes for the noise generally do not conform to the smoothness properties required. Further the group and phase times, t_g and t_p , are generally different for each mode contributing to a particular noise packet or wave group. Hence these times are explicitly indexed by both l the "wave packet" index, and m the index for the modes associated with that wave packet.

We note however, that both the group time $t_g^{(n)}$ and the phase time $t_p^{(n)}$, for the $n^{\underline{th}}$ signal pulse appearing in $Y(t;\omega_k)$, are nearly constant and equal to each other. In particular, each mode that contibutes to a given signal pulse will have values of t_g and t_p that are constant over the frequency range for which the mode has significant excitation. Since each contributing mode will have essentially the same values of t_g and t_p for a particular signal pulse, then, for seismic body wave signals, t_g and t_p are mode independent, and so are not indexed by m in (30) - (31). The same observations hold for wave types that are not pulse-like initially, but that have been rendered pulse-like and undispersed by matched filtering. In this case the dispersed modes of interest have been mapped, by the filtering, into nearly undispersed pulse-like arrivals.

Consequently, for such signals we can formally carry out the sum over modes indicated in (30), taking account of the fact that the exponential terms do not depend on m for seismic body waves and/or matched filtered signals, and rewrite the results in the simpler form:

$$Y(t;\omega_k) \approx \frac{1}{2\pi}\mathrm{Re}\left\{\sum_n \left[M_n(t-t_g^{(n)};\Delta\omega_k)\, e^{\frac{-\Delta\omega_k^2}{4\beta}(t-t_g^{(n)})^2}\right] e^{i\omega_k(t-t_p^{(n)})}\right\} \qquad (34)$$

with

$$M_n(t-t_g^{(n)};\Delta\omega_k) \approx A_n^{(0)}(\omega_k) + \frac{\Delta\omega_k^2}{2\beta}\left[iA_n^{(1)}(\omega_k)(t-t_g^{(n)}) + \frac{1}{2}A_n^{(2)}(\omega_k)\right] \qquad (35)$$

Here the amplitude factors $A_n^{(p)}(\omega_k)$, representing the p^{th} order frequency derivatives of the amplitude spectrum of the n^{th} signal pulse, correspond to sums over only the modes contributng to the n^{th} signal. That is:

$$A_n^{(p)}(\omega_k) \equiv \sum_m A_{nm}^{(p)}(\omega_k) \qquad (36)$$

where m is restricted to the mode index set (I_n) that corresponds to the n^{th} signal. (We do not, a-priori, know what mode set does in fact belong to a particular signal, but it is sufficient for the present to know that such finite sets exist. At a given frequency it is typical that only one or two modes contribute to a particular body wave phase - as illlustrated in Figure 1. Thus, the sum in (36) is generally over only one or two mode indices, m, at a fixed frequency ω_k.)

The principal use of the narrow band filtering output is to provide measurements of signal group arrival time (t_g values) and the amplitudes and phase of the signals *at these times*. Thus the essential feature of the output from a set of narrow band filters is the behaviour of the filter output at, or near, the energy or group arrival times t_g. At a group time of a particular signal, say the j^{th} signal, a properly designed filter with center frequency ω_k has an output:

$$X(t_g^{(j)};\omega_k) \approx \frac{1}{2\pi}\left[A_j^{(0)}(\omega_k)\cos\omega_k(t_g^{(j)}-t_p^{(j)}) + \sum_{n\neq j}\left\{ A_n^{(0)}(\omega_k)e^{\frac{-\Delta\omega_k^2}{4\beta}(t_g^{(j)}-t_g^{(n)})^2}\right\}\cos\omega_k(t_g^{(j)}-t_p^{(n)})\right.$$

$$\left. + \mathrm{Re}\sum_{l,m}\left\{ M_{lm}(t_g^{(j)}-t_g^{(l,m)};\Delta\omega_k)e^{\frac{-\Delta\omega_k^2}{4\beta}(t_g^{(j)}-t_g^{(l,m)})^2}\right\}\cdot e^{i\omega_k(t_g^{(j)}-t_p^{(l,m)})}\ldots\ldots\right] \qquad (37)$$

where M_{lm} in the final sum is the modulation function for the noise, and has the form given by (20).

The first term in this expression is just equal to the Fourier component of

the j^{th} signal at ω_k , while the second term is a sum over all other ($n \neq j$) pulse like signals, and the final term is the sum over all the noise arrivals. The latter two terms can be viewed as interference terms relative to the j^{th} signal, whose properties (eg. spectrum) are to be estimated. Clearly, because of the Gaussian exponential factor contained in both these terms, the sums will be small relative to the first term if

$$\left| t_g^{(j)} - t_g^{(n)} \right| \gg \frac{2\sqrt{\beta}}{\Delta\omega_k} \tag{38}$$

In this case

$$X(t_g^{(j)};\omega_k) \approx \left[\frac{1}{2\pi}\right] A_j^{(0)}(\omega_k) e^{i\omega_k (t_g^{(j)} - t_j^{(j)})}$$

and we get an uncontaminated result for the j^{th} signal. If on the other hand, the time separation between this signal and other signals and noise is not very large, then some of the terms in the two series may contribute significantly to the value of X *at* $t = t_g^{(j)}$. However, measurements of X at a signal group arrival time can be corrected for such "contamination" to give an estimate of the Fourier component of the signals, and equation (37) can be used as the basis for this correction. The details will be considered in a later section.

VI. MEASUREMENTS OF FILTER OUTPUT CHARACTERISTICS USING ASSOCIATED FILTER FUNCTIONS: ENVELOPE, INSTANTANEOUS PHASE AND FREQUENCY FUNCTIONS

In order to obtain signal spectrum and dispersion estimates from the narrow band filtering operations, it is convenient to define a set of "associated" filter functions, derived from the analytical forms obtained for the filter output, which permit simple computer controlled determinations of signal and noise group arrival times and amplitude spectra. Clearly the most important task, considering the emphasis placed on measuring the filter output at group times t_g, is to be able to determine the t_g values for all signal and noise arrivals within the time series. We will therefore first consider the filter envelope

function, from which we can obtain estimates of the t_g values.

The Quadrature Signal

As a preliminary, it is necessary to define the "quadrature signal", which can be formed from the original time series spectrum, as

$$\hat{X}(\omega) = -i\, sgn(\omega)\, X(\omega) \tag{39}$$

where $sgn(\omega)$ denotes the algebraic sign of ω, and $X(\omega)$ is the Fourier spectrum of the original time series, while $\hat{X}(\omega)$ denotes the spectrum of the quadrature time series. In the time domain, $\hat{x}(t)$ is the Hilbert transform of $x(t)$. The property of $\hat{x}$ which is useful here is that its Fourier components are shifted in phase by $-\pi/2$, as is easily seen from (39). This is the origin of its designation as the "quadrature signal".

How, for any time series, $x(t)$:

$$x(t) = \frac{1}{2\pi}\int_{-\infty}^{+\infty} X(\omega)e^{i\omega t}\,d\omega = \frac{1}{2\pi}\int_0^{\infty}\left[X(\omega)e^{i\omega t} + X(-\omega)e^{-i\omega t}\right]d\omega$$

However, since $x(t)$ is real, then $X(\omega)$ must have the property that $X(-\omega) = X^*(\omega)$, where $X^*(\omega)$ is the complex conjugate of $X(\omega)$. Thus, with

$$X(\omega) = \left|X(\omega)\right|e^{i\Phi(\omega)},$$

then it follows from this property that:

$$x(t) = \frac{1}{\pi}\int_0^{\infty}\left|X(\omega)\right|\cos\left[\omega t + \Phi(\omega)\right]d\omega = \frac{1}{\pi}\mathrm{Re}\int_0^{+\infty}\left\{\left|X(\omega)\right|e^{i\Phi(\omega)}\right\}e^{i\omega t}\,d\omega \tag{40}$$

Similarily the quadrature time function $\hat{x}(t)$, with spectrum given in (39), is represented by:

$$\hat{x}(t) = \frac{1}{2\pi}\int_{-\infty}^{+\infty}\hat{X}(\omega)e^{i\omega t}\,d\omega = \frac{1}{2\pi}\int_0^{\infty}\left\{X(\omega)e^{-\frac{i\pi}{2}+i\omega t} + X(-\omega)e^{\frac{i\pi}{2}-i\omega t}\right\}d\omega$$

But again, since $X(-\omega) = X^*(\omega)$, we have

$$\hat{x}(t) = \frac{1}{2\pi}\int_0^{\infty} |X(\omega)| \left\{ e^{i(\omega t + \phi - \pi/2)} + e^{-i(\omega t + \phi - \pi/2)} \right\} d\omega$$

or

$$\hat{x} = \frac{1}{\pi}\int_0^{\infty} |X(\omega)| \cos[\omega t + \phi - \pi/2] d\omega = \frac{1}{\pi} \mathrm{Re} \int_0^{+\infty} \left\{ |X(\omega)| e^{i(\phi(\omega) - \pi/2)} \right\} e^{i\omega t} d\omega \qquad (41)$$

(Comparison of this Fourier expansion for $\hat{x}(t)$ with that for $x(t)$ now explictly shows that $\hat{x}(t)$ has Fourier components that are shifted in phase, from those for $x(t)$, by a factor of $-\pi/2$.)

The Complex or Analytic Signal

The quadrature signal can be used, together with the original signal, to define what is usually termed the complex or analytic signal . A complex signal representation provides the basis for the definition of instantaneous phase and frequency functions, as well as an envelope function. Specifically, we define the complex signal, $x_c(t)$, as:

$$x_c(t) = x(t) + i\,\hat{x}(t) \qquad (42)$$

and from this definition it follows immediately , from the representations (40) and (41) for $x(t)$ and $\hat{x}(t)$, that

$$x_c(t) = \int_0^{\infty} X(\omega) e^{i\omega t} d\omega = \frac{1}{\pi}\int_0^{\infty} |X(\omega)| e^{i(\omega t + \phi)} d\omega \qquad (43)$$

Clearly, $x_c(t)$ is a complex valued function of time, rather than being real as are $x(t)$ and $\hat{x}(t)$, and, in particular, can be written in the forms

$$x_c(t) = \mathrm{Re}\left[x_c(t)\right] + i\ \mathrm{Im}\left[x_c(t)\right] = |x_c(t)| e^{i\phi_c(t)} \qquad (44)$$

where

$$|x_c(t)| = \sqrt{x^2(t) + \hat{x}^2(t)}$$

$$\phi_c = \tan^{-1}\left[\frac{\hat{x}(t)}{x(t)}\right] \qquad (45)$$

Thus, $x_c(t)$, can be written in polar form, since it is complex, and can easily be computed using (43), which is simply the transform of $x(t)$ over only the positive frequencies. Further, it follows from these definitions that

$$x(t) = \mathrm{Re}\left\{ x_c(t) \right\} = \left| x_c(t) \right| \cos\left[\Phi_c(t) \right]$$
$$\hat{x}(t) = \mathrm{Im}\left\{ x_c(t) \right\} = \left| x_c(t) \right| \sin\left[\Phi_c(t) \right] \tag{46}$$

Thus, an arbitrary time series, that may not have sinusoid form, can nevertheless be expressed in this "sinusoid form" through the use of its quadrature function.

In analogy with the ordinary frequency of a sinusoid, the phase factor, $\Phi_c(t)$, appearing in (44) - (46), can be expressed in terms of some fixed frequency, say ω_0, and a frequency modulation function, $\Psi(t)$, through the definition:

$$\Phi_c(t) = \omega_0 t + \int_0^t \Psi(\tau) d\tau \tag{47}$$

Thus, the time derivitaive of Φ_c corresponds to a frequency, in particular the instantaneous frequency $\Omega(t)$, and we have from (47)

$$\Omega(t) = \frac{d\Phi_c(t)}{dt} = \omega_0 + \Psi(t) \tag{48}$$

in terms of the "carrier" frequency ω_0 and frequency modulation function $\Psi(t)$. From the definiton of $\Phi_c(t)$ in (45) we also have

$$\Omega(t) = \left[x(t) \frac{d\hat{x}(t)}{dt} - \hat{x}(t) \frac{dx(t)}{dt} \right] / \left| x_c(t) \right|^2 \tag{49}$$

Envelope, Instantaneous Phase and Frequency Functions

For Quasi-Harmonic Time Series

For a quasi-harmonic time series the amplitude and phase functions in (45)

are usefully defined as the envelope and instantaneous phase of the quasi-harmonic time series. That is, with $x_k(t;\omega_k)$ denoting the quasi-harmonic time series, the envelope and instantaneous phase are defined

$$E_k(t;\omega_k) \equiv \left| x_k^c(t;\omega_k) \right| = \sqrt{x_k^2(t;\omega_k) + \hat{x}_k^2(t;\omega_k)}$$

$$\chi_k(t;\omega_k) \equiv \varphi_k^c(t;\omega_k) = \tan^{-1}\left[\frac{\hat{x}_k(t;\omega_k)}{x_k(t;\omega_k)}\right] \tag{50}$$

where $\left|x_k^c\right|$ and φ_k^c are the amplitude and phase of the complex signal formed, using (43), from the *Gaussian filtered* time series $x(t)$. Similarily the instantaneous frequency associated with each quasi-harmonic time series $x_k(t;\omega_k)$ is

$$\Omega_k(t;\omega_k) \equiv \frac{d\varphi_k^c}{dt} = \left[x_k \frac{d\hat{x}_k}{dt} - \hat{x}_k \frac{dx_k}{dt}\right] / E_k^2 \tag{51}$$

For a time series consisting of pulse-like signals, then we have:

$$x_k(t;\omega_k) \equiv \sum_n \overline{S_n}(t;\omega_k)$$

where, from (20)

$$\overline{S}_n(t;\omega_k) = \frac{1}{2\pi} \mathrm{Re}\left[e^{i\omega_k (t - t_p^{(n)})} M_n(t - t_g^{(n)};\Delta\omega_k)\, e^{\frac{-\Delta\omega_k^2}{4\beta\gamma^2}(t - t_g^{(n)})^2} \right] \tag{52}$$

with the phase time variable, defined in (15), having the form

$$t_p^{(n)} = \frac{r}{C_n(\omega_k)} + \frac{\Phi_n(\omega_k)}{\omega_k} \tag{53}$$

and with the modulation function, given by (20), having the form

$$M_n(t - t_g^{(n)};\Delta\omega_k) = \frac{1}{\gamma}\left[A_n^{(0)} + iA_n^{(1)}\left\{ \frac{\Delta\omega_k^2}{2\beta\gamma^2}(t - t_g^{(n)}) \right\} + \frac{A_n^{(2)}}{2}\left[\frac{\Delta\omega_k^2}{2\beta\gamma^2}\right] + O(\Delta\omega_k^4) \right]$$

(54)

Here the factor γ is such that:

$$\gamma^{-1} \approx 1 - \frac{i}{2}\left[\frac{\Delta\omega_k^2}{2\beta}\right]\left[\frac{dt_g^{(n)}}{d\omega}\right]_{\omega_k} \approx e^{\frac{-i}{2}\phi_g}$$

$$\gamma^{-2} \approx 1 - i\left[\frac{\Delta\omega_k^2}{2\beta}\right]\left[\frac{dt_g^{(n)}}{d\omega}\right]_{\omega_k} \approx e^{-i\phi_g}$$

where

$$\phi_g = \tan^{-1}\left[\frac{\Delta\omega_k^2}{2\beta}\left[\frac{dt_g^{(n)}}{d\omega}\right]_{\omega_k}\right]$$

as shown in (24)-(26). Now we can express M_n in polar form as

$$M_n = |M_n| e^{i[\psi_n - \phi_g/2]} \tag{55}$$

where

$$|M_n| = A_n^{(0)}\left[1 + \frac{A_n^{(2)}}{2A_n^{(0)}}\left[\frac{\Delta\omega_k^2}{2\beta}\right] + O(\Delta\omega_k^4)\right]$$

(56)

$$\psi_n = \tan^{-1}\left[\frac{A_n^{(1)}}{A_n^{(0)}}\left[\frac{\Delta\omega_k^2}{2\beta}\right](t - t_g^{(n)}) + O(\Delta\omega_k^4)\right]$$

and rewrite S_n as:

$$\tilde{S}_n(t;\omega_k) = \frac{|M_n|}{2\pi} e^{\frac{-\Delta\omega_k^2}{4\beta}(t-t_g^{(n)})^2} \cos\omega_k\left[t - t_p^{(n)} + \frac{\psi_n}{\omega_k} - \frac{\phi_g}{2\omega_k}\right] \tag{57}$$

Similarly, the quadrature signal has the form

$$S_n(t;\omega_k) = \frac{|M_n|}{2\pi} e^{\frac{-\Delta\omega_k^2}{4\beta}(t-t_g^{(n)})^2} \sin\omega_k\left[t - t_p^{(n)} + \frac{\psi_n}{\omega_k} - \frac{\phi_g}{2\omega_k}\right] \tag{58}$$

All these expressions are accurate up to terms of order $\Delta\omega_k^4$. We observe, however, that the phase of M_n, as expressed by ψ_n above, is only meaningful when t is near $t_g^{(n)}$, that is when $|t-t_g^{(n)}|<1$. It is also true that the higher order terms in $|M_n|$ involve $(t-t_g^{(n)})$, and these terms become large as $t-t_g^{(n)}$ becomes large. Thus while the Gaussian exponential factors in $\bar{S}_n$ and S_n produce a rapid convergence of these functions to zero when $t-t_g^{(n)}$ is large, it is nevertheless clear that the analytical expressions for these functions, involving truncated power series in $(t-t_g^{(n)})$, are only accurate for t near $t_g^{(n)}$.

We now observe that the envelope function, $E_k(t;\omega_k)$, for the whole filtered time series, can be related analytically to envelope functions for the individual "signals". In particular, (see also equation ( )):

$$E_k(t;\omega_k)\,e^{i\chi_k(t;\omega_k)} = \sum_n E_k^{(n)}(t;\omega_k)\,e^{i\chi_k^{(n)}(t;\omega_k)} \tag{59-a}$$

with

$$E_k^{(n)}(t;\omega_k) \equiv |S_n^c| = \sqrt{S_n^2+\bar{S}_n^2} \tag{59-b}$$

and

$$\chi_k^{(n)}(t;\omega_k) \equiv \varphi_n^c(t;\omega_k) = \tan^{-1}\left[\frac{\bar{S}_n}{S_n}\right] \tag{59-c}$$

where $|S_n^c|$ is the modulus of the "complex signal" associated with the filtered signal pulse $\bar{S}_n$, and φ_n^c is the phase.

Now from (57) and (58) we have,

$$E_k^{(n)}(t;\omega_k) = \frac{1}{2\pi}\left[(M_n^{(1)})^2+(M_n^{(2)})^2\right]^{1/2} e^{-\frac{\Delta\omega_k^2}{4\beta}(t-t_g^{(n)})^2} \tag{60}$$

where

$$M_n^{(1)} = \mathrm{Re}[M_n] \; ; \; M_n^{(2)} = \mathrm{Im}[M_n]$$

Therefore, with all terms to order $\Delta\omega_k^2$ retained in M_n, and assuming $A_n^{(0)} \neq 0$,

$$E_k^{(n)}(t;\omega_k) = \frac{A_n^{(0)}(\omega_k)}{2\pi} e^{\frac{-\Delta\omega_k^2}{4\beta}(t-t_g^{(n)})^2} \left[(1+\delta_1)+\delta_2(t-t_g^{(n)})^2\right]^{1/2} \tag{61}$$

where

$$\delta_1 = \frac{A_n^{(2)}}{A_n^{(0)}}\left[\frac{\Delta\omega_k^2}{2\beta}\right]\left[1+\frac{1}{4}\frac{A_n^{(2)}}{A_n^{(0)}}\left[\frac{\Delta\omega_k^2}{2\beta}\right]\right]$$

$$\delta_2 = \left[\frac{A_n^{(1)}}{A_n^{(0)}}\right]^2\left[\frac{\Delta\omega_k^2}{2\beta}\right]^2 \tag{62}$$

It is evident from (61) that the envelope functions are, nearly, simple Gaussian exponentials with a constant coefficient equal to the spectral amplitude of the signal at $\omega = \omega_k$. The departure from this simple form involves modulation by the square root of a polynomial function of $(t-t_g^{(n)})$, where in the case when M_n is truncated after terms of order $\Delta\omega_k^2/2\beta$, this polynominal is of second order. For pulse-like signals conforming with our criteria of smoothness, that is with

$$\left|A_n^{(0)}(\omega_k)\right| > \left|A_n^{(1)}(\omega_k)\right| > \left|A_n^{(2)}(\omega_k)\right| > \cdots$$

$$\left|t_g^{(n)}\right|_{\omega_k} > \left|\frac{dt_g^{(n)}}{d\omega}\right|_{\omega_k} > \left|\frac{d^2t_g^{(n)}}{d\omega^2}\right|_{\omega_k} > \cdots$$

and for narrow-band filters designed according to the criteria of (28) or (29), then

$$|\delta_2| < |\delta_1| \ll 1$$

and the effect of this extra modulation term is small.

The instantaneous phase for a single pulse is, from the definitions in (59) and the relations (57) and (58),

$$\chi_k^{(n)} = \tan^{-1}\left[\frac{S_n}{\bar{S}_n}\right] = \omega_k\left[t - t_p^{(n)} + \frac{\psi_n}{\omega_k} - \frac{\Phi_g}{2\omega_k}\right] \tag{63}$$

with $t_p^{(n)}, \psi_n$ and Φ_g defined previously. This result is, of course, accurate when t is close to $t_g^{(n)}$, the group arrival time for the nth signal pulse. When t is, in fact, equal to $t_g^{(n)}$, then the phase factor ψ_n is negligible, as can be seen from (56). Since $\chi_k^{(n)}$ is a calculable function of time, then (63) can be used to compute the phase time $t_p^{(n)}$; given that the group time can be otherwise determined (see the next section) and the phase factor Φ_g is either entirely negligible, which is usually the case, or has been estimated from the variation of the measured $t_g^{(n)}$ versus frequency. In this case, $t_p^{(n)}$ can be used to obtain a phase velocity estimate, as a function of frequency, using its definition given in (15). In addition, the instantaneous phase, when measured for three components of the displacement, can be used to determine the polarization of the wave field as a function of frequency. In all cases, the functions derived are valid approximations to the true variable, such as phase velocity and polarization, only at the times very near the group times, t_g, for the signal in question.

The instantaneous frequency for the nth signal pulse $\Omega_k^{(n)}$, is, from (51):

$$\Omega_k^{(n)}(t;\omega_k) = \frac{d\chi_k^{(n)}}{dt} = \left[\bar{S}_n \frac{dS_n}{dt} - S_n \frac{d\bar{S}_n}{dt}\right] / [\bar{S}_n^2 + S_n^2] \tag{64}$$

The time derivatives appearing here are, using (57) and (58):

$$\begin{aligned} \frac{dS_n}{dt} &= \omega_k\left[1 + \frac{A_n^{(1)}}{A_n^{(0)}}\left[\frac{\Delta\omega_k^2}{2\beta}\right]\right]\bar{S}_n - \left[\frac{\Delta\omega_k^2}{2\beta}\right](t - t_g^{(n)})\, S_n + O(\Delta\omega_k^4) \\ \frac{d\bar{S}_n}{dt} &= -\omega_k\left[1 + \frac{A_n^{(1)}}{A_n^{(0)}}\left[\frac{\Delta\omega_k^2}{2\beta}\right]\right]S_n - \left[\frac{\Delta\omega_k^2}{2\beta}\right](t - t_g^{(n)})\, \bar{S}_n + O(\Delta\omega_k^4) \end{aligned} \tag{65}$$

Forming the relation for $\Omega_k^{(n)}$ therefore gives, from (64):

$$\Omega_k^{(n)}(t;\omega_k) = \omega_k \left[1 + \frac{A_n^{(1)}}{A_n^{(0)}} \left[\frac{\Delta\omega_k^2}{2\beta} \right] \right] + O(\Delta\omega_k^4) \qquad (66)$$

where the terms involving the time factor $(t - t_g^{(n)})$, appearing in the relations of (65), cancel out.

From (66) it is apparent that, to first order the instantaneous frequency function is constant and equal to the center frequency of the Gaussian filter used. However, accounting for terms of second order in the filter bandwidth $\Delta\omega_k$, produces the interesting result that the constant frequency value is shifted somewhat and in a manner proportional to the first frequency derivative of the amplitude spectrum of the signal. More specifically, when the ratio of the first frequency derivative of the spectrum to the spectral amplitude itself (i.e., $A_n^{(1)}/A_n^{(0)}$) becomes relatively large, as would occur in the vicinity of a sharp spectral minimum, then this term can become quite significant in size and result in a large deviation from the filter center frequency, ω_k. In particular this second order term should give a double spike similar to a derivative of a delta function centered at the spectral minimum of the signal. Such behavior is, in fact, observed to occur, as is noted in the examples of later sections.

Relationships between Envelope Function Maxima and Signal Group Arrival Times

The most important and useful feature of the envelope function is the fact that its maxima occur at, or more accurately near, the times $t = t_g^{(n)}$. This allows the group arrival times to be estimated for each frequency ω_k. Further at these times the amplitude of the envelope will be near $A_n^{(0)}(\omega_k)$.

To show this explicitly and to obtain quantitative results, consider the location of the envelope function maxima at $t = t_m^{(n)}$ as given by

$$\left[\frac{dE_k^{(n)}}{dt} \right]_{t_m^{(n)}} = 0$$

We have, using (61) and (62):

$$\frac{dE_k^{(n)}}{dt} = A_n^{(0)} e^{\frac{-\Delta\omega_k^2}{4\beta}(t-t_g^{(n)})^2}(t-t_g^{(n)})\left[\frac{\delta_2}{(1+\delta_1)+\delta_2(t-t_g^{(n)})^2} - \frac{\Delta\omega_k^2}{2\beta}\right]\left\{(1+\delta_1)+\delta_2(t-t_g^{(n)})^2\right\}^{1/2}$$

Thus maxima occur at:

$$t_m^{(n)} = t_g^{(n)} \; ; \; n=1,2,\ldots,N. \tag{67}$$

with amplitudes given by

$$E_k^{(n)}(t_g^{(n)};\omega_k) = A_n^{(0)}(\omega_k)\left[1+\frac{A_n^{(2)}}{2A_n^{(0)}}\left[\frac{\Delta\omega_k^2}{2\beta}\right]\right] \tag{68}$$

when $E_k^{(n)}$ is represented by (58). That is, when terms of order $[\Delta\omega_k^2/2\beta]^2$ are negligible in the modulation function M_n, as in (54), then envelope maxima are predicted to occur at precisely the $t_g^{(n)}$ group times. Further the envelope amplitude, at its maxima, gives a measure of the signal Fourier spectrum at each frequency ω_k. Note that the maxima times do not explicitly depend on the condition that polynomial coefficients δ_1 and δ_2 be small - although for a truncated polynomial to be a valid approximation for M_n it is necessary that this be so. Clearly at some stage the "roughness" in the amplitude and group arrival time as functions of frequency must result in a shift of the maxima away from the $t_g^{(n)}$ values.

In fact, it is not difficult to obtain estimates of the shift in the envelope maxima due to non-negligible effects of dispersion and amplitude spectra roughness (as measured by the frequency derivatives of the signal amplitude spectra and group arrival times). This is simply achieved by including the next higher order terms for the representation of $M_n^{(1)}$ and $M_n^{(2)}$, in the expression (57), for the envelope function. In particular, we have:

$$E_k^{(n)}(t;\omega_k) = \frac{1}{2\pi}\left[(M_n^{(1)})^2+(M_n^{(2)})^2\right]^{1/2} e^{\frac{-\Delta\omega_k^2}{4\beta}(t-t_g^{(n)})^2} \tag{69-a}$$

with

$$M_n^{(1)} = a_1 + a_2(t - t_g^{(n)}) + a_3(t - t_g^{(n)})^2$$

$$M_n^{(2)} = a_4 + a_5(t - t_g^{(n)}) \qquad (69\text{-b})$$

where;

$$a_1 = A_n^{(0)}\left[1 + \frac{1}{2}\frac{A_n^{(2)}}{A_n^{(0)}}\left[\frac{\Delta\omega_k^2}{4\beta}\right] + \frac{1}{8}\frac{A_n^{(4)}}{A_n^{(0)}}\left[\frac{\Delta\omega_k^2}{2\beta}\right]^2 + \frac{1}{8}\left[\frac{dt_g^{(n)}}{d\omega}\right]_{\omega_k}\left[\frac{\Delta\omega_k^2}{2\beta}\right]^2\right]$$

$$a_2 = A_n^{(0)}\left[\frac{A_n^{(1)}}{A_n^{(0)}}\left[\frac{dt_g^{(n)}}{d\omega}\right]_{\omega_k} + 3\left[\frac{d^2t_g^{(n)}}{d\omega^2}\right]_{\omega_k}\right]\left[\frac{\Delta\omega_k^2}{2\beta}\right]^2$$

$$a_3 = -A_n^{(0)}\left[\frac{A_n^{(2)}}{2A_n^{(0)}}\right]\left[\frac{\Delta\omega_k^2}{2\beta}\right]^2$$

$$a_4 = -A_n^{(0)}\left[3\left[\frac{d^3t_g^{(n)}}{d\omega^3}\right]_{\omega_k} + 3\frac{A_n^{(1)}}{A_n^{(0)}}\left[\frac{d^2t_g^{(n)}}{d\omega^2}\right]_{\omega_k} + \frac{1}{2}\frac{A_n^{(2)}}{A_n^{(0)}}\left[\frac{dt_g^{(n)}}{d\omega}\right]_{\omega_k}\right]\left[\frac{\Delta\omega_k^2}{2\beta}\right]^2$$

$$a_5 = A_n^{(0)}\left[\frac{A_n^{(1)}}{A_n^{(0)}}\left[\frac{\Delta\omega_k^2}{2\beta}\right] + \frac{1}{2}\frac{A_n^{(3)}}{A_n^{(0)}}\left[\frac{\Delta\omega_k^2}{2\beta}\right]^2\right]$$

Now forming the derivative $dE_k^{(n)}/dt$ and retaining terms to order $\Delta\omega_k^4$, we find maxima of $E_k^{(n)}$ at times $t_m^{(n)}$, given by the zeros of :

$$\delta_0 + \delta_1(t_m^{(n)} - t_g^{(n)}) = 0$$

where

$$\delta_0 = a_1 a_2 + a_4 a_5$$

$$\delta_1 = -\frac{\Delta\omega_k^2}{2\beta}(a_1^2 + a_4^2) + 2a_1 a_3 + a_2^2 + a_5^2$$

With terms of order $\Delta\omega_k^6$ retained, these coefficients are:

$$\delta_0 = (A_n^{(0)})^2\left[\frac{A_n^{(1)}}{A_n^{(0)}}\left[\frac{dt_g^{(n)}}{d\omega}\right]_{\omega_k} + 3\left[\frac{d^2t_g^{(n)}}{d\omega^2}\right]_{\omega_k}\right]\left[\frac{\Delta\omega_k^2}{2\beta}\right]^2$$

$$\delta_1 = (A_n^{(0)})^2 \left[1 + \frac{2A_n^{(2)}}{A_n^{(0)}} \left[\frac{\Delta\omega_k^2}{2\beta} \right] - \left[\frac{A_n^{(1)}}{A_n^{(0)}} \right]^2 \left[\frac{\Delta\omega_k^2}{2\beta} \right] \right] \frac{\Delta\omega_k^2}{2\beta} \tag{70}$$

Thus the maxima of the envelope function are at times t_m given by:

$$t_m^{(n)} = t_g^{(n)} + \delta t_m^{(n)} \tag{71}$$

where

$$\delta t_m^{(n)} = -\left[\frac{\delta_0}{\delta_1} \right] = \left\{ \left[\frac{A_n^{(1)}}{A_n^{(0)}} \right] \left[\frac{dt_g^{(n)}}{d\omega} \right]_{\omega_k} + 3 \left[\frac{d^2 t_g^{(n)}}{d\omega^2} \right]_{\omega_k} \right\} \frac{\Delta\omega_k^2}{2\beta} \Big/ \left\{ 1 + \left[2 \left[\frac{A_n^{(2)}}{A_n^{(0)}} \right] - \left[\frac{A_n^{(1)}}{A_n^{(0)}} \right]^2 \right] \frac{\Delta\omega_k^2}{2\beta} \right\} \tag{72}$$

It is sufficient, for "well designed" narrow-band Gaussian filters operating on pulse-like signals, to retain only terms of order $\Delta\omega_k^2$ in $\delta t_m^{(n)}$, so that in this case,

$$t_m^{(n)} = t_g^{(n)} + \left\{ \left[\frac{A_n^{(1)}}{A_n^{(0)}} \right] \left[\frac{dt_g^{(n)}}{d\omega} \right]_{\omega_k} + 3 \left[\frac{d^2 t_g^{(n)}}{d\omega^2} \right]_{\omega_k} \right\} \frac{\Delta\omega_k^2}{2\beta} + O(\Delta\omega_k^4) \tag{73}$$

The form of $\delta t_m^{(n)}$ is such that the shifts in the envelope function maxima away from $t_g^{(n)}$ values are small for pulse-like signals, for which:

$$\left| \frac{dt_g^{(n)}}{d\omega} \right|_{\omega_k} > \left| \frac{d^2 t_g^{(n)}}{d\omega^2} \right|_{\omega_k} > \left| \frac{d^3 t_g^{(n)}}{d\omega^3} \right|_{\omega_k} > \cdots$$

$$\left| A_n^{(0)}(\omega_k) \right| > \left| A_n^{(1)}(\omega_k) \right| > \left| A_n^{(2)}(\omega_k) \right| > \cdots$$

if the filter design criteria of (28) or (29) are satisfied. If the signals in question do not conform to the spectral smoothness criteria above, then other design criteria based on the reduction of $\delta t_m^{(n)}$ to a small number (relative to $t_g^{(n)}$), would be required. In either case, equation (72) or (73) can be used to (iteratively) correct the estimates of $t_g^{(n)}$, using measured $t_m^{(n)}$ values and first order estimates of the various derivatives appearing in these equations.

Since it is $t_m^{(n)}$ that is measurable, then clearly it is the amplitude of the envelope function at $t = t_m^{(n)}$ that can provide the consistently measured estimate of the spectra amplitude of the signal. This peak value for $E_k^{(n)}$ at $t = t_m^{(n)}$ is, from (69) and subsequent relations,

$$E_k^{(n)}(t_m^{(n)};\omega_k) \approx A_n^{(0)}(\omega_k)\left[1 + \frac{A_n^{(2)}}{2A_n^{(0)}}\left[\frac{\Delta\omega_k^2}{2\beta}\right]\right] \tag{74}$$

when carried to terms of order $\Delta\omega_k^2$. Comparison with the results for $E_k^{(n)}$ at $t = t_g^{(n)}$, given by equation (65), shows that we get the same value for the envelope maxima at $t_m^{(n)}$ when terms of order $\Delta\omega_k^4$ are neglibible. Thus the small shift in time of the envelope peak from the group arrival time of the signal does not significantly change the envelope amplitude value, since differences in the envelope amplitudes at $t_g^{(n)}$ and $t_g^{(n)} + \delta t_m^{(n)}$ are of order $\Delta\omega_k^4$.

The value of $E_k^{(n)}$ measured at $t_m^{(n)}$, will be very nearly equal to $A_n^{(0)}(\omega_k)$ - the Fourier spectral amplitude of the signal at ω_k - when the design criteria of (28) or (29) are met - since the second term in (74) will be much less than unity. We can therefore estimate the signal spectrum using

$$E_k^{(n)}(t_m^{(n)};\omega_k) \approx A_n^{(0)}(\omega_k)$$

as a good first approximation, and then obtain first and second derivative estimates from differencing the $A_n^{(0)}$ values obtained at the set of filter center frequencies (ω_k). These derivative estimates can then be used to obtain a higher order iterative estimate of $A_n^{(0)}$, employing (74). This procedure can, of course, also be used to get higher order estimates of the $t_g^{(n)}$ values, using (73) and (74) together.

References

Alexander, S. S. (1963), Surface wave propagation in the Western United States, Ph.D Thesis, California Institute of Technology, 241 pages.

Archambeau, C. B., J. C. Bradford, P. W. Broome, W. C. Dean, E. A. Flinn and R. L. Sax (1965), Data Processing techniques for the detection and interpretation of teleseismic signals, *Proceedings of the IEEE, vol. 53, no. 12,* December, pp. 1860-1884.

Archambeau, C. B. and E. A. Flinn (1965), Automated analysis of seismic radiation for source characteristics, *Proceedings of the IEEE, vol. 53, no. 12,* December, pp. 1876-1884.

Archambeau, C. B., E. A. Flinn and D. G. Lambert (1966), Detection, analysis and interpretation of teleseismic signals (1) Compressional phases from the SALMON event, *J. Geophys. Res., 71,* pp. 3483-3501.

Archambeau, C. B., E. A. Flinn and D. G. Lambert (1969), Fine structure of the upper mantle, *J. Geophys. Res., 74,* pp. 5825-5865.

Cara, M. (1973), Filtering of dispersed wave trains, *Geophys. J. R. Astr. Soc., 33,* pp. 6580.

Denny, M. D. and R. C. Y. Chin (1976), Gaussian filters for determining group velocities, *Geophys. J. R. Astr. Soc., 45,* pp. 495-525.

Dziewonski, A., S. Block and M. Landisman (1969), A technique for the analysis of transient seismic signals, *BSSA, 59,* no. 1, pp. 427-444.

Dziewonski, A., J. Mills and S. Block (1972), Residual dispersion measurement - A new method of surface wave analysis, *BSSA, 62,* pp. 129-139.

Flinn, E. A. (1965), Signal analysis using rectilinearity and direction of particle motion, *Proceedings of the IEEE, Vol. 53,* no. 12, pp. 1874-1876.

Harvey, D. J. (1981), Seismogram synthesis using normal mode superposition: The locked mode approximation, *Geophys. J. R. Astr. Soc., 66*, pp. 37-69.

Helstrom, C. W. (1960), *Statistical Theory of Signal Detection*, Pergamon Press, New York.

Instron, H. H., P. D. Marshall and C. Blamey (1971), Optimization of filter bandwidth in spectral analysis of wavetrains, *Geophys. J. R. Astr. Soc., 23*, pp. 243-250.

Kanamori, H. and D. Hadley (1975), Crustal structure and temporal velocity change in Southern California, *Pageoph, 113*, pp. 257-280.

Kanasewich, E. R. (1975), *Time Sequence Analysis in Geophysics*, University of Alberta Press, Edmonton, Alberta, Canada.

Lewis, B. T. R. and R. P. Meyer (1968), Seismic investigation of the upper mantle to the west of Lake Superior, *Bull. Seism. Soc. Amer., 58*, pp. 565-598.

Mims, C. H. and R. L. Sax (1965), Rectilinear motion detection: Seismic Data Laboratory Report 118, Teledyne Inc., Alexandria, Virginia, AD-460-631.

Montalbetti, J. F. and E. R. Kanasewich (1970), Enhancement of teleseismic body phases with a polarization filter, *Geophys. J. R. Astr. Soc., 21*, pp. 119-129.

Samson, J. C. (1977), Matrix and Stokes vector for polarized waveforms, with some applications to seismic waves, *Geophys. J. R. Astr. Soc., 51*, pp. 583-603.

Shimshoni, M. and S. W. Smith (1964), Seismic signal enhancement with three component detectors, *Geophysics, 29*, pp. 664-671.

Simons, R. S. (1968), A surface wave particle motion discrimination process, *Bull. Seism. Soc. Am., 58*, pp. 629-637.

CHAPTER I

INTRODUCTION

Historically, normal mode theory has been restricted in its applications to low frequency bandwidths; namely to low frequency spherical earth normal modes and to Rayleigh and Love surface waves for flat layered structures. In this dissertation I will show how spectral solutions of the elastic wave equation can be used to compute complete, high frequency synthetic seismograms for flat, plane layered, and laterally homogeneous structural models in an efficient manner. The method which I developed is most useful for computing synthetic seismograms in the zero to ten Hertz frequency range and for source-receiver distances of 10 to 1000 km. I have also been able to successfully apply the method to exploration geophysics problems with frequency bandwidths of 100 Hertz and source-receiver distances of several km. By making a simple modification to the structural model I am able to use this method to compute the P and S body waves, in addition to the surface waves, using only normal modes with real eigenwavenumbers. I am thus able to approximate a complete solution of the elastic wave equation with a mode sum which makes this approach much more efficient than existing complete solution methods which are based upon direct numerical integration such as the reflectivity method.

A variety of approachs have been used to synthesize the P and S body waves for laterally homogeneous structures, and all of these approachs start with a doubly transformed version of the elastic wave equation which remove the derivatives of time and the horizontal space coordinates. The

Part II - A Spectral Method for Computing Complete Synthetic Seismograms

Blank Page

methods differ by the solution of the transformed wave equation which is used and by the way in which the two inverse transform integrals are evaluated. The asymptotic methods evaluate either one or both of these integrals analytically by approximating the integrand function with suitable asymptotic expansions, and the resulting solution is a decomposition of the complete solution in terms of rays. These ray theories work well for synthesizing particular phases, but they can be cumbersome to use when trying to compute the complete solution, especially in certain distance ranges. For very near field distances (zero to ten km) and at teleseismic distances (greater than 1000 km) and for sources at typical earthquake depths, the elastic energy is propagating in a fundamentally vertical direction in the crust. This means that the scattering off of the large discontinuities in the P and S wave velocities that can occur in the crust and at the Mohorovicic discontinuity (Moho) can be represented by a relatively small number of ray paths, and so the major applications of ray theory have been in these distance ranges. In the 10 to 1000 km distance range however the crust acts as a waveguide and most of the elastic energy is contained within this waveguide and propagates in a fundamentally horizontal direction. In this distance range, when using a detailed crust and upper mantle model, ray theories require the a priori specification of a very large number of ray paths to synthesize the complete solution for the P and S body waves (a typical example of this is the P_g coda which is seen in the western United States).

Another category of seismogram synthesis techniques which have been used over the past fifteen years are the complete solution methods and these methods all differ from the ray theoretical methods by the solution of the doubly transformed elastic wave equation which is used. The complete

solution methods, as the name implies, use a complete solution of the doubly transformed elastic wave equation by allowing for all possible P and S wave propagation throughout the structural model and by treating this as a boundary value problem. When one uses a complete solution method it is only necessary to specify the structural model and frequency bandwidth to compute synthetic seismograms and these synthetics contain an infinity of rays. In contrast, ray theoretical methods require the user to specify ray paths and, based upon these specified ray paths, an incomplete solution is obtained. It is the use of this incomplete solution, in addition to certain other approximations which are usually made, that causes the ray theoretical methods to be much more efficient than complete solution methods and it is primarily this efficiency that has made ray theoretical methods so popular.

The complete solution methods are themselves broken down into two general categories which I refer to as the reflectivity method and the spectral method and these methods differ in the way in which the two inverse transform integrals are evaluated. I am using the reflectivity method to refer to all methods which compute both integrals in a direct numerical manner although the original reflectivity method, as developed by Fuchs and Muller (1971), is rather restrictive in terms of the horizontal phase velocity range over which it works. Owing to recent developments (Kind (1978), Kennett and Kerry (1979), Kennett (1980), Cormier (1980), Bouchon (1981)) the reflectivity method can now be used to compute complete seismic codas for arbitrary frequency bandwidths and source depths and for vertically inhomogeneous structural models. If the reflectivity method were also efficient, then the problem of computing complete synthetic seismograms for flat, laterally homogeneous earth models could be

considered to be solved however the reflectivity methods are very computationally expensive and this expense is proportional to the product of the frequency bandwidth and the maximum source-receiver distance. In fact the computational expense is so high that it limits the use of these methods to low frequency bandwidths for cases where the complete seismic coda is computed.

One obvious way of increasing the efficiency of complete solution methods is to analytically evaluate at least one of the inverse transform integrals as is done by most ray theoretical methods. Unfortunately the complexity of the complete solution integrand function, for generally complex structural models, frustrates efforts to apply the types of techniques which are used by ray theoretical methods to eliminate the numerical evaluation of the inverse transform integrals. There is one straightforward method however which we can always use to evaluate at least part of one of the inverse transform integrals analytically and this method makes use of the residue theorem. We can extend the integration path in the complex plane into a closed contour and then evaluate the original integral in terms of a sum of residues which are caused by the poles of the integrand function which are contained within the contour of integration. These poles correspond to flat earth normal modes and for structural models which have totally reflective top and bottom boundaries, one of the inverse integral transforms can be expressed as an infinite sum of normal modes. The cases of most interest in seismology are for structural models which have a free top boundary and an infinite homogeneous half space on the bottom and for these situations one of the inverse integral transforms can be expressed as a finite sum of normal modes along with branch cut integrals which come about due to the semi-infinite nature of the structural model.

I refer collectively to methods which use the residue theorem to evaluate one of the inverse transform integrals as the spectral method. Although this method has not been as popular as the reflectivity method for computing complete synthetic seismograms, it has undergone parallel developments and improvements with the reflectivity method. The first uses of the spectral method actually predate the reflectivity method since the spectral method is the basis behind the computation of synthetic, flat earth, Rayleigh and Love fundamental surface waves however, among the earliest uses of the spectral method for computing a substantial portion of the complete seismic coda, are those of Knopoff, et. al. (1973), Nakanishi, et. al. (1977), and Mantovani, et. al. (1977) who used a sum of SH normal modes to compute synthetic SH seismograms. More recently Swanger and Boore (1978) computed both SH and P-SV synthetic seismograms for near field strong motion studies using a normal mode sum. All of these uses of the spectral method had one thing in common which was that a small number of normal modes was included in the mode sum and this resulted in rather incomplete solutions to the elastic wave equation.

One fundamental difficulty, which had a large effect on both the development of the complete solution methods and their ranges of applicability, was a numerical instability which seened to be inherent in the complete solution form of the P-SV integrand function. This numerical instability was always associated with the presence of inhomogeneous or evanescent waves within the elastic medium which exist at horizontal phase velocities that are less than the local P or S wave velocity. This problem was first recognized by Dorman, et. al. (1960) when the complete matrix solution formalism of Thomson (1950) and Haskell (1953) was applied to the problem of computing Rayleigh dispersion curves using an early digital computer.

Although the numerical problem was circumvented for the computation of the fundamental Rayleigh dispersion curve by the use of structural layer reduction, it wasn't until Knopoff (1964) applied Laplace's development by minors to the problem of computing the Rayleigh characteristic function that the numerical problem was formally addressed in an analytical manner. Knopoff's work was the seed for an area of research which was followed by Dunkin (1965), Watson (1970) and most recently by Abo-Zena (1979) and all of this research was aimed at streamlining Knopoff's original method and understanding why it worked as well as it did. The method completely solved the numerical instability problem, as related to computing the Rayleigh characteristic function and thus the Rayleigh dispersion curves, for all frequency bandwidths and structural models.

Although Knopoff's method works quite well for computing the Rayleigh characteristic function it does not address the problem of numerical instabilities which are present in the computation of the depth dependent stress and displacement eigenfunctions. Because of this it has not been possible to use the spectral method to compute P-SV synthetic seismograms for buried sources and at high frequencies when using the Knopoff modified version of the Thomson-Haskell matrix formalism. Thus we can see that there are actually two numerical instability problems which must be solved in order to use the spectral method to compute P-SV synthetic seismograms for arbitrary sources and frequencies, and my research has focused on extending Knopoff's method to solve the eigenfunction numerical problem.

The same numerical difficulties that plagued the spectral method were encountered with the reflectivity method. The original method as given by Fuchs and Muller was based directly on the original Thomson-Haskell matrix method and they avoided the numerical problems by

limiting the range of phase velocities to those for which there were no evanescent waves within the structure. This narrowed the range of applicability of the reflectivity method until Kind (1978) applied Knopoff's method to remove the numerical instabilities. Kind also reformulated the integrand function in a manner which he claimed eliminated the numerical instabilities associated with buried sources. A completely different and novel approach was taken by Kennett, et. al. (1978), Kennett and Kerry (1979) and Kennett (1980) to solve the numerical problems of the reflectivity method which was not an extension of Knopoff's original work. They showed how the doubly transformed complete solution of the elastic wave equation could be expressed in terms of a set of generalized reflection and transmission functions. They then showed how all growing exponential solutions could be eliminated in this ray-like representation of the complete solution and this eliminated the numerical instabilities for all source depths.

The most recent developments of the spectral method have focused on solving the numerical problems for arbitrary frequencies, source depths, and structural models and extending the completeness of the spectral solutions. All of the earlier uses of the spectral method used only a small number of normal modes and thus produced rather incomplete solutions. Harvey (1981) and Kerry (1981) were the first researchers to use all of the normal modes with real eigenwavenumbers and I refer to spectral synthetic seismograms produced in this manner as locked mode synthetics. The branch cut integral contributions are ignored when using the locked mode method which gives the most complete spectral solution possible without using numerical integration or without locating poles off of the real wavenumber axis. At about the same time Wang and Herrmann (1980) developed a truly complete spectral solution by including both a numerical

integration of the branch cuts along with all of the locked mode residues.

As with the reflectivity method, the development of numerically stable algorithms to use in the spectral method has followed two paths. Kerry (1981) directly applied the methods developed by Kennett, et. al. which reformulated the frequency-wavenumber solution of the elastic wave equation in terms of generalized reflection and transmission functions. I chose to extend Knopoff's method, which operates directly with the Thomson-Haskell matrix formalism and uses stress and displacement functions to describe the elastic propagation, and the numerical algorithms which I developed constitute a substantial portion of my research. Kerry's locked mode method comes the closest to my own both in terms of the basic way in which it works and its range of applicability and I will be comparing these two methods throughout this dissertation.

The research which I will be describing in the following chapters has as its basic objective the development of an optimally fast, accurate and complete spectral method for computing P-SV synthetic seismograms for flat, plane layered, laterally homogeneous structural models. An equally important criterion which I placed on the method is that it work for the widest possible range of frequency bandwidths and structural models. I adopted this last criterion to cover problems such as high frequency P_n and S_n wave propagation in oceanic structural models with liquid and near-liquid layers and very high frequency near surface wave propagation in structural models which have numerous strong low velocity zones for problems in earthquake hazards engineering and geophysical exploration.

Since eigensolutions of the elastic wave equation can be thought of as providing optimal sampling in the wavenumber domain, spectral methods should be able to provide the most efficient way to compute

complete synthetic seismograms. I feel that one of the fundamental reasons that the spectral has not seen the popularity of the reflectivity method has been the lack of an efficient and reliable normal mode searching algorithm. A substantial portion of my research has been devoted to developing a truly fast, accurate and completely reliable mode searching algorithm in order to realize the potential efficiency of the spectral method. Also, in order to maximize the efficiency, it was desirable to compute nearly complete synthetic seismograms without making numerical evaluations of the branch cut integrals. For normal structural models locked mode synthetic seismograms will not contain any P wave arrivals since they are typically part of the branch cut integral contribution however, by making a simple modification to the structural model, one can significantly extend the phase velocity range which will be represented in the locked mode synthetic seismograms while simultaneously insuring that a certain time window within the synthetic seismograms will be uncontaminated by the structural modification. When the locked method is applied to such modified structural models, I refer to this as the locked mode approximation which produces nearly complete synthetic seismograms while only using normal modes with real eigenwavenumbers.

In chapter two I review the basic theory for computing flat earth normal modes and the resulting displacements. Most of this draws upon previously published work however I will present a complete and consistent derivation starting with the elastic wave equation and ending with the spectral solution for flat, plane layered, isotropic and laterally homogeneous models. During this derivation I will indicate the departure points of the various seismogram synthesis methods and I will also point out the sources of the numerical instabilities. The final solution which I derive will be

expressed in terms of proper and improper eigenfunctions representing respectively the discrete normal modes and the continuous branch cut integrals.

In chapter three I will address the numerical instabilities which are inherent in the Thomson-Haskell matrix formulation and I will present two methods which overcome these instabilities. I start by reviewing Knopoff's method, along with the later work which was based upon it, and I give the derivation of a numerically stable computation of the Rayleigh characteristic function. I then describe a simple method for stabilizing the depth dependent stress and displacement eigenfunctions which works quite well for completely elastic structural models with monotonically increasing velocities with depth except for no more than one weak low velocity zone. The locked mode method when using this algorithm is functionally equivalent to the method developed by Kerry and I discuss the restrictions which these methods have in common. I then proceed to derive a much more robust method of computing numerically stable eigenfunctions which has virtually no restrictions. This method works for oceanic models as well as for complex elastic models with multiple strong low velocity zones and at arbitrary frequency bandwidths. I finally show numerical examples of depth dependent eigenfunctions using the two methods for several different structural models.

In chapter four I describe the numerical algorithms and computer programs which I developed to implement the computation of locked mode synthetic seismograms from a starting structural model to the final, three component time traces at specified receiver locations. The first step in this process is the normal mode searching algorithm which locates the Rayleigh and Love dispersion curves and I go into considerable detail to describe the

algorithm which I developed. The next step involves the computation of certain partial derivatives which are necessary for eigenfunction normalization and which I use in a first order perturbation approximation to account for the effects of frequency dependent anelastic attenuation in the structural model. I give analytic expressions for these derivatives and I show how the first order attenuation approximation can be computed and applied in a fast manner which does not require the use of complex arithmetic. In the next section I describe the actual computer programs which I wrote and the user interface with these programs. I discuss practical matters such as the algorithms which require the use of double precision arithmetic, the amount of core memory required by each program, the approximate run times of the programs, and the structure and size of the intermediate data files which link the programs together. I then formally present the locked mode approximation and show when the approximation breaks down. In this section I also show synthetic seismograms produced by the locked mode approximation and how spurious arrivals caused by the approximation can be controlled. Finally I show comparisons of synthetic seismograms produced by the locked mode approximation with synthetics for the same structural models which were generated using other complete solution methods.

Chapter five is devoted to showing examples of synthetic seismograms produced by the locked mode approximation for a variety of frequency bandwidths, structural models and source-receiver distances. In the first part of the chapter I show a number of examples which illustrate the characteristics of elastic wave propagation which can be seen when using a complete solution method. I then show an example in which theoretical seismograms using the locked mode approximation are compared to real observed data. This example involves modelling an underground nuclear

explosion which took place in northern New Mexico and for which receivers recorded seismograms in the 10 to 100 km distance range and the 0 to 10 Hertz frequency range. This is a well constrained example since both the source and the structure were known and since the structure was closely approximated by a flat layered half space.

In chapter six I conclude the dissertation by summarizing the relative advantages and disadvantages of the locked mode approximation when compared to other seismogram synthesis techniques. The possibility of future extensions of my research are discussed which would extend the range of applicability of the methods which I have developed while maintaining the efficiency.

CHAPTER II

THE FUNDAMENTALS OF NORMAL MODE THEORY FOR FLAT LAYERED STRUCTURES

Although the development of the theoretical basis for elastic wave propagation can be traced all the way back to Lord Rayleigh's time, the first occurrence of the complete solution of the elastic wave equation in cylindrical coordinates and for flat, plane layered, isotropic and laterally homogeneous elastic media is given by Sezawa (1931). He uses a transformed version of the elastic wave equation which eliminates all derivatives except for the depth derivatives and thus he reduces the problem of solving the elastic wave equation to one of solving several ordinary differential equations and evaluating inverse integral transforms. The form of the solution which Sezawa presents is identical to that used by all modern day seismologists who work in cylindrical coordinates.

Sezawa did not give solutions for the depth dependent ordinary differential equations for arbitrary vertical velocity distributions and the next major development was aimed at solving these equations. Thomson (1950) derived a solution for the depth dependent differential equations which was expressed in terms of recursive matrix multiplications. Thomson's method applied to elastic structures which were composed of planar, isotropic and completely homogeneous layers which were welded together along their top and bottom surfaces. Although each layer had to be homogeneous there was no restriction on the number of different layers that were welded together or on the thinness of each layer and so, in the limit of

an infinite number of infinitesimally thin layers, Thomson's method provided complete solutions of the depth dependent differential equations for arbitrary vertical velocity profiles. Haskell (1953) embraced Thomson's approach and basically streamlined it and applied it to produce numerical computations of the fundamental Rayleigh dispersion curve for several simple structural models. The Thomson-Haskell matrix method has provided a formalism for obtaining complete solutions of the elastic wave equation and, as with Sezawa's work, this has become one of the basic tenets of a large branch of subsequent research.

It wasn't until digital computers became generally available that the next major developments in the theory of seismic wave propagation in cylindrical coordinates took place. In the early sixties a number of researchers applied the Thomson-Haskell matrix method to write computer programs for locating Rayleigh dispersion curves (e.g. Dorman, et. al. (1960), Press, et. al. (1961)). Numerical instabilities in the Thomson-Haskell method were discovered at this time however these instabilities occurred at frequencies which were above the range of interest of the researchers. Harkrider (1964) made the next major contribution by showing how to compute time domain synthetic seismograms for Rayleigh and Love surface waves and for arbitrary point sources at arbitrary depths. This research was based directly on the Thomson-Haskell matrix method and it suffered an additional numerical instability associated with the source depth.

In the following chapter I give a condensed yet complete summary of linear elastic wave theory for flat, plane layered, laterally homogeneous structures. This treatment will draw primarily from the work of Harkrider (1964) and Ben-Menahem and Singh (1972 and 1981) who show how a complete solution of the elastic wave equation can be expressed in

terms of vector cylindrical harmonics, but in order to preserve continuity, I will use my own notation and layering conventions. I will show how normal mode solutions are derived from the general solutions of the elastic wave equation and to what extent these solutions are related to other types of solutions such as ray theoretical and reflectivity solutions. I will also point out both accuracy and efficiency problems which come up in the numerical implementation of the theory. These problems will be addressed in detail in subsequent chapters and constitute the major portion of my research.

2.1 Basic Assumptions

In order to obtain tractable solutions of the elastic wave equation it is necessary to make a number of assumptions. Most of the assumptions I have made fall in this category and are absolutely necessary in order to solve the problem at all. I have however made a few additional assumptions which were made primarily to narrow the range of the problem and I will outline the necessary steps which must be taken to remove these assumptions.

The first assumption is that of a linearized elastic wave equation. This is widely used and accepted by seismologists and is justified by the small amplitudes of differential strains that are produced globally by most seismic disturbances. The exception to this is in the near vicinity of a large, non-linear seismic source such as an earthquake or a nuclear explosion. Even in these cases we can consider the elastic wave field to be linear beyond some volume which encloses the non-linear source region and represent the source by an equivalent linear point source (e.g. Bache and Harkrider (1976)). In this case our solution will be invalid within the non-linear region but will be valid outside that region.

The second assumption is an earth structure which is laterally homogeneous. This is the most restrictive assumption and considering the attention that seismogram synthesis for laterally homogeneous structures has received in the past, some justification is deserved at this point. I justified the laterally homogeneous assumption based upon the following three premises:

1. A starting point for the solution of certain laterally inhomogeneous problems is an accurate, efficient and complete solution to the laterally homogeneous problem.
2. Although much work has been directed towards the laterally homogeneous problem, an accurate efficient and complete solution is yet to be realized.
3. Spectral solutions of the elastic wave equation promise the most efficient solution to the problem, at least when compared to the methods used presently.

The second premise can be justified by a quick review of existing methods for synthesizing seismograms for laterally homogeneous structures. These methods fall into two general categories: ray theoretical methods and complete solutions methods. Ray theoretical methods, although efficient and accurate, do not, in general, provide complete solutions (Hartzell and Helmberger (1982)). The complete solution methods are all closely related to the original reflectivity method (Fuchs and Muller, (1972)) and suffer from being rather inefficient. This is due to the direct numerical integration approach used by all of these methods to compute the inverse Hankel transform. Discrete spectral representations of the solution, however, allow for the inverse Hankel transform to be evaluated analytically in terms of a residue sum which, in addition to avoiding the accuracy problems associated

with direct numerical integration, also provides a more efficient solution as I will show later.

The third assumption is the flat earth approximation. This is not at all restrictive and can be easily justified for several reasons. First of all, as will be shown later, the major applicability of the spectral method will be for near field problems where the flat earth approximation is quite good on its own. If the source receiver distances become large, a flattening correction can be applied to the vertical structural dependence which will give very good solutions out to teleseismic distances. It should be pointed out that *all* ray theoretical solutions end up making the flat earth approximation implicitly by using the Poisson sum formula to convert discrete sum solutions in terms of spherical wave functions to continuous integral solutions in terms of cylindrical or Cartesian wave functions.

The fourth assumption is that the earth structure will be made up of homogeneous layers connected by flat plane interfaces. At first this may appear to be a restrictive assumption, but we can represent any arbitrary depth dependence for some finite wave length by specifying a large number of suitably thin layers. The question, then, is whether it is more efficient and accurate to use a large number of homogeneous layers or a smaller number of inhomogeneous layers and I will address this question in more detail in a later section.

The fifth assumption is that the earth structure will be isotropic. This restriction can be reduced to that of lateral isotropy without any fundamental change in the analytical development of the solution although with the expense of significantly increased algebraic complexity.

The sixth assumption is that the source of seismic energy will be a spatial point source. Once again this is not a restrictive assumption since any distributed source can be represented as either an equivalent point source or a linear superposition of a large number of point sources placed along the boundary of the distributed source.

2.2 Differential Equations, Coordinate Systems, and Boundary Conditions

The most general representation of the linearized elastic wave equation in Cartesian coordinates is:

$$\sigma_{ij,j} + \rho f_i = \rho \ddot{u}_i \tag{2.2.1}$$

where σ_{ij} is the space and time dependent stress tensor, f_i is the space and time dependent applied body forces, ρ is the space dependent density and u_i is the space and time dependent displacement vector. Integer indices range from one to three with the implied summation convention. Partial differentiation is indicated by $,j = \partial/\partial x_j$ and $\ddot{} = \partial^2/\partial t^2$.

The stress tensor is related to the displacements through the constitutive tensor, C_{ijkl}:

$$\sigma_{ij} = C_{ijkl}\, u_{k,l}. \tag{2.2.2}$$

Using the first law of thermodynamics and assuming adiabatic elastic deformations, one can show:

$$C_{ijkl} = C_{klij}, \tag{2.2.3}$$

and since the stress and strain tensors are symmetric,

$$C_{ijkl} = C_{jikl} = C_{ijlk} = C_{jilk}. \tag{2.2.4}$$

Equations (2.2.3) and (2.2.4) reduce the number of independent components

in C_{ijkl} to 21 and this is the number of elastic constitutive parameters which must be specified for a general anisotropic material. Since we have assumed a linearized elastic wave equation, each of these parameters depend only on the spatial coordinates and not on the displacement or any of its derivatives. Also, since we assumed a laterally homogeneous structure, the elastic constitutive parameters (along with the density) will only be dependent on one spatial coordinate, x_3.

If we assume lateral isotropy about the x_3 axis, the number of independent elastic constitutive parameters reduces from 21 to 5 and following the notation of Takeuchi and Saito (1972) we represent these parameters with the coefficients A, C, F, L and N in expression (2.2.2).

$$\sigma_{11} = A(u_{1,1} + u_{2,2}) - 2Nu_{2,2} + Fu_{3,3} \tag{2.2.5}$$

$$\sigma_{22} = A(u_{1,1} + u_{2,2}) - 2Nu_{1,1} + Fu_{3,3}$$

$$\sigma_{33} = F(u_{1,1} + u_{2,2}) + Cu_{3,3}$$

$$\sigma_{23} = L(u_{2,3} + u_{3,2}) = \sigma_{32}$$

$$\sigma_{31} = L(u_{3,1} + u_{1,3}) = \sigma_{13}$$

$$\sigma_{12} = N(u_{1,2} + u_{2,1}) = \sigma_{21}$$

For the case of a completely isotropic material,

$$A = C = \lambda + 2\mu \,, L = N = \mu \,, F = \lambda \tag{2.2.6}$$

where λ and μ are the Lamé elastic parameters and we can rewrite equation (2.2.2) in the following familiar form:

$$\sigma_{ij} = \lambda \, \delta_{ij} u_{k,k} + \mu(u_{i,j} + u_{j,i}) \,. \tag{2.2.7}$$

Typically the elastic parameters are redefined in terms of the P and S wave

velocities in a homogeneous isotropic material

$$\alpha = \sqrt{(\lambda + 2\mu)/\rho}\,, \quad \beta = \sqrt{\mu/\rho} \tag{2.2.8}$$

For the case of a laterally isotropic material we can also define the elastic parameters in terms of horizontal and vertical propagating P and S wave velocities.

$$\alpha_H = \sqrt{A/\rho}\,, \alpha_V = \sqrt{C/\rho}\,,$$
$$\beta_H = \sqrt{N/\rho}\,, \beta_V = \sqrt{L/\rho} \tag{2.2.9}$$

and we are left over with a fifth coefficient, F.

The constitutive relations (2.2.5) and (2.2.7) along with the elastic parameters allow us to model either a full elastic material or an acoustic, liquid material by setting $\beta = 0$. We can also model an anelastic material by allowing the elastic moduli to have non-zero imaginary components and this will be addressed in more detail in a later chapter.

In order to easily represent the radiation field from point sources and to match boundary conditions at horizontal layer interfaces, the coordinates will be changed from Cartesian to a cylindrical coordinate system and all of the following analytical developments will be done in cylindrical coordinates. The cylindrical coordinate system is shown in Figure 2-1 along with layer numbering conventions. At a later point in the theoretical development the assumption of a layered structure will be made and since I will be writing solutions of the wave equation in each individual layer and then matching boundary conditions throughout the stack, I employ both a global coordinate system and a set of local coordinates, each relative to an individual layer. The origin of the global coordinate system will be at the free surface with the positive z-axis pointing down. The origin of a local

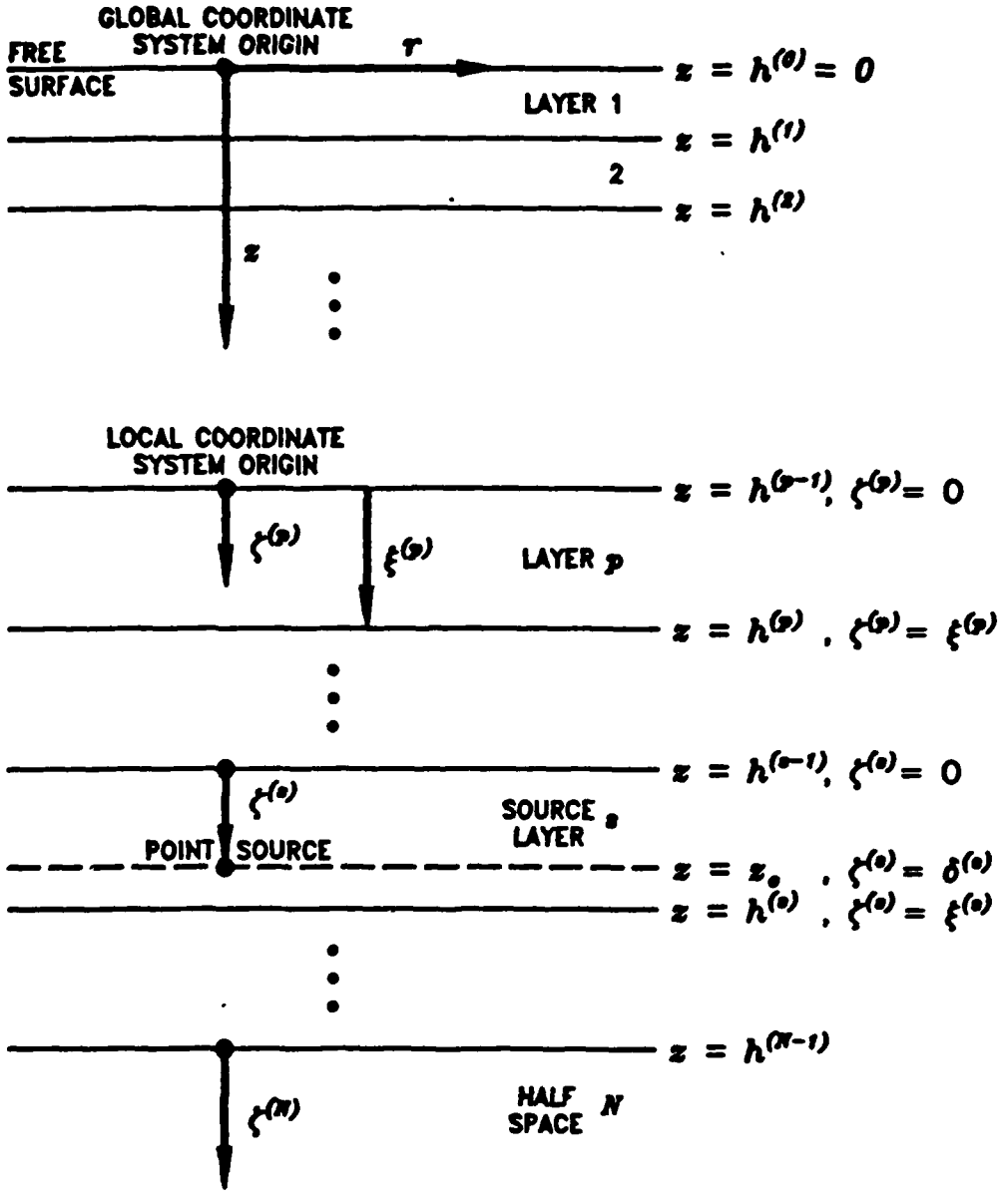

Figure 2-1. These are the coordinate systems and layer numbering conventions which are used in the theoretical development.

coordinate system will be at the top of the layer, with the radial and azimuthal coordinates being the same for all of the coordinate systems.

I distinguish between the global and local vertical coordinates by using an unsubscripted or unsuperscripted z for the global coordinate and a superscripted $\zeta^{(p)}$ for local coordinates where p is the layer index. The depth of the bottom of the p^{th} layer in global coordinates is $z = h^{(p)}$ whereas the thickness of the p^{th} layer is $\xi^{(p)}$, $(\xi^{(p)} = h^{(p)} - h^{(p-1)})$. This dual representation is used for all of the functions of z as well. Whenever a function of z appears without a layer superscript it is understood that the argument will be in global coordinates and whenever a layer superscript does appear, then the argument of the function will be in local coordinates. Thus for some function, f(z)

$$f(z) \Big|_{z = h^{(p-1)} + \zeta^{(p)}} = f^{(p)}(\zeta^{(p)}) \qquad (2.2.10)$$

By making the flat earth and laterally homogeneous assumptions, the elastic moduli and density will be dependent only on the z coordinate and the lateral isotropy assumption will imply isotropy about the z-axis.

The boundary conditions will be specified either in terms of displacements and tractions, or in terms of wave field functions (radiation condition). The displacements are denoted by $u_r(r,\theta,z;t)$, $u_\theta(r,\theta,z;t)$, $u_z(r,\theta,z;t)$, and the tractions across a horizontal plane are $T_r(r,\theta,z;t)$, $T_\theta(r,\theta,z;t)$, and $T_z(r,\theta,z;t)$. The boundary conditions are as follows:

1. A traction-free surface will exist at the top of the structure ($z = 0$),

$$T_r(r,\theta,0;t) = T_\theta(r,\theta,0;t) = \qquad (2.2.11)$$
$$= T_z(r,\theta,0;t) = 0 \quad \text{for all } r,\theta,t\ .$$

2. Either a radiation condition will exist for a semi-infinite bottom layer,

$$\text{no sources at } z = \infty\ , \qquad (2.2.12)$$

or a plate boundary condition will exist for the underside of the bottom layer at $z = H$ which can be specified in several ways; either

$$T_r(r,\theta,H;t) = T_\theta(r,\theta,H;t) = T_z(r,\theta,H;t) = 0 \text{ for all } r,\theta,t, \qquad (2.2.13)$$

or

$$u_r(r,\theta,H;t) = u_\theta(r,\theta,H;t) = u_z(r,\theta,H;t) = 0 \text{ for all } r,\theta,t, \qquad (2.2.14)$$

or

$$T_r(r,\theta,H;t) = T_\theta(r,\theta,H;t) = u_z(r,\theta,H;t) = 0 \text{ for all } r,\theta,t\ . \qquad (2.2.15)$$

The mixed boundary condition given by (2.2.15) insures no conversion of P to S energy at the plate bottom or vice versa.

3. Tractions and displacements will be continuous along the z-axis for all r,θ, and t as long as the elastic moduli are continuous except at the source location.

4. For a horizontal interface at $z = h$ where the elastic moduli change discontinuously, the boundary conditions will be specified according to the type of discontinuity. For a solid-solid discontinuity,

$$T_r(r,\theta,h^+;t) = T_r(r,\theta,h^-;t)\ ,$$

$$T_\theta(r,\theta,h^+;t) = T_\theta(r,\theta,h^-;t),$$

$$T_z(r,\theta,h^+;t) = T_z(r,\theta,h^-;t), \qquad (2.2.16)$$

$$u_r(r,\theta,h^+;t) = u_r(r,\theta,h^-;t),$$

$$u_\theta(r,\theta,h^+;t) = u_\theta(r,\theta,h^-;t),$$

$$\text{and } u_z(r,\theta,h^+;t) = u_z(r,\theta,h^-;t),$$

for all r,θ, and t, where h^+ is just below the interface and h^- is just above the interface.

For a solid-liquid and liquid-liquid discontinuity

$$T_r(r,\theta,h^+;t) = T_\theta(r,\theta,h^+;t) = 0\,,$$

$$T_r(r,\theta,h^-;t) = T_\theta(r,\theta,h^-;t) = 0,$$

$$T_z(r,\theta,h^+;t) = T_z(r,\theta,h^-;t), \qquad (2.2.17)$$

$$u_z(r,\theta,h^+;t) = u_z(r,\theta,h^-;t),$$

for all r,θ, and t.

2.3 Separable Solutions of the Elastic Wave Equation in Cylindrical Coordinates

The elastic wave equation (2.2.1), can be written in cylindrical coordinates as follows:

$$\rho\ddot{u}_r = \rho f_r + \frac{1}{r}\frac{\partial}{\partial r}(r\sigma_{rr}) + \frac{1}{r}\frac{\partial \sigma_{r\theta}}{\partial \theta} + \qquad (2.3.1)$$

$$+ \frac{\partial \sigma_{rz}}{\partial z} - \frac{1}{r}\sigma_{\theta\theta}$$

$$\rho\ddot{u}_\theta = \rho f_\theta + \frac{1}{r}\frac{\partial}{\partial r}(r\sigma_{\theta r}) + \frac{1}{r}\frac{\partial \sigma_{\theta\theta}}{\partial \theta} +$$

$$+ \frac{\partial \sigma_{\theta z}}{\partial z} + \frac{1}{r}\sigma_{r\theta}$$

$$\rho\ddot{u}_z = \rho f_z + \frac{1}{r}\frac{\partial}{\partial r}(r\sigma_{zr}) + \frac{1}{r}\frac{\partial \sigma_{\theta z}}{\partial \theta} + \frac{\partial \sigma_{zz}}{\partial z}$$

Likewise, the constitutive equations (2.2.5) can also be written in cylindrical coordinates for the case of lateral isotropy.

$$\sigma_{rr} = A\frac{\partial u_r}{\partial r} + (A-2N)\left(\frac{1}{r}\frac{\partial u_\theta}{\partial \theta} + \frac{1}{r}u_r\right) + F\frac{\partial u_z}{\partial z} \qquad (2.3.2)$$

$$\sigma_{\theta\theta} = (A-2N)\frac{\partial u_r}{\partial r} + A\left(\frac{1}{r}\frac{\partial u_\theta}{\partial \theta} + \frac{1}{r}u_r\right) + F\frac{\partial u_z}{\partial z}$$

$$\sigma_{zz} = F\frac{\partial u_r}{\partial r} + F\left(\frac{1}{r}\frac{\partial u_\theta}{\partial \theta} + \frac{1}{r}u_r\right) + C\frac{\partial u_z}{\partial z}$$

$$\sigma_{\theta z} = L\left(\frac{1}{r}\frac{\partial u_z}{\partial \theta} + \frac{\partial u_\theta}{\partial z}\right) = \sigma_{z\theta}$$

$$\sigma_{zr} = L\left(\frac{\partial u_r}{\partial z} + \frac{\partial u_z}{\partial r}\right) = \sigma_{rz}$$

$$\sigma_{r\theta} = N\left(\frac{\partial u_\theta}{\partial r} - \frac{1}{r}u_\theta + \frac{1}{r}\frac{\partial u_r}{\partial \theta}\right) = \sigma_{\theta r},$$

where the coefficients A, C, L, N, and F are functions only of z. For the case of a completely isotropic structure equations (2.3.2) reduce to the following:

$$\sigma_{rr} = (\lambda + 2\mu)\frac{\partial u_r}{\partial r} + \lambda\left(\frac{1}{r}u_r + \frac{1}{r}\frac{\partial u_\theta}{\partial \theta} + \frac{\partial u_z}{\partial z}\right) \qquad (2.3.3)$$

$$\sigma_{\theta\theta} = (\lambda + 2\mu)\left(\frac{1}{r}u_r + \frac{1}{r}\frac{\partial u_\theta}{\partial \theta}\right) + \lambda\left(\frac{\partial u_r}{\partial r} + \frac{\partial u_z}{\partial z}\right)$$

$$\sigma_{zz} = (\lambda + 2\mu)\frac{\partial u_z}{\partial z} + \lambda\left(\frac{1}{r}u_r + \frac{1}{r}\frac{\partial u_\theta}{\partial \theta} + \frac{\partial u_r}{\partial r}\right)$$

$$\sigma_{\theta z} = \mu\left(\frac{1}{r}\frac{\partial u_z}{\partial \theta} + \frac{\partial u_\theta}{\partial z}\right) = \sigma_{z\theta}$$

$$\sigma_{zr} = \mu\left(\frac{\partial u_r}{\partial z} + \frac{\partial u_z}{\partial r}\right) = \sigma_{r\theta}$$

$$\sigma_{r\theta} = \mu\left(\frac{\partial u_\theta}{\partial r} - \frac{1}{r}u_\theta + \frac{1}{r}\frac{\partial u_r}{\partial \theta}\right) = \sigma_{\theta r},$$

where once again λ and μ are functions only of z.

Equations (2.3.2) or (2.3.3) could be substituted back into equations (2.3.1) to eliminate the stress variables and produce a system of three coupled, second order, partial differential equations in the three displacement unknowns, u_r, u_θ, and u_z. The next step, normally, would be to define three potential functions of the displacements in order to decouple the system of equations (2.3.1). The P wave dilatational potential and the SV and SH wave shear potential functions will only decouple equations (2.3.1) when the structure is completely homogeneous and, in the case of an arbitrarily inhomogeneous material, the representation of equations (2.3.1) in terms of the potential functions would be completely coupled. Ben-Menahem and Singh (1981) have shown, however, how separable solutions of the elastic wave equation in cylindrical coordinates for the case of an arbitrary vertically inhomogeneous structure can be represented in terms of vector cylindrical harmonics. When these separable functions are substituted into equations (2.3.1), the t, r and θ dependence are eliminated and we are left with a set of coupled ordinary differential equations (ODE) in the depth variable, z.

I will thus assume the following solutions for the displacements, $\mathbf{u} = (u_r, u_\theta, u_z)$.

$$\mathbf{u} = e^{i\omega t}\Big(u_P(\omega,k,m,z)\,\mathbf{P}_k^m(r,\theta) - \tag{2.3.4}$$

$$+\, u_B(\omega,k,m,z)\,\mathbf{B}_k^m(r,\theta) + u_C(\omega,k,m,z)\,\mathbf{C}_k^m(r,\theta)\Big)$$

where ω is the constant angular frequency,

k is the constant horizontal wavenumber,

m is the constant integer azimuthal order,

and **P**, **B** and **C** are the vector cylindrical harmonics and are given by

$$\mathbf{P}_k^m(r,\theta) = \mathbf{e}_z\, Y_k^m(r,\theta)$$

$$\mathbf{B}_k^m(r,\theta) = \left(\mathbf{e}_r \frac{\partial}{\partial(kr)} + \mathbf{e}_\theta \frac{1}{kr}\frac{\partial}{\partial\theta}\right) Y_k^m(r,\theta) \qquad (2.3.5)$$

$$\mathbf{C}_k^m(r,\theta) = \left(\mathbf{e}_r \frac{1}{kr}\frac{\partial}{\partial\theta} - \mathbf{e}_\theta \frac{\partial}{\partial(kr)}\right) Y_k^m(r,\theta)\,,$$

where $\mathbf{e}_r$, $\mathbf{e}_\theta$ and $\mathbf{e}_z$ are unit vectors in the r, θ and z directions and $Y_k^m(r,\theta)$ is the scalar horizontal wavefunction and is

$$Y_k^m(r,\theta) = J_m(kr)\, e^{im\theta}\,. \qquad (2.3.6)$$

$J_m(kr)$ is the integer order Bessel function of the first kind.

In order to satisfy the boundary conditions it will be necessary to compute the tractions across the z=constant plane as well as the displacements. Separable solutions for the tractions in terms of vector cylindrical harmonics will also be used.

$$\mathbf{T} = e^{i\omega t}\left(T_P(\omega,k,m,z)\,\mathbf{P}_k^m(r,\theta) + \right. \qquad (2.3.7)$$

$$\left. + T_B(\omega,k,m,z)\,\mathbf{B}_k^m(r,\theta) + T_C(\omega,k,m,z)\,\mathbf{C}_k^m(r,\theta)\right)$$

where $\mathbf{T} = (T_r, T_\theta, T_z)$ and

$$T_r = \sigma_{rz}$$

$$T_\theta = \sigma_{\theta z}$$

$$T_z = \sigma_{zz}\,.$$

Finally, I will represent the body forces, $\rho\mathbf{f} = (\rho f_r,\ \rho f_\theta,\ \rho f_z)$, in the same manner as the displacements and tractions.

$$\rho f = e^{i\omega t}\left[f_P(\omega k,m,z)\, P_k^m(r,\theta) + \right. \tag{2.3.8}$$

$$\left. + f_B(\omega,k,m,z)\, B_k^m(r,\theta) + f_C(\omega,k,m,z)\, C_k^m(r,\theta)\right]$$

If we substitute equations (2.3.4), (2.3.7), and (2.3.8) into equations (2.3.1) and (2.3.2) and use relations (2.3.5) and (2.3.6) along with various properties of integer order Bessel functions, the t, r and θ dependences can be factored out leaving a system of six coupled ordinary differential equations of z, in the dependent variables u_P, u_B, u_C, T_P, T_B, and T_C. The resulting z-dependent ODEs can be written as follows:

$$\frac{d}{dz}\begin{Bmatrix} u_P \\ u_B \\ T_P \\ T_B \\ u_C \\ T_C \end{Bmatrix} = \begin{bmatrix} 0 & k\frac{F}{C} & \frac{1}{C} & 0 & 0 & 0 \\ -k & 0 & 0 & \frac{1}{L} & 0 & 0 \\ -\omega^2\rho & 0 & 0 & k & 0 & 0 \\ 0 & \left[k^2\left(A - \frac{F^2}{C}\right) - \omega^2\rho\right] & -\frac{kF}{C} & 0 & 0 & 0 \\ 0 & 0 & 0 & 0 & 0 & \frac{1}{L} \\ 0 & 0 & 0 & 0 & (k^2N - \omega^2\rho) & 0 \end{bmatrix} \begin{Bmatrix} u_P \\ u_B \\ T_P \\ T_B \\ u_C \\ T_C \end{Bmatrix}$$

$$- \begin{Bmatrix} 0 \\ 0 \\ f_P \\ f_B \\ 0 \\ f_C \end{Bmatrix} \tag{2.3.9}$$

Once gain the elastic moduli A, C, L, N, and F are arbitrary functions of z and at this point we have made no approximations or assumptions other than linearity, laterally homogeneous structure and laterally isotropic structure.

Because of the separable form of the solutions expressed by equations (2.3.4) and (2.3.7), equations (2.3.7) must hold at a fixed ω, k and m for all t, r and θ. Thus the boundary conditions expressed by equations (2.2.11) through (2.2.17) will be insured by applying them to the depth dependent spectral functions in equations (2.3.9).

2.4 Solutions of the Depth Dependent ODEs: The Propagator Matrix

We can write equations (2.3.9) in a more convenient form as follows:

$$\frac{d}{dz}\{y(z)\} = [U(z)]\{y(z)\} - \{w(z)\}, \tag{2.4.1}$$

where $\{y(z)\}$ is the six component displacement-stress vector, and is given by

$$\begin{Bmatrix} y_1(z) \\ y_2(z) \\ y_3(z) \\ y_4(z) \\ y_5(z) \\ y_6(z) \end{Bmatrix} = \begin{Bmatrix} u_P \\ u_B \\ T_P \\ T_B \\ u_C \\ T_C \end{Bmatrix}, \tag{2.4.2}$$

$\{w(z)\}$ is the six component forcing function vector and for a time and space distribution of simple body forces is given by

$$\begin{Bmatrix} w_1(z) \\ w_2(z) \\ w_3(z) \\ w_4(z) \\ w_5(z) \\ w_6(z) \end{Bmatrix} = \begin{Bmatrix} 0 \\ 0 \\ f_P \\ f_B \\ 0 \\ f_C \end{Bmatrix}, \tag{2.4.3}$$

and [U(z)] is a six by six matrix whose element are functions only of ω,k and depth dependent elastic moduli.

It is obvious from equations (2.3.9) that we can partition equations (2.4.1) as follows,

$$\frac{d}{dz}\{_R y(z)\} = |_R U(z)|\,\{_R y(z)\} - \{_R w(z)\}, \tag{2.4.4}$$

and

$$\frac{d}{dz}\{_L y(z)\} = |_L U(z)|\,\{_L y(z)\} - \{_L w(z)\}, \tag{2.4.5}$$

Where

$$\{_R y(z)\} = \begin{Bmatrix} y_1(z) \\ y_2(z) \\ y_3(z) \\ y_4(z) \end{Bmatrix}, \{_R w(z)\} = \begin{Bmatrix} w_1(z) \\ w_2(z) \\ w_3(z) \\ w_4(z) \end{Bmatrix},$$

$$|_R U(z)| = \begin{bmatrix} 0 & \frac{kF}{\alpha_V^2\rho} & \frac{1}{\alpha_V^2\rho} & 0 \\ -k & 0 & 0 & \frac{1}{\beta_V^2\rho} \\ -\omega^2\rho & 0 & 0 & k \\ 0 & \left[k^2\left(\alpha_H^2\rho - \frac{F^2}{\alpha_V^2\rho}\right) - \omega^2\rho\right] & -\frac{kF}{\alpha_V^2\rho} & 0 \end{bmatrix}, \tag{2.4.6}$$

and

$$\{_L y(z)\} = \begin{Bmatrix} y_5(z) \\ y_6(z) \end{Bmatrix}, \{_L w(z)\} = \begin{Bmatrix} w_5(z) \\ w_6(z) \end{Bmatrix}, \tag{2.4.7}$$

$$|_L U(z)| = \begin{bmatrix} 0 & \frac{1}{\beta_V^2\rho} \\ (k^2\beta_H^2\rho - \omega^2\rho) & 0 \end{bmatrix},$$

and where the R subscript denotes Rayleigh or P-SV wave motion, the L subscript denotes Love or SH wave motion, and the elastic moduli A, C, L and N have been replaced by the P and S wave vertical and horizontal velocities, α_V, β_V, α_H, and β_H from equations (2.2.9). We can easily determine $[_RU]$ and $[_LU]$ for a completely isotropic structure by setting $\alpha_V = \alpha_H = \alpha$, $\beta_V = \beta_H = \beta$ and $F = \lambda$.

Consider the homogeneous or unforced part of equation (2.4.1), namely,

$$\frac{d}{dz}\{y\} = [U]\{y\}. \tag{2.4.8}$$

Gilbert and Backus (1966) studied solutions to this equation and popularized and generalized the propagator matrix method which was first employed by Thomson (1950) and Haskell (1953) for the case of a plane homogeneous layered structure. In order to solve (2.4.8) the matrizant of [U] is defined as follows,

$$[A(z,z_0)] = [I] + \int_{z_0}^{z}[U(\varsigma_1)]\,d\varsigma_1 + \tag{2.4.9}$$

$$+ \int_{z_0}^{z}[U(\varsigma_1)]\int_{z_0}^{\varsigma_1}[U(\varsigma_2)]\,d\varsigma_2 d\varsigma_1 + \cdots$$

where [I] is the unit matrix. Differentiating the matrizant with respect to z gives,

$$\frac{d}{dz}[A(z,z_0)] = [U(z)] + [U(z)]\int_{z_0}^{z}[U(\varsigma_1)]\,d\varsigma_1 + \cdots$$

or

$$\frac{d}{dz}[A(z,z_0)] = [U(z)]\,[A(z,z_0)]. \tag{2.4.10}$$

If we post multiply (2.4.10) by $\{y(z_0)\}$ we arrive at,

$$\frac{d}{dz} [A(z,z_0)] \{y(z_0)\} = [U(z)] [A(z,z_0)] \{y(z_0)\} , \qquad (2.4.11)$$

and comparing this to equation (2.4.8) it follows that,

$$\{y(z)\} = [A(z,z_0)] \{y(z_0)\} . \qquad (2.4.12)$$

When we include the forcing function vector $\{w\}$, equation (2.4.12) becomes

$$\{y(z)\} = [A(z,z_0)] \{y(z_0)\} - \int_{z_0}^{z} [A(z,\varsigma)] \{w(\varsigma)\} d\varsigma . \qquad (2.4.13)$$

The matrizant of [U] given by equation (2.4.9) allows us to propagate the solution for $\{y\}$ from some initial depth, z_0, to some other depth, z, and thus the matrizant is usually called the propagator matrix. One obvious property of the propagator matrix which must be true in order for relation (2.4.12) to be valid is that,

$$[A(z,z)] = [I] . \qquad (2.4.14)$$

Another important property of the propagator matrix is that it is only dependent on ω, k, z, and the depth dependent elastic moduli, and is independent of r, θ and the azimuthal order m. The major difficulty, then in determining spectral solutions of the elastic wave equation for a laterally homogeneous structure, is in computing the propagator matrix.

Consider the $\{y\}$ vector at three depths, z_0, z_1, and z_2, such that $z_2 > z_1 > z_0$. From equation (2.4.13),

$$\{y(z_1)\} = [A(z_1,z_0)] \{y(z_0)\} - \int_{z_0}^{z_1} [A(z_1,\varsigma)] \{w(\varsigma)\} d\varsigma$$

and

$$\{y(z_2)\} = [A(z_2,z_1)] \{y(z_1)\} - \int_{z_1}^{z_2} [A(z_2,\varsigma)] \{w(\varsigma)\} d\varsigma ,$$

or

$$\{y(z_2)\} = [A(z_2,z_1)]\ [A(z_1,z_0)]\ \{y(z_0)\}$$

$$- [A(z_2,z_1)] \int_{z_0}^{z_1} [A(z_1,\varsigma)]\ \{w(\varsigma)\}\, d\varsigma$$

$$- \int_{z_1}^{z_2} [A(z_2,\varsigma)]\ \{w(\varsigma)\}\, d\varsigma \ ,$$

but since

$$\{y(z_2)\} = [A(z_1,z_0)]\ \{y(z_0)\} - \int_{z_0}^{z_2} [A(z_2,\varsigma)]\ \{w(\varsigma)\}\, d\varsigma \ ,$$

$$[A(z_2,z_0)] = [A(z_2,z_1)]\ [A(z_1,z_0)] \ . \qquad (2.4.15)$$

Equation (2.4.15) expresses an important property of the propagator matrix which is especially useful when dealing with layered structures. The depth restriction, $z_2 > z_1 > z_0$, is actually not necessary and as a corollary to (2.4.15),

$$[A(z_0,z_0)] = [I] = [A(z_0,z_1)]\ [A(z_1,z_0)] \ ,$$

or

$$[A(z_0,z_1)] = [A(z_1,z_0)]^{-1} \ . \qquad (2.4.16)$$

Thus the upward propagator matrix between two depths is the inverse of the downward propagator matrix between the same two depths.

For the case of a general heterogeneous structure with depth, equation (2.4.9) cannot be solved analytically and the only method presently available is that of numerical integration. In practice equation (2.4.1) is integrated with respect to z so that,

$$\{y(z)\} = \{y(z_0)\} + \int_{z_0}^{z} [U(\varsigma)]\ \{y(\varsigma)\}\, d\varsigma - \int_{z_0}^{z} \{w(\varsigma)\}\, d\varsigma \ .$$

(2.4.17)

The six by six propagator matrix can be determined by ignoring the forcing function contribution in (2.4.17) and then numerically integrating $[U(z)]$ $\{y(z)\}$ six times with each element of the starting value of $\{y(z_0)\}$ set consecutively to unity, the other elements being zero. The resulting six values of the vector $\{y(z)\}$ will constitute the six columns of $[A(z,z_0)]$. It should be pointed out at this time that *all* solutions of the depth dependent ODEs for an arbitrary heterogeneous medium are in fact approximations to the exact solution. Thus we should evaluate candidate approximations according to accuracy, efficiency and ease of implementation.

One candidate approximation which is very popular and relatively easy to implement is to assume the structure is made up of a number of plane layers, each layer being completely homogeneous. It is obvious that any arbitrary depth dependence can be approximated by a large number of sufficiently thin homogeneous layers welded together. The approximation would then break down at wavelengths less than or equal to the individual layer thicknesses, and the approximation could be made arbitrarily accurate by decreasing the layer thicknesses.

In order to see why the homogeneous layered structure approximation is easy to implement let us first consider the case of a completely homogeneous structure. In this case [U] is independent of z and can be taken outside of the integrals in (2.4.9) which then gives

$$[A(z,z_0)] = [I] + (z - z_0)[U] + \frac{1}{2}(z - z_0)^2[U][U] + \cdots$$

$$= \exp\Big((z - z_0)[U]\Big) . \qquad (2.2.18)$$

We can apply Sylvester's formula (Hildebrand (1952)) to compute any func-

tion of a matrix in terms of the eigenvalues of that matrix.

$$f([U]) = \sum_{k=1}^{n} f(\lambda_k) \frac{\prod_{m \neq k} ([U] - \lambda_m[I])}{\prod_{m \neq k} (\lambda_k - \lambda_m)} \tag{2.4.19}$$

where [U] is a square n × n matrix with distinct eigenvalues, λ_i, i = 1,2,...,n. We now have an explicit analytical solution for the propagator matrix in terms of the eigenvalues of $(z - z_0)[U]$. From equations (2.4.18) and (2.4.19) we can see right away that the solutions for the propagator matrix will be exponential functions in z which is what we might have expected for a homogeneous structure. It is the exact solution for the propagator matrix given by (2.4.19) along with the simple functional dependence with depth that makes the homogeneous layered approximation easy to implement, relatively efficient and arbitrarily accurate. As for as I can determine, there is no other structural approximation for which an exact analytical solution for the propagator matrix can be obtained.

The eigenvalues of $(z - z_0)[U]$ for SH waves are easy to compute and from equation (2.4.7) are

$$\lambda_1 = + (z - z_0) \left(\frac{\beta_H^2}{\beta_V^2} k^2 - \frac{\omega^2}{\beta_V^2} \right)^{1/2}$$

$$\lambda_2 = - (z - z_0) \left(\frac{\beta_H^2}{\beta_V^2} k^2 - \frac{\omega^2}{\beta_V^2} \right)^{1/2} . \tag{2.4.20}$$

The Love wave propagator matrix can now be expressed as follows for a solid laterally isotropic homogeneous material.

$$[{}_L A(z,z_0)] = \exp \left[(z - z_0) [{}_L U] \right] ,$$

$$= \exp(\lambda_1) \frac{([{}_L U] - \lambda_2[I])}{(\lambda_1 - \lambda_2)} \tag{2.4.21}$$

$$- \exp(\lambda_2) \frac{([{}_L U] - \lambda_1[I])}{(\lambda_1 - \lambda_2)} ,$$

$$[{}_L A(z,z_0)] = [{}_L U] \frac{1}{i\,{}_L\nu} \sinh\left(i(z - z_0)\,{}_L\nu\right)$$

$$+ [I] \cosh\left(i(z - z_0)\,{}_L\nu\right) ,$$

$$[{}_L A(z,z_0)] = [{}_L U] \frac{1}{{}_L\nu} \sin\left((z - z_0)\,{}_L\nu\right)$$

$$+ [I] \cos\left((z - z_0)\,{}_L\nu\right) , \qquad (2.4.22)$$

where ${}_L\nu$ is the Love wave vertical wavenumber and is given by,

$${}_L\nu = - i\left(\frac{\beta_H^2}{\beta_V^2} k^2 - \frac{\omega^2}{\beta_V^2}\right)^{1/2} . \qquad (2.4.23)$$

I have chosen the vertical wavenumber by analogy with the horizontal wavenumber so that when ${}_L\nu$ is real, propagating solutions occur in the z-direction and when ${}_L\nu$ is imaginary, inhomogeneous or evanescent solutions exist. The propagator matrix, however, remains real for all real values of ω, k, β_H, β_V and ρ. Also, even though ${}_L\nu$ is a dual valued function due to the square root, the propagator matrix itself is single valued. This is because both values of ${}_L\nu$ are included in the propagator matrix which can be more easily seen in equation (2.4.21) where $\lambda_1 = + i(z - z_0)\,{}_L\nu$ and $\lambda_2 = - i(z - z_0)\,{}_L\nu$.

Consider the transformation matrix, [B], which diagonalizes [U].

$$[B]^{-1}\,[U][B] = \begin{bmatrix} \lambda_1 & 0 & 0 \\ 0 & \lambda_2 & 0 \\ 0 & 0 & \lambda_n \end{bmatrix} = [\Lambda] \qquad (2.4.24)$$

Obviously, the diagonalized version of [U] will consist of diagonal elements equal to the eigenvalues of [U] and the columns of [B] will be equal to the n eigenvectors of [U]. Let us use [B] to transform the stress-displacement vector, {y}, also.

$$\{v\} = [B]^{-1}\{y\},$$

or

$$\{y\} = [B]\{v\} \tag{2.4.25}$$

Substituting into equation (2.4.8) and assuming a completely homogeneous material,

$$[B]\frac{d}{dz}\{v\} = [U][B]\{v\},$$

$$\frac{d}{dz}\{v\} = [B]^{-1}[U][B]\{v\},$$

or

$$\frac{d}{dz}\{v\} = [A]\{v\}. \tag{2.4.26}$$

defining the propagator matrix for the transformed vector, {v}, as $[V(z,z_0)]$ and applying Sylvester's formula we get,

$$\{v(z)\} = [V(z,z_0)]\{v(z_0)\}, \tag{2.4.27}$$

$$[V(z,z_0)] = \exp\Big((z - z_0)[A]\Big),$$

$$[V(z,z_0)] = \begin{bmatrix} \exp((z - z_0)\lambda_1) & & & \\ & \exp((z - z_0)\lambda_2) & 0 & \\ & 0 & & \\ & & & \exp((z - z_0)\lambda_n) \end{bmatrix} \tag{2.4.28}$$

This transformed version of the stress-displacement vector has been used extensively by Kennett, Kerry and Woodhouse (1978) and Kennett and Kerry (1979) who show how complete, numerically stable solutions to the elastic wave equation for plane homogeneous layered structures can be expressed in terms of a generalized ray expansion. They refer to the vector, {v}, as the wave or wavefield vector and its elements are decoupled from each other in a homogeneous material due to the diagonal form of the wavefield propagator matrix, [V]. The six elements of {v} are, in fact, the ω, k and z dependent factors in the P, SV and SH potential functions for upward and downward propagating waves. Thus the elements of the wavefield vector are the ω, k and z dependent complex amplitudes of P, SV and SH rays travelling either upward or downward through the homogeneous material. The matrix [B], then, transforms the z-dependent solutions from a ray representation to a stress-displacement representation. Using [B] we can easily relate the stress-displacement propagator matrix directly to the wave field propagator matrix.

$$[A(z,z_0)] = [B]\,[V(z,z_0)]\,[B]^{-1} \tag{2.4.29}$$

The [B] matrix also proves useful in computing reflection and transmission coefficients across layer interfaces. Because of the usefulness of [B], I will compute the P-SV propagator matrix using (2.4.29) instead of Sylvester's formula. The first step is to compute the eigenvalues of $[{}_R U]$ given by equation (2.4.6). This reduces to solving for the roots of the following characteristic equation:

$$ {}_R\lambda^4 + {}_R\lambda^2 \left({}_R\nu_\alpha^2 + {}_R\nu_\beta^2 + \frac{k^2}{\beta^2}\left(\alpha^2(1-\eta^2) + \xi\right)\right) \tag{2.4.30}$$

$$ + \left({}_R\nu_\alpha^2 {}_R\nu_\beta^2 + k^2 {}_R\nu_\beta^2 (1-\eta^2)\right) = 0$$

where ${}_R\lambda$ is an eigenvalue of $[{}_RU]$, and

$$\alpha = \alpha_V \,, \beta = \beta_V \,, \eta = \frac{\alpha_H}{\alpha_V} \,, \xi = \frac{F}{\rho} - \alpha_V^2 + 2\beta_V^2 \qquad (2.4.31)$$

$$k_\alpha = \frac{\omega}{\alpha_V} \,, k_\beta = \frac{\omega}{\beta_V},$$
$${}_R\nu_\alpha^2 = k_\alpha^2 - k^2 \,, {}_R\nu_\beta^2 = k_\beta^2 - k^2 \,.$$

${}_R\nu_\alpha$ and ${}_R\nu_\beta$ are P and S wave vertical wavenumbers and when they are real, the z-dependent solutions are propagating and when they are imaginary, the z-dependent solutions are evanescent as with ${}_L\nu$. For a completely isotropic material,

$$\eta = 1, \xi = 0 \,,$$

and we can write equation (2.4.30) as follows:

$${}_R\lambda^4 + {}_R\lambda^2 ({}_R\nu_\alpha^2 + {}_R\nu_\beta^2) + {}_R\nu_\alpha^2 {}_R\nu_\beta^2 = 0 \,, \qquad (2.4.32)$$

which can be factored as,

$$\left({}_R\lambda^2 + {}_R\nu_\alpha^2\right) \left({}_R\lambda^2 + {}_R\nu_\beta^2)\right) = 0 \,,$$

so that

$${}_R\lambda^2 = - {}_R\nu_\alpha^2 \qquad (2.4.33)$$

or

$${}_R\lambda^2 = - {}_R\nu_\beta^2 \,.$$

This then gives the following four solutions for ${}_R\lambda$ which corresponds to upward and downward travelling P and SV waves.

$${}_R\lambda_1 = + i\nu_\alpha = + i\sqrt{k_\alpha^2 - k^2} = + {}_R\lambda_\alpha \qquad (2.4.34)$$

$${}_R\lambda_2 = - i\nu_\alpha = - i\sqrt{k_\alpha^2 - k^2} = - {}_R\lambda_\alpha$$

$${}_R\lambda_3 = + i\nu_\beta = + i\sqrt{k_\beta^2 - k^2} = + {}_R\lambda_\beta$$

$$ {}_R\lambda_4 = -i\nu_\beta = -i\sqrt{k_\beta^2 - k^2} = -{}_R\lambda_\beta $$

We can certainly obtain an explicit algebraic solution for ${}_R\lambda^2$ even for the anisotropic case, however, the form of the solution will generally be complicated. For the isotropic case the roots ${}_R\lambda^2$, are always real and distinct for real ω, k, α, β and ρ and as long as $\alpha \neq \beta$. For the anisotropic case the roots, ${}_R\lambda^2$, may be either real or complex depending on the sign of the discriminant of equation (2.4.30). As long as η is close to one and ξ is close to zero (weak anisotropy) we would expect the roots to remain real and distinct and the resulting wave motion would correspond approximately to P and SV type wave motion. There will be values of η and ξ, however, for which the roots, ${}_R\lambda^2$, will be complex, but since the coefficients in equation (2.4.30) are always real, complex values of ${}_R\lambda^2$ will occur as complex conjugate pairs.

In order to compute $[{}_RB]$ we need to compute the eigenvectors of $[{}_RU]$. We will compose $[{}_RU]$ from the four eigenvectors of $[{}_RU]$ as follows:

$$ [{}_RB] = \left[\{{}_Rb\}_1 \mid \{{}_Rb\}_2 \mid \{{}_Rb\}_3 \mid \{{}_Rb\}_4 \right] , \qquad (2.4.35) $$

where $\{{}_Rb\}$ is a column vector with four components equal to the i^{th} eigenvector of $[{}_RU]$, and

$$ \left[[{}_RU] - {}_R\lambda_i [I] \right] \{{}_Rb\}_i = \{0\} , i = 1,2,3,4 . \qquad (2.4.36) $$

The normalization of the eigenvectors is arbitrary and so we will chose the first component in each eigenvector to be unity so that ${}_RB_{11} = {}_RB_{12} = {}_RB_{13} = {}_RB_{14} = 1$. Solving for the remaining components of the eigenvectors in (2.4.36) we get

$$ {}_RB_{1i} = 1 \qquad (2.4.37) $$

$$ {}_{R}B_{2i} = \frac{1}{\delta_i}\left(\frac{\omega^2}{\alpha_V^2\beta_V^2\rho} + \frac{{}_{R}\lambda_i^2}{\beta_V^2\rho} - \frac{k^2}{\alpha_V^2\rho}\right) $$

$$ {}_{R}B_{3i} = \frac{1}{\delta_i}\left(-\frac{kF\omega^2}{\alpha_V^2\beta_V^2\rho} + {}_{R}\lambda_i^2 k + \frac{k^3F}{\alpha_V^2\rho}\right) $$

$$ {}_{R}B_{4i} = \frac{1}{\delta_i}\left(\frac{{}_{R}\lambda_i\omega^2}{\alpha_V^2} + {}_{R}\lambda_i^3 + \frac{{}_{R}\lambda_i k^2 F}{\alpha_V^2\rho}\right) $$

where $\delta_i = \frac{k_R\lambda_i}{\alpha_V^2}\left(\frac{F}{\beta_V^2\rho} + 1\right)$, and i = 1,2,3,4.

Since ${}_{R}\lambda_2 = -{}_{R}\lambda_1$ and ${}_{R}\lambda_4 = -{}_{R}\lambda_3$, we can see that,

$$ {}_{R}B_{22} = -{}_{R}B_{21}\,,\ {}_{R}B_{24} = -{}_{R}B_{23}, \qquad (2.4.38) $$

$$ {}_{R}B_{32} = -{}_{R}B_{31}\,,\ {}_{R}B_{34} = -{}_{R}B_{33}, $$

$$ {}_{R}B_{42} = {}_{R}B_{41}\,,\ {}_{R}B_{44} = {}_{R}B_{43}\,. $$

We can obviously compute $[{}_{R}B]^{-1}$ and from equation (2.4.29) obtain an explicit solution for the stress-displacement propagator matrix for the anisotropic case.

At this point I am going to assume a completely isotropic structure. This assumption is being made primarily to simplify the form of the solutions for [B] and [A] which will result in a computationally efficient algorithm, however, there is no fundamental reason why the anisotropic case cannot be handled in the same manner as the isotropic case. I am also going to redefine the stress-displacement vector, {y}, as,

$$ \{{}_{R}\bar{y}(z) = \begin{Bmatrix} y_1(z) \\ y_2(z) \\ y_3(z)/k \\ y_4(z)/k \end{Bmatrix}, \qquad (2.4.39) $$

and

$$\{{}_L\bar{y}(z)\} = \begin{Bmatrix} y_5(z) \\ y_6(z)/k \end{Bmatrix}.$$

Similarly, I redefine the forcing function vector, {w}, as

$$\{{}_R\bar{w}(y)\} = \begin{Bmatrix} w_1(z) \\ w_2(z) \\ w_3(z)/k \\ w_4(z)/k \end{Bmatrix}, \{{}_L\bar{w}(z)\} = \begin{Bmatrix} w_5(z) \\ w_6(z)/k \end{Bmatrix}. \qquad (2.4.46)$$

I will drop the overbar in the following development in order to simplify the notation. From the definition of the matrix, $[{}_RB]$, and assuming an isotropic homogeneous structure we arrive at

$$[{}_RB] = \begin{bmatrix} i\phi_\alpha & -i\phi_\alpha & 1 & 1 \\ 1 & 1 & i\phi_\beta & -i\phi_\beta \\ \rho c^2(\gamma-1) & \rho c^2(\gamma-1) & \rho c^2\gamma i\phi_\beta & -\rho c^2\gamma i\phi_\beta \\ \rho c^2\gamma i\phi_\alpha & -\rho c^2\gamma i\phi_\alpha & \rho c^2(\gamma-1) & \rho c^2(\gamma-1) \end{bmatrix},$$

where we have changed the normalization from that defined by (2.4.37) and,

$c = \frac{\omega}{k}$ is the horizontal phase velocity, (2.4.42)

$\phi_\alpha = \sqrt{(c/\alpha)^2 - 1}$, $\phi_\beta = \sqrt{(c/\beta)^2 - 1}$ are the cotangents of the incidence angles for plane propagating P and S waves,

and $\gamma = 2(\beta/c)^2$.

Note that $\nu_\alpha = k\phi_\alpha$ and $\nu_\beta = k\phi_\beta$ and that by redefining the stress-displacement vector with equation (2.4.39) we have eliminated ω dependence from $[{}_RB]$. We can easily compute $[{}_RB]^{-1}$ from (2.4.41)

$$[{}_{R}B]^{-1} = \frac{1}{2}\begin{bmatrix} \frac{-(\gamma-1)}{i\phi_\alpha} & \gamma & -\frac{1}{\rho c^2} & \frac{1}{\rho c^2 i\phi_\alpha} \\ \frac{(\gamma-1)}{i\phi_\alpha} & \gamma & -\frac{1}{\rho c^2} & -\frac{1}{\rho c^2 i\phi_\alpha} \\ \gamma & -\frac{(\gamma-1)}{i\phi_\beta} & \frac{1}{\rho c^2 i\phi_\beta} & -\frac{1}{\rho c^2} \\ \gamma & \frac{(\gamma-1)}{i\phi_\beta} & -\frac{1}{\rho c^2 i\phi_\beta} & -\frac{1}{\rho c^2} \end{bmatrix} \qquad (2.4.43)$$

Using equations (2.4.28), (2.4.34), (2.4.41), (2.4.43), and (2.4.29) we can solve for the Rayleigh wave stress-displacement propagator matrix for a solid material.

$${}_{R}A_{11}(z,z_0) = -(\gamma-1)\cos(\theta_\alpha) + \gamma\cos(\theta_\beta) \qquad (2.4.44)$$

$${}_{R}A_{12}(z,z_0) = -\gamma\phi_\alpha\sin(\theta_\alpha) - \frac{(\gamma-1)}{\phi_\beta}\sin(\theta_\beta)$$

$${}_{R}A_{13}(z,z_0) = \frac{\phi_\alpha}{\rho c^2}\sin(\theta_\alpha) + \frac{1}{\rho^2\phi_\beta}\sin(\theta_\beta)$$

$${}_{R}A_{14}(z,z_0) = \frac{1}{\rho c^2}\cos(\theta_\alpha) - \frac{1}{\rho c^2}\cos(\theta_\beta)$$

$${}_{R}A_{21}(z,z_0) = -\frac{(\gamma-1)}{\phi_\alpha}\sin(\theta_\alpha) - \gamma\phi_\beta\sin(\theta_\beta)$$

$${}_{R}A_{22}(z,z_0) = \gamma\cos(\theta_\alpha) - (\gamma-1)\cos(\theta_\beta)$$

$${}_{R}A_{23}(z,z_0) = -{}_{R}A_{14}(z,z_0)$$

$${}_{R}A_{24}(z,z_0) = \frac{1}{\rho c^2\phi_\alpha}\sin(\theta_\alpha) + \frac{\phi_\beta}{\rho c^2}\sin(\theta_\beta)$$

$${}_{R}A_{31}(z,z_0) = -\frac{\rho c^2(\gamma-1)^2}{\phi_\alpha}\sin(\theta_\alpha) - \rho c^2\gamma^2\phi_\beta\sin(\theta_\beta)$$

$$_{R}A_{32}(z,z_0) = \rho c^2\gamma(\gamma-1)\cos(\theta_\alpha) - \rho c^2\gamma(\gamma-1)\cos(\theta_\beta)$$

$$_{R}A_{33}(z,z_0) = {}_{R}A_{11}(z,z_0)$$

$$_{R}A_{34}(z,z_0) = -\,{}_{R}A_{21}(z,z_0)$$

$$_{R}A_{41}(z,z_0) = -\,{}_{R}A_{32}(z,z_0)$$

$$_{R}A_{42}(z,z_0) = -\,\rho c^2\gamma^2\phi_\alpha\sin(\theta_\alpha) - \frac{\rho c^2(\gamma-1)^2}{\phi_\beta}\sin(\theta_\beta)$$

$$_{R}A_{43}(z,z_0) = -\,{}_{R}A_{12}(z,z_0)$$

$$_{R}A_{44}(z,z_0) = {}_{R}A_{22}(z,Z0)\,,$$

where

$$\theta_\alpha = (z - z_0)\,\nu_\alpha = (z - z_0)\,k\phi_\alpha\,, \tag{2.4.45}$$

and

$$\theta_\beta = (z - z_0)\,\nu_\beta = (z - z_0)\,k\phi_\beta\,,$$

Once again, as with the SH case, we can see that although ϕ_α, ν_α, ϕ_β and ν_β are dual valued, the elements of the propagator matrix are all single valued.

In order to compute the propagator matrix for a liquid or acoustic layer let us renormalize the last two columns in $[_{R}B]$ with $1/(i\phi_\beta)$ and then let $\beta \to 0$. We can see from (2.4.41) that the last two columns and the last row of $[_{R}B]$ will go to zero and the 4×4 $[_{R}B]$ matrix will be singular and non-invertible. For an acoustic layer only the upward and downward P-wave solutions will exist and so we need to partition out a 2×2 non-singular matrix from the 4×4 $[_{R}B]$ matrix in order to determine a solution for the acoustic propagator matrix. We define the acoustic [B] matrix as follows.

$$\begin{Bmatrix} y_1(z) \\ y_3(z) \end{Bmatrix} = [{}_A B] \begin{Bmatrix} v_1(z) \\ v_2(z) \end{Bmatrix} \tag{2.4.46}$$

where

$$[{}_A B] = \begin{bmatrix} i\phi_a & -i\phi_a \\ -\rho c^2 & -\rho c^2 \end{bmatrix} . \tag{2.4.47}$$

We should note that the second and third rows of $[{}_R B]$ are linearly dependent for $\beta = 0$ and so for an acoustic layer,

$$y_3(z) = -\rho c^2 \, y_2(z) . \tag{2.4.48}$$

We can invert $[{}_A B]$ to get

$$[{}_A B]^{-1} = \frac{1}{2} \begin{bmatrix} \frac{1}{i\phi_a} & -1/\rho c^2 \\ -\frac{1}{i\phi_a} & -1/\rho c^2 \end{bmatrix} , \tag{2.4.49}$$

and obtain the 2 × 2 acoustic propagator matrix.

$$\begin{Bmatrix} y_1(z) \\ y_3(z) \end{Bmatrix} = [{}_A A(z,z_0)] \begin{Bmatrix} y_1(z_0) \\ y_3(z_0) \end{Bmatrix} \tag{2.4.50}$$

$$[{}_A A(z,z_0)] = \begin{bmatrix} \cos(\theta_a) & -\phi_a \sin(\theta_a) \\ \frac{-\rho c^2 \sin(\theta_a)}{\phi_a} & -\rho c^2 \cos(\theta_a) \end{bmatrix} . \tag{2.4.51}$$

We can also rewrite (2.4.51) in terms of a 4 × 4 matrix using equation (2.4.48).

$$[{}_A A(z,z_0)] = \begin{bmatrix} \cos(\theta_a) & -\phi_a \sin(\theta_a) & 0 & 0 \\ \frac{\sin(\theta_a)}{\phi_a} & \cos(\theta_a) & 0 & 0 \\ -\frac{\rho c^2}{\phi_a} \sin(\theta_a) & -\rho c^2 \cos(\theta_a) & 0 & 0 \\ 0 & 0 & 0 & 0 \end{bmatrix} \tag{2.4.52}$$

We have already dealt with the Love wave propagator matrix, but we will write down the solutions for $[_L B]$, $[_L B]^{-1}$, and $[_L A(z,z_0)]$ for the case of an isotropic homogeneous material.

$$[_L B] = \begin{bmatrix} 1 & 1 \\ \rho\beta^2 i\phi_\beta & -\rho\beta^2 i\phi_\beta \end{bmatrix}, \tag{2.4.53}$$

$$[_L B]^{-1} = \begin{bmatrix} 1 & \dfrac{1}{\rho\beta^2 i\phi_\beta} \\ 1 & -\dfrac{1}{\rho\beta^2 i\phi_\beta} \end{bmatrix}, \tag{2.4.54}$$

$$[_L A(z,z_0)] = \begin{bmatrix} \cos(\theta_\beta) & \dfrac{\sin(\theta_\beta)}{\rho\beta^2\phi_\beta} \\ -\rho\beta^2\phi_\beta \sin(\theta_\beta) & \cos(\theta_\beta) \end{bmatrix} \tag{2.4.55}$$

Equations (2.4.44), (2.4.55), and (2.4.52) give the stress-displacement propagator matrices for P-SV, SH, and acoustic materials which are completely homogeneous and isotropic. In order to compute propagator matrices for a homogeneous layered structure we need to apply the layer interface boundary conditions given by equations (2.2.16) and (2.2.17). First we start by defining the layer propagator matrix, $[\boldsymbol{a}^{(p)}]$, which relates the stress-displacement vector at some point within the p^{th} homogeneous layer to the stress-displacement vector at the top of the layer.

$$\{y^{(p)}(\varsigma^{(p)})\} = [\boldsymbol{a}^{(p)}(\varsigma^{(p)})]\ \{y^{(p)}(0)\}, \tag{2.4.56}$$

$$[\boldsymbol{a}^{(p)}(\varsigma^{(p)})] = [A(z,h^{(p-1)})], \tag{2.4.57}$$

where $\varsigma^{(p)} = z - h^{(p-1)}$, $0 \leq \varsigma^{(p)} < \xi^{(p)}$,

and $\varsigma^{(p)}$, $\xi^{(p)}$ and $h^{(p-1)}$ are shown in figure 1.

When $\varsigma^{(p)} = \xi^{(p)}$ then the layer propagator matrix will relate the stress-

displacement vector at the bottom of a layer to the vector at the top of the layer.

For a solid material we can now start at any layer interface, p, and propagate the stress-displacement vector to any other interface, q, (where $p < q$) by applying the welded interface boundary conditions expressed by equations (2.2.16) and by repeating equation (2.4.56) and in doing so we define the interlayer propagator matrix, $[A^{(q,p)}]$,

$$\{y(h^{(q)})\} = [A^{(q,p)}]\ \{y(h^{(p)})\}\ . \tag{2.4.58}$$

The interlayer propagator matrix is,

$$[A^{(q,p)}] = \prod_{l=p+1}^{q} \left[a^{(q+p+1-l)}(\xi^{(q+p+1-l)}) \right] \tag{2.4.59}$$

For a solid-liquid, liquid-solid, or liquid-liquid interface, the situation is a little more complicated and I will cover these cases in the next section.

Equations (2.4.44), (2.4.52), (2.4.55), (2.4.57), and (2.4.59) give the *exact* solution for the stress-displacement propagator matrix in a vertically heterogeneous material made up of plane homogeneous layers. Thus the approximation made here is in the representation of the structural model and not in the solution itself. As I stated previously, candidate approximations for the propagator matrix in an arbitrarily heterogeneous material with depth must be compared on the basis of accuracy, efficiency and ease of implementation. The plane homogeneous layered approximation is exact for the structural model it represents and can be made arbitrarily accurate to represent any structural model in a straightforward and physically interpretable manner. Also this approximation is relatively efficient and easy to implement due to the simple algebraic-trigonometric form of the solution.

I was able to compare the homogeneous layered approximation directly with the full wave theory or Langer approximation which has been used extensively by Paul Richards and was modified by Vernon Cormier (1980) to compute the stress-displacement propagator matrix in a layered structure in which the layer elastic moduli vary linearly with depth. The Langer approximation ran about ten to twenty times slower than the homogeneous layered approximation on a per layer basis. Also the Langer approximation is an approximation of the solution and not in the representation of the structure and it breaks down when velocity gradients within a layer become large. When this happens the structure must be broken up into thin layers as with the homogeneous layered approximation.

2.5 Integral and Spectral Representations for the Solution of the Elastic Wave Equation

Equation (2.3.4) represents a solution of the elastic wave equation for all t, r, θ, and z in terms of the constant parameters ω, k and m. The final solution will be some appropriate linear combination of solutions of form (2.3.4) spanning the range of the parameters ω, k, and m, and this appropriate combination will be determined by the source vector, $\{w(\omega,k,m,z)\}$, in equation (2.4.13). In order to determine the source vector we first define the following transforms:

$$F(f(t)) = \int_{-\infty}^{+\infty} f(t)\, e^{-i\omega t}\, dt, \quad -\infty \leqslant \omega \leqslant +\infty \tag{2.5.1}$$

$$F^{-1}(f(\omega)) = \frac{1}{2\pi} \int_{-\infty}^{+\infty} f(\omega)\, e^{+i\omega t}\, d\omega, \tag{2.5.2}$$

where $F(\cdot)$ is the integral Fourier transform and $F^{-1}(\cdot)$ is the inverse integral Fou r transform,

$$G(f(\theta)) = \int_0^{2\pi} f(\theta)\, e^{-im\theta}\, d\theta,\ m = -\infty, \cdots, -1, 0, 1, \cdots \infty \qquad (2.5.3)$$

$$G^{-1}(f(m)) = \frac{1}{2\pi} \sum_{m=-\infty}^{+\infty} \left(f(m)\, e^{+im\theta} \right), \qquad (2.5.\ )$$

where $G(\cdot)$ is the discrete Fourier transform $G^{-1}(\cdot)$ is the inverse discrete Fourier transform,

$$H(f(r)) = \int_0^{\infty} f(r)\, J_m(kr) r dr\ , \qquad (2.5.5)$$

$$0 \leq k \leq +\infty,\ m = -\infty, \cdots, -1, 0, 1, \cdots, +\infty$$

$$H^{-1}(f(k,m)) = \int_0^{\infty} f(k,m)\, J_m(kr) k dk\ , \qquad (2.5.6)$$

$H(\cdot)$ is the Hankel transform and $H^{-1}(\cdot)$ is the inverse Hankel transform. Note that these transforms are normalized so that,

$$F^{-1}\left(F(f(t)) \right) = f(t)\ ,$$

$$G^{-1}\left(G(f(\theta)) \right) = f(\theta)\ ,$$

$$H^{-1}\left(H(f(r)) \right) = f(r)\ ,\ \text{for all } m.$$

Ben-Menahem and Singh (1981) show how any vector, $\chi(r,\theta)$, can be expanded in terms of vector cylindrical harmonics

$$\chi(r,\theta) = \sum_{m=-\infty}^{+\infty} \frac{1}{2\pi} \int_0^{\infty} k dk \left[\chi_P(k,m)\, P_k^m(r,\theta) + \right.$$

$$\left. \chi_B(k,m)\, B_k^m(r,\theta) + \chi_C C_k^m(r,\theta) \right]\ , \qquad (2.5.7)$$

where using the vector cylindrical harmonic orthogonality relations,

$$\chi_P(k,m) = \int_0^{\infty} r\,dr \int_0^{2\pi} d\theta\ \chi(r,\theta) \cdot \mathbf{P}_k^{m^*}(r,\theta)\ , \tag{2.5.8}$$

$$\chi_B(k,m) = \int_0^{\infty} r\,dr \int_0^{2\pi} d\theta\ \chi(r,\theta) \cdot \mathbf{B}_k^{m^*}(r,\theta)\ ,$$

$$\chi_C(k,m) = \int_0^{\infty} r\,dr \int_0^{2\pi} d\theta\ \chi(r,\theta) \cdot \mathbf{C}_k^{m^*}(r,\theta)\ ,$$

and * denotes complex conjugate. We can express the body force vector, $\rho f(\omega,r,\theta,z)$, as (2.5.7) and thus the displacement vector $u(\omega,r,\theta,z)$, as

$$u(\omega,r,\theta,z) = \frac{1}{2\pi} \sum_{m=-\infty}^{+\infty} \int_0^{\infty} k\,dk \Big[u_P(\omega,k,m,z)\ \mathbf{P}_k^m(r,\theta) + \tag{2.5.9}$$

$$+ u_B(\omega,k,m,z)\ \mathbf{B}_k^m(r,\theta) + u_C(\omega,k,m,z)\ \mathbf{C}_k^m(r,\theta) \Big]\ .$$

In order to obtain the time domain solution, we apply the inverse integral Fourier transform to $u(\omega)$.

$$u(t,r,\theta,z) = \frac{1}{2\pi} \int_{-\infty}^{+\infty} d\omega\ e^{i\omega t}\ u(\omega,r,\theta,z) \tag{2.5.10}$$

The actual values of the stress-displacement vector, {y} and thus the values of u_P, u_B and u_C will be functions of f_P, f_B and f_C in equation (2.3.8) and using (2.5.8) these are,

$$f_P(\omega,k,m,z) = \int_0^{\infty} r\,dr \int_0^{2\pi} d\theta\ \rho f(\omega,r,\theta,z) \cdot \mathbf{P}_k^{m^*}(r,\theta)\ , \tag{2.5.11}$$

$$f_B(\omega,k,m,z) = \int_0^{\infty} r\,dr \int_0^{2\pi} d\theta\ \rho f(\omega,r,\theta,z) \cdot \mathbf{B}_k^{m^*}(r,\theta)\ ,$$

$$f_C(\omega,k,m,z) = \int_0^{\infty} r\,dr \int_0^{2\pi} d\theta\ \rho f(\omega,r,\theta,z) \cdot \mathbf{C}_k^{m^*}(r,\theta)\ ,$$

where

$$\rho f(\omega,r,\theta,z) = \int_{-\infty}^{+\infty} d\omega\, e^{-i\omega t}\, \rho f(t,r,\theta,z)\,.$$

Equations (2.5.11) allow us to express any space and time distribution of body forces in terms of frequency and depth dependent vector cylindrical harmonics. Using equations (2.4.3) and (2.4.13) along with the expressions for the propagator matrix and the boundary conditions at the top and the bottom of the structure, we can compute the stress-displacement vector at any depth. Finally, with equations (2.4.2), (2.5.9) and (2.5.10) we can compute the displacement vector, u, for all space and time.

At this point I will make the following assumption regarding the source vector, {w}.

$$\{w(\omega,k,m,z)\} = \delta(z - z_s)\,\{\Sigma(\omega,k,m)\} \qquad (2.5.12)$$

I am thus restricting the source to a horizontal plane at depth z_s. We can see from equation (2.4.13) that if $z_s < z < z_0$, or if $z_s < z_0 < z$, or if $z_s > z > z_0$, or if $z_s > z_0 > z$ (i.e. z_s, is not between z and z_0), then the integral in (2.4.13) will be zero. On the other hand, if $z < z_s < z_0$, or $z_0 < z_s < z$, then

$$\{y(z)\} = [A(z,z_0)]\,\{y(z_0)\} - [A(z,z_s)]\,\{\Sigma\}\,, \qquad (2.5.13)$$

$$z < z_s < z_0 \text{ or } z_0 < z_s < z\,.$$

The vector function {Σ} is called the source jump vector since it causes a discontinuous jump in the stress-displacement vector. Notice that this "jump" condition only exists when the source is restricted to a horizontal plane (or a point) and that for a spatially distributed source in depth, the

stress-displacement vector will remain continuous everywhere.

The problem of computing the stress-displacement vector for a given source at depth z_s has now been reduced to a linear algebra problem. For a completely solid material we can relate the stress-displacement vector at the top interface to the stress-displacement vector at the bottom interface as follows:

$$\{y(0)\} = [A(0,z_s)]\ \{y(z_s^-)\}\,, \tag{2.5.14}$$

$$\{y(H)\} = [A(H,z_s)]\ \{y(z_s^+)\}\,,$$

$$\{y(z_s^+)\} = \{y(z_s^-)\} - \{\Sigma\}\,,$$

where z_s^- is immediately above the source,

and z_s^+ is immediately below the source,

and $0 = z_T$ is the depth of the top boundary,

and $H = z_B$ is the depth of the bottom boundary.

We now need to apply boundary conditions at the top and bottom of the structure. These boundary conditions can be expressed in terms of zeroing out some linear combinations of the stress-displacement vector and so we define the [E] matrices as,

$$[^T E]\ \{y(0)\} = \{0\}\,, \tag{2.5.15}$$

$$[^B E]\ \{y(H)\} = \{0\}\,,$$

where the superscript T denotes the top interface and B denotes the bottom interface.

The two [E] matrices will, in general, not be square and may have different dimensions. For a solid structure both $[^{T}E]$ and $[^{B}E]$ will have six columns and the sum of the number of rows for both matrices will be six. The number of rows for each matrix will be equal to the number of boundary conditions at that interface and in practice there will be three boundary conditions at each of the top and bottom interfaces. The [E] matrices are given below for the various boundary conditions expressed by equations (2.2.11) through (2.2.15).

1. A traction free surface,

$$[E] = \begin{bmatrix} 0 & 0 & 1 & 0 & 0 & 0 \\ 0 & 0 & 0 & 1 & 0 & 0 \\ 0 & 0 & 0 & 0 & 0 & 1 \end{bmatrix} \tag{2.5.16}$$

2. A rigid surface,

$$[E] = \begin{bmatrix} 1 & 0 & 0 & 0 & 0 & 0 \\ 0 & 1 & 0 & 0 & 0 & 0 \\ 0 & 0 & 0 & 0 & 1 & 0 \end{bmatrix} \tag{2.5.17}$$

3. Zero shear tractions and zero vertical displacement,

$$[E] = \begin{bmatrix} 1 & 0 & 0 & 0 & 0 & 0 \\ 0 & 0 & 0 & 1 & 0 & 0 \\ 0 & 0 & 0 & 0 & 0 & 1 \end{bmatrix} \tag{2.5.18}$$

4. No upward propagating P or S wave radiation (Sommerfield radiation condition for a bottom half space). In order to do this we must first transform the stress-displacement vector to the wavefield vector using the transformation matrix, $[B]^{-1}$. We then pick out the first, third and fifth rows of $[B]^{-1}$ to give for a solid half space,

$$[E] = \frac{1}{2}\begin{bmatrix} -\frac{(\gamma-1)}{i\phi_\alpha} & \gamma & -\frac{1}{\rho c^2} & \frac{1}{\rho c^2 i\phi_\alpha} & 0 & 0 \\ \gamma & -\frac{(\gamma-1)}{i\phi_\beta} & \frac{1}{\rho c^2 i\phi_\beta} & -\frac{1}{\rho c^2} & 0 & 0 \\ 0 & - 0 & 0 & 0 & 1 & \frac{1}{\rho\beta^2 i\phi_\beta} \end{bmatrix}, \quad (2.5.19)$$

where the elastic moduli are those of the half space,

5. No downward propagating P or S wave radiation (Sommerfeld radiation condition for a top half space). In this case we pick out the second, fourth, and sixth rows of $[B]^{-1}$.

$$[E] = \frac{1}{2}\begin{bmatrix} \frac{(\gamma-1)}{i\phi_\alpha} & \gamma & -\frac{1}{\rho c^2} & -\frac{1}{\rho c^2 i\phi_\alpha} & 0 & 0 \\ \gamma & \frac{(\gamma-1)}{i\phi_\beta} & \frac{-1}{\rho c^2 i\phi_\beta} & -\frac{1}{\rho c^2} & 0 & 0 \\ 0 & 0 & 0 & 0 & 1 & -\frac{1}{\rho\beta^2 i\phi_\beta} \end{bmatrix}. \quad (2.5.20)$$

As with the propagator matrix, it is obvious that we can partition the [E] matrix into a 2×4 $[{}_R E]$ matrix and a 1×2 $[{}_L E]$ matrix.

From equations (2.5.14) and (2.5.15) we arrive at,

$$[{}^T E]\,[A(0,z_s)]\,\{y(z_s^-)\} = \{0\} \quad (2.5.21)$$

$$[{}^B E]\,[A(H,z_s)]\,\{y(z_s^+)\} = \{0\},$$

$$[{}^B E]\,[A(H,z_s)]\,\{y(z_s^-)\} = [{}^B E]\,[A(H,z_s)]\,\{\Sigma\}. \quad (2.5.22)$$

we now define the [D] matrices as follows,

$$[{}^T D(z)] = [{}^T E]\,[A(0,z)], \quad (2.5.23)$$

$$[{}^B D(z)] = [{}^B E]\,[A(H,z)], \quad (2.5.24)$$

so that

$$[^{T}D(z)]\ \{y(z)\} = \{0\}\ ,z < z_s\ , \tag{2.5.25}$$

and

$$[^{B}D(z)]\ \{y(z)\} = \{0\}\ ,z > z_s\ , \tag{2.5.26}$$

Equations (2.5.25) and (2.5.26) are important relations and will constitute the basis for numerically stable computations of the stress-displacement vector. We can now specify the stress-displacement vector immediately above the source as,

$$[^{T}D(z_s)]\ \{y(z_s^-)\} = \{0\}\ , \tag{2.5.27}$$

$$[^{B}D(z_s)]\ \{y(z_s^-)\} = [^{B}D(z_s)]\ \{\Sigma\}\ .$$

This gives us six equations in the six unknowns, $\{y(z_s^-)\}$, so we can solve for $\{y(z_s^-)\}$. We can then compute the stress-displacement vector at any other depth by using the propagator matrix

$$[D(z_s)]\ \{y(z_s^-)\} = \left\{ \begin{array}{c} \{0\} \\ \hline [^{B}(z_s)]\ \{\Sigma\}\ , \end{array} \right\}\ , \tag{2.5.28}$$

$$\{y(z)\} = [A(z,z_s)]\ \{y(z_s^-)\}\ ,z < z_s\ , \tag{2.5.29}$$

$$\{y(z)\} = [A(z,z_s)]\ \left(\{y(z_s^-)\} - \{\Sigma\}\right)\ ,z > z_s\ , \tag{2.5.30}$$

where $[D(z_s)]$ is a six by six matrix composed of $[^{T}D(z_s)]$ and $[^{B}D(z_s)]$ as,

$$[D(z_s)] = \left[\begin{array}{c} [^{T}D(z_s)] \\ \hline [^{B}D(z_s)] \end{array} \right]\ . \tag{2.5.31}$$

Once again $|D(z_s)|$ can be partitioned into a four by four Rayleigh matrix and a two by two Love matrix.

So far, in order to compute the various [D] matrices, we have assumed solid-solid welded interfaces and this approach must be modified somewhat to handle acoustic layers. Of course, Love waves will be completely blocked at a solid-liquid interface and so we will only need to address the P-SV problem. Let us first consider the case of the P-SV stress-displacement vector being propagated upward through a solid to liquid interface. In this case we will denote the stress-displacement vector in the solid material immediately below the interface as $\{_R y\}$ and the stress-displacement vector in the liquid material immediately above the interface as $\{_A y\}$. From equations (2.2.17), the boundary conditions at the interface require the following:

$$ {}^R y_1 = {}^A y_1 , \qquad (2.5.32) $$

$$ {}^R y_3 = {}^A y_3 , $$

$$ {}^R y_4 = 0 , $$

$$ {}^A y_4 = 0 . $$

In this case the shear displacement will generally be discontinuous. Within the solid layer there are generally four linearly independent components of the stress-displacement vector with a four column (and usually two rows) $|{}^B_R D|$ matrix. Within the liquid layer there are two linearly independent components of the stress-displacement vector with a two column (and usually one row) $|{}^B_A D|$ matrix. The problem then is to apply the boundary conditions given by equations (2.5.32) to determine the elements of $|{}^B_A D|$ from

the elements of $[{}^{B}_{R}D]$ at the interface. This is a straightforward problem and the results are as follows:

$$ {}^{B}_{A}D_1 = {}^{B}_{R}D_{11}\,{}^{B}_{R}D_{22} - {}^{B}_{R}D_{12}\,{}^{B}_{R}D_{21}\,, \tag{2.5.33} $$

$$ {}^{B}_{A}D_2 = {}^{B}_{R}D_{13}\,{}^{B}_{R}D_{22} - {}^{B}_{R}D_{12}\,{}^{B}_{R}D_{23}\,, $$

where

$$ 0 = [{}^{B}_{A}D]\,\{{}_{A}y\} = [{}^{B}_{A}D_1 \;\; {}^{B}_{A}D_2] \begin{Bmatrix} y_1 \\ y_3 \end{Bmatrix} \tag{2.5.34} $$

For the case of the stress-displacement vector being propagated upward through a liquid to solid interface, the same boundary conditions apply and the resulting $[{}^{B}_{R}D]$ matrix is as follows:

$$ {}^{B}_{R}D_{11} = {}^{B}_{A}D_1\,, \tag{2.5.35} $$

$$ {}^{B}_{R}D_{13} = {}^{B}_{A}D_2\,, $$

$$ {}^{B}_{R}D_{24} = 1 $$

$$ {}^{B}_{R}D_{12} = {}^{B}_{R}D_{14} = {}^{B}_{R}D_{21} = {}^{B}_{R}D_{22} = {}^{B}_{R}D_{23} = 0\,. $$

The results for downward propagating $[{}^{T}D]$ matrices are identical.

Given the stress-displacement vector, we can write the integral equations for the displacement vector given by (2.5.9) as Rayleigh and Love wave components.

$$ {}^{R}u_r(\omega,r,\theta,z) = \frac{1}{2\pi} \sum_{m=-\infty}^{+\infty} \int_0^{\infty} y_2(\omega,k,m,z;z_s) \left(\frac{m}{kr} J_m(kr) - J_{m+1}(kr) \right) e^{im\theta}\, k\,dk \tag{2.5.36} $$

$$R^{u_\theta}(\omega,r,\theta,z) = \frac{1}{2\pi} \sum_{m=-\infty}^{+\infty} \int_0^\infty y_2(\omega,k,m,z;z_s)\, J_m(kr) \left(\frac{im}{kr}\right) e^{im\theta}\, kdk$$

$$R^{u_z}(\omega,r,\theta,z) = \frac{1}{2\pi} \sum_{m=-\infty}^{+\infty} \int_0^\infty y_1(\omega,k,m,z;z_s)\, J_m(kr)\, e^{im\theta}\, kdk$$

and

(2.5.37)

$$L^{u_r}(\omega,r,\theta,z) = \frac{1}{2\pi} \sum_{m=-\infty}^{+\infty} \int_0^\infty y_5(\omega,k,m,z;z_s)\, J_m(kr) \left(\frac{im}{kr}\right) e^{im\theta}\, kdk$$

$$L^{u_\theta}(\omega,r,\theta,z) = \frac{1}{2\pi} \sum_{m=-\infty}^{+\infty} \int_0^\infty y_5(\omega,k,m,z;z_s) \left(-\frac{m}{kr} J_m(kr) + J_{m+1}(kr)\right) e^{im\theta}\, kdk$$

$$L^{u_z}(\omega,r,\theta,z) = 0\,,$$

where y_1, y_2 and y_5 come from equations (2.5.28), (2.5.29) and (2.5.30).

Equations (2.5.36) and (2.5.37) are the basis for the various numerical integration approaches which I refer to collectively as the reflectivity method. First popularized by Fuchs and Muller (1971) this direct integration method has been modified and expanded by Kind (1978), Kennett and Kerry (1979), who eliminated certain numerical instabilities, Cormier (1980), who applied the Langer approximation to model inhomogeneous layers and deformed the contour of integration to avoid singularities in the integrand function and Bouchon (1981), who established a spatial sampling theorem with respect to the Hankel transforms and applied this theorem in a discrete wavenumber method for evaluating the wavenumber integrals. All of the reflectivity methods have in common the direct numerical integration of the wavenumber (or slowness) integrals in equations (2.5.36) and (2.5.37).

Another approach for evaluating the wavenumber integrals is to deform the contour of integration in the complex wavenumber plane so as to encircle the singularities of the integrand function and then apply the residue theorem. The integrals given by equations (2.5.36) and (2.5.37) are not amenable to this since the Bessel functions blow up as $|k| \to \infty$, however, Lapwood (1949) and more recently Hudson (1969) have shown how the Bessel functions can be changed to Hankel functions of the second kind by extending the contour of integration to $-\infty$.

$$\int_0^{\infty} f(k,m)\, J_m(kr)\, k\,dk = \frac{1}{2} \int_{-\infty}^{+\infty} f(k,m)\, H_m^{(2)}(kr)\, k\,dk\,, \qquad (2.5.38)$$

where $f(k,n) = (-1)^{n+1} f(-k,n)$,

and $H_m^{(2)}$ is the integer order Hankel function of the second kind.

The Hankel functions go to zero as $|k| \to \infty$ and $\mathrm{Im}(k) < 0$, so the contour of integration can be closed by including a semicircular arc at infinity in the lower half of the complex wavenumber plane. We now need to consider the locations and characteristics of the singularities of the integrand functions.

The singularities of the Hankel functions are well known and so we turn our attention to the singularities of the stress-displacement vector, $\{y\}$, as a function of complex wavenumber. First of all we will address the question of when $\{y\}$ is a multivalued function of wavenumber with attendant branch points and branch cuts. The only multivalued functions to appear in the propagator matrices or boundary condition ([E]) matrices are the dual valued vertical wavenumber functions, ν_α and ν_β (as ϕ_α and ϕ_β). In the case of the propagator matrices, these functions always appear either as arguments of even functions (e.g. $\cos((z - z_0)\nu_\alpha)$) or in products or quo-

tients (e.g. $\nu_\alpha \sin((z - z_0)\,\nu_\alpha)$, $\sin((z - z_0)\,\nu_\alpha)/\nu_\alpha$) such that the result is single valued, and thus the propagator matrices are single valued. The boundary condition matrices, $[^{T}E]$ and $[^{B}E]$, however, may be either single valued or multivalued depending on the type of boundary condition.

For conditions where all incident seismic energy is reflected for all wavenumbers (equations (2.5.16), (2.5.17), and (2.5.18)), the [E] matrix is single valued and if both $[^{T}E]$ and $[^{B}E]$ are determined by one of these conditions then we will refer to this as the plate problem. For the plate problem the various [D] matrices will also be single valued, as can be seen from equations (2.5.23), (2.5.24) and (2.5.31) and since the source jump vector, $\{\Sigma\}$, is always single valued, the stress-displacement vector will also be single valued as can be seen from equations (2.5.28) to (2.5.30). Thus the contour of integration can encircle the lower half of the complex wavenumber plane without being required to detour around any branch cuts or branch points.

The case of most interest in seismology is what we will refer to as the half space problem, that is, a reflectivity boundary condition at the top and a radiation boundary condition at the bottom of the structure. The free surface boundary condition will be applied at the top of the structure and thus $[^{T}E]$ will be single valued and given by equation (2.5.16). The radiation condition given by equation (2.5.19) will specify the boundary condition matrix at the bottom $[^{B}E]$, but in this case the matrix will be four valued for P-SV waves due to the ν_α and ν_β functions (in the form of ϕ_α and ϕ_β), and two valued for SH waves due to ν_α (ϕ_β). We can see then that the P-SV stress-displacement vector will be four valued with two branch points at $\nu_\alpha = 0$ and $\nu_\beta = 0$ and two branch cuts emanating from

these branch points and the SH stress-displacement vector will be two valued with one branch point at $\nu_\beta = 0$ and one associated branch cut. The contour of integration must be deformed around these branch cuts and branch points in order to stay on an analytic path and the resulting branch cut integral contributions are well known and physically attributable to the energy which "leaks" away into the bottom half space (Gilbert (1964)). We have been somewhat remiss in this analysis since ν_α and ν_β are functions of k^2 and so for every branch point at +k there is another at -k. Consequently, there are actually four branch points and branch cuts for the P-SV case and two branch points and branch cuts for the SH case, however since the integration contour circles only half of the complex wavenumber plane, only two branch cut integrals will occur for the P-SV case and one for the SH case. As we will see this symmetry will also be characteristic of the poles of {y} as well as the branch points and branch cuts.

The remaining singularities of the stress-displacement vector are the Rayleigh and Love poles which occur at values of ω and k for which the [D] matrix in equation (2.5.28) is singular. For a fixed frequency these poles will occur at discrete wavenumbers, however in the (ω,k) space these poles form continuous functions of ω and k which are commonly called dispersion curves. Thus, in order to locate the poles, we can either fix frequency and look for discrete poles as a function of wavenumber (or phase velocity, slowness, etc.), or fix wavenumber and look for discrete poles as a function of frequency. Whenever the [D] matrix is singular, we can write equation (2.5.28) as follows:

$$[D(K(n,\omega),z_s)]\,\{E(n,\omega,z_s)\} = \{0\}\,, \qquad (2.5.39)$$

where $K(n,\omega)$ is the n^{th} value of wavenumber which at frequency ω for

(2.5.39) is true given $\{E(z_s)\} \neq \{0\}$. Note that equations (2.5.39) and (2.5.28) are identical if $\{y\} = \{E\}$ and if $\{\Sigma\} = \{0\}$. Thus the $\{E\}$ vector is the stress-displacement vector for the unforced vibration problem, or in other words, $\{E(n,\omega,z)\}$ is the depth dependence of the n^{th} flat earth normal mode at frequency ω.

Kazi (1976) shows how (2.5.39) can be written as an eigenvalue problem for SH waves and defines a Love wave operator whose eigenvalues are ${}_LK^2(n,\omega)$ and eigenfunctions are $\{{}_LE(n,\omega,z)\}$ The definition of a Rayleigh wave operator is not so straightforward because of the P-SV coupling, however, we can still compute Rayleigh wave eigenvalues and eigenfunctions by searching out the singular values of $[{}_RD(\omega,k)]$. In order to do this we will first propagate the eigenfunctions from the source depth to the surface so that,

$$[D(K(n,\omega),0)]\,\{E(n,\omega,0)\} = \{0\}\,, \tag{2.5.40}$$

where

$$[D(K(n,\omega),0)] = \begin{bmatrix} [{}^TE(K(n,\omega))] \\ \hline [{}^BD(K(n,\omega),0)] \end{bmatrix}. \tag{2.5.41}$$

Note that since the $\{E\}$ vector is a particular type of stress-displacement vector, it has most of the properties of the stress-displacement vector and, in particular, it can be computed at different depths by applying the correct propagator matrix. One property of $\{E\}$ which is not true of $\{y\}$, however, is that $\{E\}$ is continuous everywhere with depth and does not suffer a discontinuity at the source depth. In fact, from equation (2.5.39) we can see that the eigenvalues and eigenfunctions are completely independent of any source characteristics since z_s in that equation can be replaced by any

other depth we chose (as in equation (2.5.40)) which of course is what we would expect for normal mode solutions. It is this decoupling of structural wave propagation characteristics, as manifested by its spectra or normal modes, from the source and receiver characteristics that makes the normal mode method an efficient solution of the elastic wave equation.

Returning to (2.5.40) we now need to compute the determinant of [D] which we will refer to as the characteristic function

$$ {}_R\Delta(\omega,k) = \det([{}_RD(\omega,k,0)]) , \tag{2.5.42} $$

$$ {}_L\Delta(\omega,k) = \det([{}_LD(\omega,k,0)]). $$

Assuming a free surface boundary condition we can write the [D] matrices as follows:

$$ [{}_RD(\omega,k,0)] = \begin{bmatrix} 0 & 0 & 1 & 0 \\ 0 & 0 & 0 & 1 \\ {}^B_RD_{11}^{(0)} & {}^B_RD_{12}^{(0)} & {}^B_RD_{13}^{(0)} & {}^B_RD_{14}^{(0)} \\ {}^B_RD_{21}^{(0)} & {}^B_RD_{22}^{(0)} & {}^B_RD_{23}^{(0)} & {}^B_RD_{24}^{(0)} \end{bmatrix} , \tag{2.5.43} $$

and

$$ [{}_LD(\omega,k,0)] = \begin{bmatrix} 0 & 1 \\ {}^B_LD_1^{(0)} & {}^B_LD_2^{(0)} \end{bmatrix} \tag{2.5.44} $$

We can easily solve for the characteristic functions which are as follows:

$$ {}_R\Delta(\omega,k) = {}^B_RD_{11}(\omega,k,0)\,{}^B_RD_{22}(\omega,k,0) \tag{2.5.45} $$

$$ - {}^B_RD_{12}(\omega,k,0)\,{}^B_RD_{21}(\omega,k,0) , $$

$$ {}_L\Delta(\omega,k) = - {}^B_LD_1(\omega,k,0) \tag{2.5.46} $$

The characteristic functions are scalar functions of ω and k and implicitly

define the eigenvalues by,

$$ {}_R\Delta(\omega,{}_RK(n,\omega)) = 0 , \tag{2.5.47} $$

and

$$ {}_L\Delta(\omega,{}_LK(n,\omega)) = 0 . $$

The normalization of the eigenfunctions is arbitrary and so we will assume a vertical displacement and SH shear displacement of unity at the free surface. We can solve for the remaining non-zero eigenfunction, the P-SV radial shear displacement in terms of the [D] matrix elements so that

$$ {}_RE_1(n,\omega,0) = 1 \tag{2.5.48} $$

$$ {}_RE_2(n,\omega,0) = - \left({}^B_RD_{11}(\omega,{}_RK(n,\omega),0)\ {}^B_RD_{24}(\omega,{}_RK(n,\omega),0) \right. $$

$$ \left. - {}^B_RD_{14}(\omega,{}_RK(n,\omega),0)\ {}^B_RD_{21}(\omega,{}_RK(n,\omega),0) \right) $$

$$ / \left({}^B_RD_{12}(\omega,{}_RK(n,\omega),0)\ {}^B_RD_{24}(\omega,{}_RK(n,\omega),0) \right. $$

$$ \left. - {}^B_RD_{14}(\omega,{}_RK(n,\omega),0)\ {}^B_RD_{22}(\omega,{}_RK(n,\omega),0) \right) $$

$$ {}_RE_3(n,\omega,0) = 0 $$

$$ {}_RE_4(n,\omega,0) = 0 $$

$$ {}_LE_1(n,\omega,0) = 1 \tag{2.5.49} $$

$$ {}_LE_2(n,\omega,0) = 0 $$

With the surface values of the eigenfunctions defined, we can compute the eigenfunctions at any other depth simply by using the appropriate propagator matrices.

In order to use the normal modes we must say something about where the modes will be located. As with the branch points, for every eigenvalue at +k there will be one at -k due to the fact that the [D] matrix elements are functions of k^2 (or equivalently c^2). In general, for all of the Riemann sheets there will be both pure real and complex eigenwavenumbers (the exception to this are SH and acoustic plate problems for which the eigenwavenumbers are always either purely real or purely imaginary). The complex poles will be easy to deal with since we will include the residues of those complex poles which are within the contour of integration, however the poles on the real wavenumber axis cause a problem since the integration contour goes directly through those poles, and we cannot know off hand whether or not to include their residue contributions.

We could compute the principle values for these poles, but there is a simpler way to deal with this problem. Basically, we will apply a perturbation to the frequency, ω, such that the poles move off of the real wavenumber axis and can be easily identified as being within or outside of the contour of integration. We can allow the frequency to have a small, constant imaginary component as long as $\mathrm{Im}(\omega) < 0$ in order to insure that the Fourier transform remains analytic. For each pole on the real wavenumber axis for real frequency, we can compute the group velocity, U, as the slope of the dispersion curve in the ω, k space, or,

$$U(n,\omega) = d\omega/dk \Big|_{\omega,\,{}_{R}K(n,\omega)} . \qquad (2.5.50)$$

A small change in ω, $\delta\omega$, will thus cause a small change in ${}_{R}K(n,\omega)$, δK, such that,

$$\delta K = \delta\omega/U . \qquad (2.5.51)$$

So for poles on the positive real wavenumber axis, if the group velocity is positive then a small negative imaginary perturbation of frequency will move the poles into the fourth quadrant where they would be within the integration contour, and if the group velocity is negative then the frequency perturbation will move the poles into the first quadrant where they will be outside of the integration contour. However, for every pole at +k there will be one at -k and it is easy to show that a pole at +k with group velocity U will have a companion pole at -k with group velocity -U. So the companion poles to those on the positive real wavenumber axis with positive group velocities will have negative group velocities and will move into the second quadrant where they will be outside of the contour of integration. The companion poles to those on the positive real wavenumber axis with negative group velocities will have positive group velocities and will move into the third quadrant where they will be within the contour of integration. The net result is that all poles with positive real wavenumbers and positive group velocity will contribute their residues to the wavenumber integral and those poles with positive real wavenumbers and negative group velocity will contribute with their companion poles at -k. The wavenumber integration contour in the complex wavenumber plane along with the branch points, branch cuts and poles are shown in figure 2-2 for the general P-SV half space problem. We can see from figure 2-2 that

$$\int_{-\infty}^{+\infty} + R_\alpha I + R_\beta I = -2\pi i \sum_{a} \text{residues}, \qquad (2.5.52)$$

where the arcs at infinity do not contribute and the sum of residues are those within the integration contour, Γ.

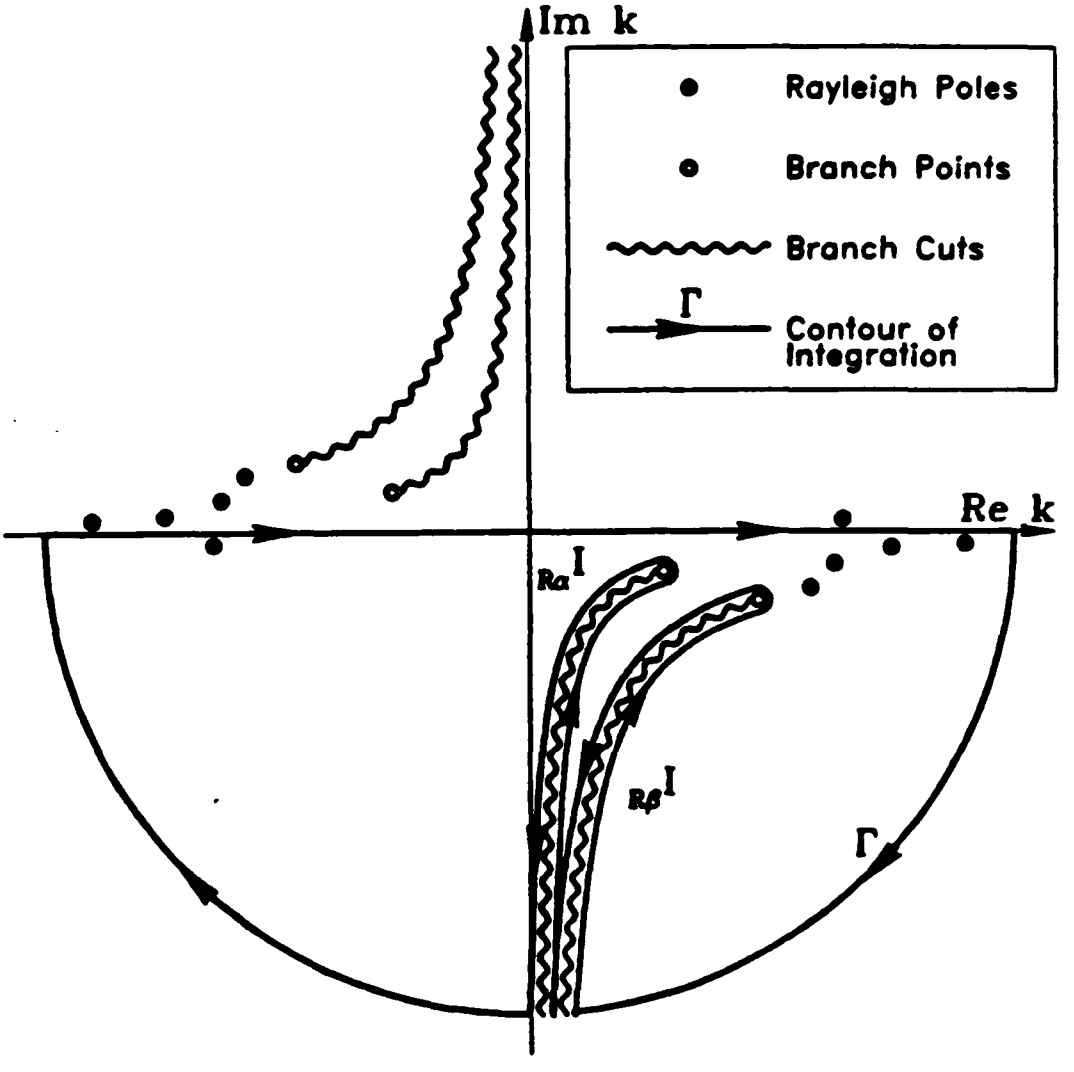

Figure 2-2. Wavenumber integration contour for a complex frequency with a small, negative imaginary component.

We now turn our attention to the evaluation of the residues. Returning to equation (2.5.28), we can write the solution for the stress-displacement vector at the top of the structure as we did with the eigenfunctions

$$[D(0)]\ \{y(0)\} = \begin{Bmatrix} \{0\} \\ \hline [{}^{B}D(0)]\ [A(0,z_s)]\ \{\Sigma\} \end{Bmatrix} \tag{2.5.53}$$

Once gain we assume a free surface so that $[D(0)]$ is given by equations (2.5.43) and (2.5.44). Substituting these relations in (2.5.53) it follows that,

$$\begin{Bmatrix} {}_{R}y_1(0) \\ {}_{R}y_2(0) \end{Bmatrix} = \frac{1}{{}_{R}\Delta} \begin{bmatrix} {}^{B}_{R}D_{11}(0) & -{}^{B}_{R}D_{12}(0) \\ -{}^{B}_{R}D_{21}(0) & {}^{B}_{R}D_{11}(0) \end{bmatrix} [{}^{B}_{R}D(0)]\ [{}_{R}A(0,z_s)]\ \{{}_{R}\Sigma\} \tag{2.5.54}$$

$${}_{R}y_3(0) = {}_{R}y_4(0) = 0\ ,$$

and

$${}_{L}y_1(0) = -\frac{1}{{}_{L}\Delta}\ [{}^{B}_{L}D(0)]\ [{}_{L}A(0,z_s)]\ \{{}_{L}\Sigma\}\ , \tag{2.5.55}$$

$${}_{L}y_2(0) = 0.$$

We can see that the two by two minors of the two by four P-SV $[{}^{B}_{R}D]$ matrix appear repeatedly throughout the analytical development of the eigenvalues, eigenfunctions and the stress-displacement vector. In order to save writing we will define the four by four anti-symmetric minor matrix, $[M]$, as,

$$M_{ij}(\omega,k,z) = {}_{R}D_{1i}(\omega,k,z)\ {}_{R}D_{2j}(\omega,k,z) \tag{2.5.56}$$

$$-\ {}_{R}D_{1j}(\omega,k,z)\ {}_{R}D_{2i}(\omega,k,z)\ .$$

Obviously,

$$M_{ij}(\omega,k,z) = - M_{ji}(\omega,k,z) ,$$
$$M_{11} = M_{22} = M_{33} = M_{44} = 0.$$

We will also have two versions of the minor matrix, $[^{B}M]$ and $[^{T}M]$ corresponding to $[^{B}_{R}D]$ and $[^{T}_{R}D]$. The minor matrix can now be used to simplify the solution to equation (2.5.54) as follows,

$$\begin{Bmatrix} {}_{R}y_1(0) \\ {}_{R}y_2(0) \end{Bmatrix} = \frac{1}{{}_{R}\Delta} \begin{bmatrix} {}^{B}M_{12}(0) & 0 & -{}^{B}M_{23}(0) & -{}^{B}M_{24}(0) \\ 0 & {}^{B}M_{12}(0) & {}^{B}M_{13}(0) & {}^{B}M_{14}(0) \end{bmatrix} [{}_{R}A(0,z_s)] \{{}_{R}\Sigma\} . \tag{2.5.57}$$

We can also see from equation (2.5.45) that,

$${}_{R}\Delta = {}^{B}M_{12}(0) . \tag{2.5.58}$$

The P-SV radial displacement eigenfunction at the surface, given by equation (2.5.48), can be written as follows

$${}_{R}\epsilon(n,\omega) = \frac{{}_{R}E_2(n,\omega,0)}{{}_{R}E_1(n,\omega,0)} = {}_{R}E_2(n,\omega,0) = \tag{2.5.59}$$

$$= - \frac{{}^{B}M_{14}(\omega,{}_{R}K(n,\omega),0)}{{}^{B}M_{24}(\omega,{}_{R}K(n,\omega),0)}$$

$$= - \frac{{}^{B}M_{13}(\omega,{}_{R}K(n,\omega),0)}{{}^{B}M_{23}(\omega,{}_{R}K(n,\omega),0)} ,$$

where ${}_{R}\epsilon(n,\omega)$ is the Rayleigh wave surface ellipticity for the n^{th} mode at frequency ω.

Poles of equation (2.5.52) will occur whenever ${}_{R}\Delta = 0$ which implicitly defines the eigenwavenumbers. We can simplify equation (2.5.57) further when k is an eigenwavenumber and express it in terms of the

eigenfunctions, but first we must state two general properties.

$$M_{13}(\omega,k,z) = -M_{24}(\omega,k,z) \tag{2.5.60}$$

This is true for all ω, k and z. It is obviously true for the boundary conditions given by equations (2.5.16) through (2.5.20) at the top and bottom of the structure, and, with much tedious algebraic manipulation, it can be shown to be true at all depths. The second property allows one to relate the elements of a P-SV propagator matrix which propagates the stress-displacement vector upward between two depths to the elements of the downward propagator matrix.

$$[{}_R A(z,z_0)] = \begin{bmatrix} {}_R A_{33}(z_0,z) & {}_R A_{43}(z_0,z) & -{}_R A_{13}(z_0,z) & -{}_R A_{23}(z_0,z) \\ {}_R A_{34}(z_0,z) & {}_R A_{44}(z_0,z) & -{}_R A_{14}(z_0,z) & -{}_R A_{24}(z_0,z) \\ -{}_R A_{31}(z_0,z) & -{}_R A_{41}(z_0,z) & {}_R A_{11}(z_0,z) & {}_R A_{21}(z_0,z) \\ -{}_R A_{32}(z_0,z) & -{}_R A_{42}(z_0,z) & {}_R A_{12}(z_0,z) & {}_R A_{22}(z_0,z) \end{bmatrix} \tag{2.5.61}$$

This can be shown by using the relations that exist among the elements of the P-SV layer propagator matrix (equations (2.4.44)) and then reversing the order of layer multiplications. Equation (2.5.6) is a general property of the propagator matrix; it is true for all ω, k, z, and z_0 and it is true even for an arbitrarily inhomogeneous structure with depth. We now define the numerator vector in (2.5.57) as

$$\begin{Bmatrix} {}_R y_1(z_0) \\ {}_R y_2(z_0) \end{Bmatrix} = \frac{1}{{}_R\Delta} \begin{Bmatrix} {}_R N_1(z) \\ {}_R N_2(z) \end{Bmatrix}. \tag{2.5.62}$$

Using equations (2.5.58), (2.5.59), and (2.5.60) we can solve for [N] evaluated at an eigenwavenumber as,

$$\left\{\begin{matrix} {}_R N_1^{(0)} \\ {}_R N_2^{(0)} \end{matrix}\right\} \Bigg|_{k = {}_R K(n,\omega)} = - {}^B M_{23}(0) \begin{bmatrix} 0 & 0 & 1 & R^{\epsilon} \\ 0 & 0 & R^{\epsilon} & R^{\epsilon 2} \end{bmatrix} [{}_R A(0,z_s)] \{{}_R \Sigma\} \Bigg|_{k={}_R K(n,\omega)} \tag{2.5.63}$$

Using (2.5.61) this can be expressed as follows,

$${}_R N_1^{(0)} \Big|_{k={}_R K(n,\omega)} = \tag{2.5.64}$$

$$= - {}^B M_{23}(0) [1 \; R^{\epsilon}] \begin{bmatrix} - {}_R A_{31}(z_s,0) & - {}_R A_{41}(z_s,0) & {}_R A_{11}(z_s,0) & {}_R A_{21}(z_s,0) \\ - {}_R A_{32}(z_s,0) & - {}_R A_{42}(z_s,0) & {}_R A_{12}(z_s,0) & {}_R A_{22}(z_s,0) \end{bmatrix} \cdot$$

$$\cdot \{{}_R \Sigma\} \Big|_{k={}_R K(n,\omega)},$$

$${}_R N_2^{(0)} \Big|_{k={}_R K(n,\omega)} = R^{\epsilon} \; {}_R N_1^{(0)} \Big|_{k={}_R K(n,\omega)}$$

We can write the Rayleigh wave eigenfunctions at the source depth as

$$\{{}_R E(n,\omega,z_s)\} = \begin{bmatrix} {}_R A_{11}(z_s,0) & {}_R A_{12}(z_s,0) \\ {}_R A_{21}(z_s,0) & {}_R A_{22}(z_s,0) \\ {}_R A_{31}(z_s,0) & {}_R A_{32}(z_s,0) \\ {}_R A_{41}(z_s,0) & {}_R A_{42}(z_s,0) \end{bmatrix} \Bigg|_{k={}_R K(n,\omega)} \begin{Bmatrix} 1 \\ R^{\epsilon}(n,\omega) \end{Bmatrix} \tag{2.5.65}$$

If we redefine a new vector for the source jump vector as,

$$[{}_R \Sigma(n,\omega)] = [{}_R \Sigma_3 \; {}_R \Sigma_4 \; - {}_R \Sigma_1 \; - {}_R \Sigma_2] \Big|_{k={}_R K(n,\omega)}, \tag{2.5.66}$$

and using (2.5.65) we can write (2.5.64) as

$$\left\{\begin{matrix} {}_R N_1^{(0)} \\ {}_R N_2^{(0)} \\ {}_R N_3^{(0)} \\ {}_R N_4^{(0)} \end{matrix}\right\} \Bigg|_{k={}_R K(n,\omega)} = \tag{2.5.67}$$

$$= - {}^B M_{23}(0) \Big|_{k={}_R K(n,\omega)} \left([{}_R \Sigma(n,\omega)] \{ {}_R E(n,\omega,z_s) \} \right) \{ {}_R E(n,\omega,0) \}$$

where we have expanded $\{{}_R N\}$ to four P-SV components. Finally, we can write the numerator vector at any other depth by applying the propagator matrix so that,

$$\{ {}_R N(z) \} \Big|_{k={}_R K(n,\omega)} = \tag{2.5.68}$$

$$= - {}^B M_{23}(0) \Big|_{k={}_R K(n,\omega)} \left([{}_R \Sigma(n,\omega)] \{ {}_R E(n,\omega,z_s) \} \right) \{ {}_R E(n,\omega,z) \}$$

We can also define a numerator vector for Love waves and without repeating the detailed derivation one can show that,

$$\{ {}_L N(z) \} \Big|_{k={}_L K(n,\omega)} = \tag{2.5.69}$$

$$= - {}^B D_2(0) \Big|_{k={}_L K(n,\omega)} \left([{}_L \Sigma(n,\omega)] \{ {}_L E(n,\omega,z_s) \} \right) \{ {}_L E(n,\omega,z) \}$$

where

$$[{}_L \Sigma(n,\omega)] = [{}_L \Sigma_2 - {}_L \Sigma_1] \Big|_{k={}_L K(n,\omega)}, \tag{2.5.70}$$

and

$$\{ {}_L y(z) \} = \frac{1}{\Delta_L} \{ {}_L N(z) \}. \tag{2.5.71}$$

We may now evaluate the wavenumber integrals given by equations (2.5.36) and (2.5.37) in terms of branch cut integrals and residue contributions. Using equations (2.5.38), (2.5.52), (2.5.58), (2.5.68), (2.5.69) and (2.5.71) we can write the frequency dependent displacements at a receiver location (r_r, θ_r, z_r) due to a source confined to a horizontal plane at depth z_s as follows,

$$ {}_R u(\omega, r_r, \theta_r, z_r) = - {}_R\alpha^I - {}_R\beta^I \qquad (2.5.72) $$

$$ - i \sum_n \sum_m \left({}_R A(n,\omega) \, [{}_R\Sigma(n,\omega,m)] \, \{ {}_R E(n,\omega,z_s) \} \, {}_R\Psi(n,\omega,m,r_r,\theta_r,z_r) \right) , $$

and

$$ {}_L u(\omega, r_r, \theta_r, z_r) = - {}_L\beta^I \qquad (2.5.73) $$

$$ - i \sum_n \sum_m \left({}_L A(n,\omega) \, [{}_L\Sigma(n,\omega,m)] \, \{ {}_L E(n,\omega,z_s) \} \, {}_L\Psi(n,\omega,m,r_r,\theta_r,z_r) \right) , $$

where the A's are scalar amplitude factors and are,

$$ {}_R A(n,\omega) = - \left. \frac{k \, {}^B M_{23}(0)}{\partial_R \Delta / \partial k} \right|_{k = {}_R K(n,\omega)} \qquad (2.5.74) $$

and

$$ {}_L A(n,\omega) = - \left. \frac{k \, {}^B L D_2(0)}{\partial_L \Delta / \partial k} \right|_{k = {}_L K(n,\omega)} , \qquad (2.5.75) $$

${}_R\Delta$ and ${}_L\Delta$ are defined by equations (2.5.45) and (2.5.46), $[{}_R\Sigma]$ and $[{}_L\Sigma]$ are defined by equations (2.5.66) and (2.5.70), and ${}_R\Psi$ and ${}_L\Psi$ are defined as follows,

$$ {}_R\Psi(n,\omega,m,r_r,\theta_r,z_r) = {}_RE_1(n,\omega,z_r)\,\hat{P}(n,\omega,m,r_r,\theta_r) \tag{2.5.76} $$

$$ + {}_RE_2(n,\omega,z_r)\,\hat{B}(n,\omega,m,r_r,\theta_r)\ , $$

$$ {}_L\Psi(n,\omega,m,r_r,\theta_r,z_r) = {}_LE_1(n,\omega,z_r)\,\hat{C}(n,\omega,m,r_r,\theta_r)\ , \tag{2.5.77} $$

where $\hat{P}$, $\hat{B}$ and $\hat{C}$ are modified vector cylindrical harmonics and are,

$$ \hat{P}(n,\omega,m,r_r,\theta_r) = e_z \left(H_m^{(2)}(kr_r)\, e^{im\theta_r} \right) \Big|_{k={}_RK(n,\omega)} \tag{2.5.78} $$

$$ \hat{B}(n,\omega,m,r_r,\theta_r) = e_r \left(\frac{\partial H_m^{(2)}(kr)}{\partial(kr)}\, e^{im\theta_r} \right) \Big|_{k={}_RK(n,\omega),\ r=r_r} \tag{2.5.79} $$

$$ + e_\theta \left(\frac{H_m^{(2)}(kr_r)}{(kr)}\, \frac{\partial e^{im\theta}}{\partial\theta} \right) \Big|_{k={}_RK(n,\omega),\ \theta=\theta_r} $$

and

$$ \hat{C}(n,\omega,m,r_r,\theta_r) = e_r \left(\frac{H_m^{(2)}(kr_r)}{(kr_r)}\, \frac{\partial e^{im\theta}}{\partial\theta} \right) \Big|_{k={}_RK(n,\omega),\ \theta=\theta_r} \tag{2.5.80} $$

$$ - e_\theta \left(\frac{\partial H_m^{(2)}(kr)}{\partial(kr)}\, e^{im\theta_r} \right) \Big|_{k={}_LK(n,\omega),\ r=r_r} . $$

2.6 The Branch Cut Integral Contributions

Finally we turn our attention to the branch cut integrals ${}_{R\alpha}I$, ${}_{R\beta}I$, and ${}_{L\beta}I$. Let us first consider the Rayleigh wave branch cut integrals as shown in figure 2-2. In order to facilitate the evaluation of the branch cut integrals we define the following complex valued functions of the real positive scalar variable η.

$$_{R\alpha}\tilde{K}(\eta,\omega) = \text{P-wave branch cut,} \tag{2.6.1}$$

$$_{R\beta}\tilde{K}(\eta,\omega) = \text{S-wave branch cut,}$$

where

$$_{R\alpha}\tilde{K}(0,\omega) = \text{P-wave branch point,}$$
$$= \omega/\alpha^{(N)}$$

$$_{R\beta}\tilde{K}(0,\omega) = \text{S-wave branch point,}$$
$$= \omega/\beta^{(N)}$$

and $0 \leqslant \eta \leqslant \infty$.

We will also denote wavenumber values immediately to the right and left of the branch cuts as viewed in figure 2-2 with + and - superscripts. We can now write the branch cut integrals as follows,

$$_{R\alpha}I = \int_{\infty}^{0} f(_{R\alpha}\tilde{K}^{+}(\eta,\omega))\ _{R\alpha}\tilde{K}'\, d\eta \tag{2.6.2}$$

$$+ \int_{0}^{\infty} f(_{R\alpha}\tilde{k}^{-}(\eta,\omega))\ _{R\alpha}\tilde{K}'\, d\eta\ ,$$

and similarly for the $_{R\beta}I$, where

$$_{R\alpha}\tilde{K}' = \frac{\partial}{\partial\eta}\left(_{R\alpha}\tilde{K}(\eta,\omega)\right)$$

and f(k) is the wavenumber integrand function. We can combine the two integrals in (2.6.2) to obtain the following

$$-\ _{R\alpha}I = \int_{0}^{\infty}\left(f(_{R\alpha}\tilde{K}^{+}(\eta,\omega)) - f(_{R\alpha}\tilde{K}^{-}(\eta,\omega))\right)\ _{R\alpha}\tilde{K}'\, d\eta \tag{2.6.3}$$

The P and S-wave branch cuts define discontinuities in the bottom half space vertical wavenumbers, $\nu_\alpha^{(N)}$ and $\nu_\beta^{(N)}$ so that as one crosses the P-wave branch cut, $\nu_\alpha^{(N)} \rightarrow -\nu_\alpha^{(N)}$, and as one crosses the S-wave branch cut, $\nu_\beta^{(N)} \rightarrow -\nu_\beta^{(N)}$. The only factors in the wavenumber integrand functions which will be discontinuous across the branch cuts will be the elements of the stress-displacement vector, and so in order to evaluate (2.5.29) we need to compute the stress-displacement difference function across the branch cut which we define as follows,

$$\{\delta y(\eta,z)\} = \{y^+(\eta,z)\} - \{y^-(\eta,z)\}\,, \tag{2.6.4}$$

where

$$\{y^+(\eta,z)\} = \{{}_R y(k,z)\}\Big|_{k = {}_R\bar{K}^+(\eta)}\,,$$

and

$$\{y^-(\eta,z)\} = \{{}_R y(k,z)\}\Big|_{k = {}_R\bar{K}^-(\eta)}\,,$$

For Rayleigh waves, we can use equation (2.5.57) to compute $\{{}_R y^+\}$ and $\{{}_R y^-\}$ at the surface. Remembering that the propagator matrix and source jump vector are both single valued functions, we can compute the stress-displacement branch cut jump at the surface as,

$$\begin{Bmatrix} \delta_R y_1(\eta,0) \\ \delta_R y_2(\eta,0) \end{Bmatrix} = \begin{bmatrix} 0 & 0 & \delta\left(-\dfrac{{}^B M_{23}(0)}{{}^B M_{12}(0)}\right) & \delta\left(-\dfrac{{}^B M_{24}(0)}{{}^B M_{12}(0)}\right) \\ 0 & 0 & \delta\left(\dfrac{{}^B M_{13}(0)}{{}^B M_{12}(0)}\right) & \delta\left(\dfrac{{}^B M_{14}(0)}{{}^B M_{12}(0)}\right) \end{bmatrix} [{}_R A(0,z_s)]\ \{{}_R \Sigma\}.$$

(2.6.6)

where $\delta(\cdot)$ defines the jump across the branch cut as with (2.6.4), so

$$\delta\left(\frac{{}^{B}M_{13}(0)}{{}^{B}M_{12}(0)}\right) = \frac{{}^{B}M_{13}^{+}(0)}{{}^{B}M_{12}^{+}(0)} - \frac{{}^{B}M_{13}^{-}(0)}{{}^{B}M_{12}^{-}(0)}, \text{ etc.}$$

From equation (2.5.60) it is easy to show that

$$\delta\left(\frac{{}^{B}M_{13}(0)}{{}^{B}M_{12}(0)}\right) = \delta\left(-\frac{{}^{B}M_{24}(0)}{{}^{B}M_{12}(0)}\right) \tag{2.6.6}$$

We can see that equation (2.6.5) resembles equation (2.5.63) which expresses the solution of the stress-displacement vector in terms of the discrete spectra of the Rayleigh wave operator. In order to derive a similar solution for the branch cut integrals, we need to determine the improper eigenfunctions which will constitute the continuous spectra of the Rayleigh wave operator. We will do this by first considering the stress-displacement vector $\{{}_{R}\chi\}$ which obeys the radiation condition in the bottom half space, but not necessarily the free surface boundary condition. In computing the $\{{}_{R}\chi\}$ vector we will also assume no sources so that from equation (2.5.26) we can write the following.

$$\begin{bmatrix} {}_{R}^{B}D_{11} & {}_{R}^{B}D_{12} \\ {}_{R}^{B}D_{21} & {}_{R}^{B}D_{22} \end{bmatrix} \begin{Bmatrix} {}_{R}\chi_1 \\ {}_{R}\chi_2 \end{Bmatrix} = - \begin{bmatrix} {}_{R}^{B}D_{13} & {}_{R}^{B}D_{14} \\ {}_{R}^{B}D_{23} & {}_{R}^{B}D_{24} \end{bmatrix} \begin{Bmatrix} {}_{R}\chi_3 \\ {}_{R}\chi_4 \end{Bmatrix} \tag{2.6.7}$$

Equation (2.6.7) will hold at all depths and so we will evaluate ${}_{R}\chi_2$ and ${}_{R}\chi_2$ at the surface where, using the [D] matrix minors we arrive at,

$$\begin{Bmatrix} {}_{R}\chi_1(0) \\ {}_{R}\chi_2(0) \end{Bmatrix} = - \frac{1}{{}^{B}M_{12}(0)} \begin{bmatrix} -{}^{B}M_{23}(0) & -{}^{B}M_{24}(0) \\ {}^{D}M_{13}(0) & {}^{B}M_{14}(0) \end{bmatrix} \begin{Bmatrix} {}_{R}\chi_3(0) \\ {}_{R}\chi_4(0) \end{Bmatrix} \tag{2.6.8}$$

Of course, equation (2.6.8) is only true if ${}^{B}M_{12}(0) \neq 0$. We will now assume that ${}_{R}\chi_3(0) = 0$ so that we can solve for ${}_{R}\chi_1(0)$ and ${}_{R}\chi_2(0)$ in terms of ${}_{R}\chi_4(0)$. We will also evaluate these at ${}_{R}\tilde{K}^{+}(\eta)$ and ${}_{R}\tilde{K}^{-}(\eta)$ so that,

$$ {}_{R}\chi_1^{+}(0) = \frac{{}^{B}M_{24}^{+}(0)}{{}^{B}M_{12}^{+}(0)} \, {}_{R}\chi_4^{+}(0) , \tag{2.6.9} $$

$$ {}_{R}\chi_2^{+}(0) = - \frac{{}^{B}M_{14}^{+}(0)}{{}^{B}M_{12}^{+}(0)} \, {}_{R}\chi_4^{+}(0) , $$

and similarly for ${}_{R}\chi_1^{-}(0)$ and ${}_{R}\chi_2^{-}(0)$. We will specify that,

$$ {}_{R}\chi_4^{+}(0) = {}_{R}\chi_4^{-}(0) , \tag{2.6.10} $$

so that,

$$ {}_{R}\chi_1^{+}(0) = \frac{{}^{B}M_{24}^{+}(0)}{{}^{B}M_{12}^{+}(0)} \cdot \frac{{}^{B}M_{12}^{-}(0)}{{}^{B}M_{24}^{-}(0)} \, {}_{R}\chi_1^{-}(0) , \tag{2.6.11} $$

and

$$ {}_{R}\chi_2^{+}(0) = \frac{{}^{B}M_{14}^{+}(0)}{{}^{B}M_{12}^{+}(0)} \cdot \frac{{}^{B}M_{12}^{-}(0)}{{}^{B}M_{14}^{-}(0)} \, {}_{R}\chi_2^{-}(0) . $$

We can now define the stress-displacement vector $\{{}_{R}\tilde{E}\}$ as follows,

$$ \{{}_{R}\tilde{E}\} = \frac{\{\delta_{R}\chi\}}{\delta_{R}\chi_1(0)} = \frac{\{{}_{R}\chi^{+}\} - \{{}_{R}\chi^{-}\}}{\{{}_{R}\chi_1^{+}(0)\} - \{{}_{R}\chi_1^{-}(0)\}} , \tag{2.6.12} $$

so that

$$ \begin{Bmatrix} {}_{R}\tilde{E}_1(0) \\ {}_{R}\tilde{E}_2(0) \\ {}_{R}\tilde{E}_3(0) \\ {}_{R}\tilde{E}_4(0) \end{Bmatrix} = \begin{Bmatrix} 1 \\ \dfrac{{}_{R}\chi_2^{+}(0) - {}_{R}\chi_2^{-}(0)}{{}_{R}\chi_1^{+}(0) - {}_{R}\chi_1^{-}(0)} \\ 0 \\ 0 \end{Bmatrix} $$

$$= \begin{Bmatrix} 1 \\ R^{\tilde{\epsilon}} \\ 0 \\ 0 \end{Bmatrix}$$

where

$$R^{\tilde{\epsilon}} = - \frac{\delta \left(\frac{B M_{14}(0)}{B M_{24}(0)} \right)}{\delta \left(\frac{B M_{24}(0)}{B M_{14}(0)} \right)} . \tag{2.6.13}$$

Following the same procedure except setting ${}_R\chi_4^+(0) = {}_R\chi_4^-(0) = 0$ we can show that

$$R^{\tilde{\epsilon}} = - \frac{\delta \left(\frac{B M_{13}(0)}{B M_{12}(0)} \right)}{\delta \left(\frac{B M_{23}(0)}{B M_{12}(0)} \right)} . \tag{2.6.14}$$

Equations (2.6.13) and (2.6.14) along with (2.6.6) allow us to express equation (2.5.5) in the following manner.

(2.6.15)

$$\begin{Bmatrix} R^{y_1}(0) \\ R^{y_2}(0) \end{Bmatrix} = \delta \left(\frac{- B M_{23}(0)}{B M_{12}(0)} \right) \begin{bmatrix} 0 & 0 & 1 & R^{\tilde{\epsilon}} \\ 0 & 0 & R^{\tilde{\epsilon}} & R^{\tilde{\epsilon}^2} \end{bmatrix} [{}_R A(0,z_0)] \{{}_R \Sigma\}.$$

We can now repeat the derivation of equations (2.5.63) through (2.5.68) to show the following.

(2.6.16)

$$\{\delta {}_R y(\eta,z)\} = \delta \left(- \frac{B M_{23}(0)}{B M_{12}(0)} \right) \left([{}_R \tilde{\Sigma}(\eta,\omega)] \left\{ {}_R \tilde{E}(\eta,\omega,z_0) \right\} \right) \left\{ {}_R \tilde{E}(\eta,\omega,z) \right\},$$

where

$$[{}_R\tilde{\Sigma}(\eta,\omega)] = [{}_R\Sigma_3 \; {}_R\Sigma_4 \; -{}_R\Sigma_1 \; -{}_R\Sigma_3] \Big|_{k={}_R\tilde{K}(\eta,\omega)}, \tag{2.6.17}$$

and

$$\{{}_R\tilde{E}(\eta,\omega,z)\} = [{}_R A(z,0)] \Big|_{k={}_R\tilde{K}(\eta,\omega)} \cdot \{{}_R\tilde{E}(\eta,\omega,0)\}. \tag{2.6.18}$$

In order to clean up the notation, we have dropped the α and β subscripts denoting P and S-wave branch cuts throughout the developments but it is understood that there will be two versions of (2.6.15) corresponding to the two branch cut integrals, ${}_{R\alpha}I$ and ${}_{R\beta}I$. Following a similar analysis for the Love waves we can express the stress-displacement vector jump across the Love wave branch cut as follows.

$$\{\delta_L y(\eta,z)\} = \delta\left(-\frac{{}^L B_2(0)}{{}^L B_1(0)}\right)\left(\left[{}_L\tilde{\Sigma}(\eta,\omega)\right]\left\{{}_L\tilde{E}(\eta,\omega,z_s)\right\}\right)\left\{{}_L\tilde{E}(\eta,\omega,z)\right\}, \tag{2.6.19}$$

where

$$\left[{}_L\tilde{\Sigma}(\eta,\omega)\right] = \left[{}_L\Sigma_2 \; -{}_L\Sigma_1\right] \Big|_{k={}_L\tilde{K}(\eta,\omega)}, \tag{2.6.20}$$

$$\{{}_L\tilde{E}(\eta,\omega,z)\} = [{}_L A(z,0)] \Big|_{k={}_L\tilde{K}(\eta,\omega)} \{{}_L\tilde{E}(\eta,\omega,0)\}, \tag{2.6.21}$$

and

$$\{{}_L\tilde{E}(\eta,\omega,0)\} = \begin{Bmatrix} 1 \\ 0 \end{Bmatrix}.$$

REFERENCES

Abo-Zena, A., 1979, Dispersion function computations for unlimited frequency values: Geophysical Journal of the Royal Astronomical Society, v. 58, p. 91-105.

Achenbach, J., 1984, in, Wave Propagation in Elastic Solids, North-Holland, Amsterdam, 209 pp.

Acton, F., 1970, in, Numerical Methods that Usually Work, Harper and Row, New York.

Aki, K. and Richards, P., 1980, in, Quantitative Seismololgy Theory and Methods, v. 1, W. H. Freeman, San Francisco

Bache, T. and Harkrider, D., 1976, The body waves due to a general seismic source in a layered earth model: 1. formulation of the theory: Bulletim of the Seismological Society of America, v. 66, p. 1805-1819.

Ben-Menahem, A. and Singh, S., 1972, Computations of models of elastic dislocations in the earth: in, Methods in Computational Physics, v. 12, Academic Press, New York, p. 300-372.

Ben-Menahem, A. and Singh, S., 1981, in, Seismic Waves and Sources, Springer-Verlag, New York.

Bouchon, M., 1981, A simple method to calculate Green's functions for elastic layered media: Bulletin of the Seismological Society of America, v. 71, p. 959-971.

Cormier, V., 1980, The synthesis of complete seismograms in an earth model specified by radially inhomogeneous layers: Bulletin of the Seismological Society of America, v. 70, p. 691-716.

Dorman, J., Ewing, M. and Oliver, J., 1960, Study of the shear-velocity distribution in the upper mantle by mantle Rayleigh waves: Bulletin of the Seismological Society of America, v. 50, p. 87-115.

Dunkin, J., 1965, Computation of modal solutions in layered elastic media at high frequencies: Bulletin of the Seismological Society of America, v. 55, p. 335-358.

Fuchs, K. and Muller, G., 1971, Computation of synthetic seismograms with the reflectivity method and comparison with observations: Geophysical

Journal of the Royal Astronomical Society, v. 23, p. 417-433.

Gilbert, F., 1964, Propagation of transient leaking modes in a stratified elastic wave-guide: Reviews of Geophysics, v. 2, p. 123-154.

Gilbert, F. and Backus, G., 1966, Propagator matrices in elastic wave and vibration problems: Geophysics, v. 31, p. 326-332.

Harkrider, D., 1964, Surface waves in multi-layered elastic media I. Rayleigh and Love waves from buried sources in a multi-layered elastic half space: Bulletin of the Seismological Society of America, v. 54, p. 627-679.

Hartzell, S. and Helmberger, D., 1982, Strong-motion modelling of the Imperial valley earthquake of 1979: Bulletin of the Seismological Society of America, v. 72, p. 571-596.

Harvey, D., 1981, Seismogram synthesis using normal mode superposition: the locked mode approximation: Geohpysical Journal of the Royal Astronomical Society, v. 66, p. 37-61.

Haskell, N., 1953, The dispersion of surface waves on multilayered media: Bulletin of the Seismological Society of America, v. 43, p. 17-34.

Herrmann, R. and Wang, C., 1985, A comparison of synthetic seismograms: Bulletin of the Seismological Society of America, v. 75, p. 41-56.

Hudson, J., 1969, A quantitative evaluation of seismic signals at teleseismic distances - II. body waves and surface waves from an extended source: Geophysical Journal of the Royal Astronomical Society, v. 18, p. 353-370.

Kanamori, H. and Hadley, D., 1975, Crustal structure and temporal velocity change in southern California: Pure and Applied Geophysics, v. 113, p. 258-280.

Kazi, M., 1976, Spectral representation of the Love wave operator: Geophysical Journal of the Royal Astronomical Society, v. 47, p. 225-249.

Kennett, B., Kerry, N. and Woodhouse, J., 1978, Symmetries in the reflection and transmission of elastic waves: Geophysical Journal of the Royal Astronomical Society, v. 52, p. 215-230.

Kennett, B. and Kerry, N., 1979, Seismic waves in a stratified half space: Geophysical Journal of the Royal Astronomical Society, v. 57, p. 557-583.

Kennett, B., 1980, Seismic waves in a stratified half space - II. theoretical seismograms: Geophysical Journal of the Royal Astronomical Society, v. 61, p. 1-10.

Kerry, N., 1981, Synthesis of seismic surface waves: Geophysical Journal of the Royal Astronomical Society, v. 64, p. 425-446.

Kind, R., 1978, The reflectivity method for a buried source: Journal of Geophysics, v. 44, p. 603-612.

Knopoff, L., 1964, A matrix method for elastic wave problems: Bulletin of the Seismological Society of America, v. 54, p. 431-438.

Knopoff, L., Schwab, F. and Kansel, E., 1973, Interpretation of L_g: Geophysical Journal of the Royal Astronomical Society, v. 33, p. 389-404.

Lapwood, E., 1949, The disturbance due to a line source in a semi-infinite elastic medium: Philosophical Transactions of the Royal Society of London, v. A242, p. 63-100.

Liu, H., Anderson, D. and Kanamori, H., 1976, Velocity dispersion due to anelasticity: implications for seismology and mantle composition: Geophysical Journal of the Royal Astronomical Society, v. 47, p. 41-58.

Mantovani, E., Schwab, F., Liuo, H. and Knopoff, L., 1977, Generation of complete theoretical seismograms for SH - II: Geophysical Journal of the Royal Astronomical Society, v. 48, p. 531-536.

Nakanishi, K., Schwab, F. and Knopoff, L., 1977, Generation of complete theoretical seismograms for SH - I: Geophysical Journal of the Royal Astronomical Society, v. 48, p. 525-530.

Press, F., Harkrider, D. and Seafeldt, C., 1961, A fast, convenient program for computation of surface-wave dispersion curves in multilayered media: Bulletin of the Seismological Society of America, v. 51, p. 495-502.

Rosenbaum, J., 1960, The long-time response of a layered elastic medium to explosion sound: Journal of Geohpysical Research, v. 65, p. 1577-1613.

Rosenbaum, J., 1964, A note on the computation of Rayleigh wave dispersion curves for layered elastic media: Bulletin of the Seismological Society of America, v. 54, p. 1013-1019.

Schwab, F. and Knopoff, L., 1970, Surface-wave dispersion computations: Bulletin of the Seismological Society of America, v. 60, p. 321-344.

Sezawa, K., 1931, On the transmission of seismic waves on the bottom surface of an ocean: Bulletin of the Earthquake Research Institute Tokyo Imperial University, v. 9, p. 115-142.

Stevens, J., 1980, Seismic radiation from the sudden creation of a spherical cavity in an arbitrarily prestressed ealstic medium: Geophysical Journal of the Royal Astronomical Society, v. 61, p. 303-328.

Swanger, H. and Boore, D., 1978, Simulation of strong-motion displacements using surface-wave modal superposition: Bulletin of the Seismological Society of America, v. 68, p. 907-922.

Takeuchi, H. and Saito, M., 1972, Seismic surface waves: in, Methods in Computational Physics, v. 11, Academic Press, New York, p. 217-295.

Thomson, W., 1950, Transmission of elastic waves through a stratified solid medium: Journal of Applied Physics, v. 21, 89 pp.

Wang, C. and Herrmann, R., 1980, A numerical study of P-, SV-, and SH-wave generation in a plane layered medium: Bulletin of the Seismological Society of America, v. 70, p. 1015-1036.

Watson, T., 1970, A note on fast computation of Rayleigh wave dispersion in the multi-layered elastic half space: Bulletin of the Seismological Society of America, v. 60, p. 161-166.